1973

Broad Spectrum Microwave Systems for Remotely Measuring Soil Moisture Content

W. P. Waite
University of Arkansas, Fayetteville

K. R. Cook
University of Arkansas, Fayetteville

B. B. Bryan
University of Arkansas, Fayetteville

BROAD SPECTRUM MICROWAVE SYSTEMS FOR REMOTELY MEASURING SOIL MOISTURE CONTENT

By

W.P. WAITE

K.R. COOK

B.B. BRYAN

WATER RESOURCES RESEARCH CENTER

Publication No. 18

In Cooperation With

ENGINEERING EXPERIMENT STATION

Research Report No. 23

UNIVERSITY OF ARKANSAS

Fayetteville

1973

PROJECT COMPLETION REPORT

Project No.: B-020-ARK II

Agreement No.: 14-31-0001-3557

Starting Date: July, 1971

Completion Date: September, 1973

BROAD SPECTRUM MICROWAVE SYSTEMS FOR REMOTELY MEASURING SOIL MOISTURE CONTENT

By

W. P. Waite, K. R. Cook, and B. B. Bryan
Co-Principal Investigators

ARKANSAS WATER RESOURCES RESEARCH CENTER
University of Arkansas
Fayetteville, Arkansas 72701

For Worked Performed by

Department of Electrical Engineering
Agricultural Experiment Station
University of Arkansas
Fayetteville, Arkansas 72701

November, 1973

ABSTRACT

A theoretical and experimental study of the microwave reflectivity of soils with varying moisture content was conducted. A system was developed to measure reflectivity over a continuous frequency range of 4 to 26.5 GHz, at incidence angles from 10^{o} to 70^{o}, and with both horizontal and vertical polarization. The measurements were found to be extremely accurate for smooth homogeneous surfaces, however, the effects of surface roughness were found to be more severe than predicted due to the discontinuous nature of naturally occurring rough surfaces.

An algorithm was developed which used the frequency dependence of the reflectivity to estimate the effective roughness of the surface and permit correction to an equivalent smooth surface reflectivity which in turn could be related to dielectric constant or percent moisture content.

For the frequency range of investigation the maximum mean square height deviation that could be accomodated was approximately one inch. From this it may be concluded that operational airborne or spacecraft sensors must operate in the 500 MHz to 1 GHz range. Even at this reduced frequency it will be impossible to neglect the effects of roughness and a diversity technique such as developed here is essential if an absolute measure of soil moisture is to be made.

ACKNOWLEDGEMENT

The work performed during this contract period was supported in part with funds provided by the Office of Water Resources Research, U. S. Department of the Interior, under Grant No. A-017-ARK, as authorized under the Water Resources Research Act of 1964, P. L. 88-379, as amended by P.L. 89-404 and P. L. 92-175.

Additional support was provided by National Science Foundation under NSF Grant No. GK-31515 and National Bureau of Standards under Contract No. CST 8145(1).

This research program was performed under the direction of the Principal Investigators:

K. R. Cook	Professor & Head	Electrical Engr. Dept.
B. B. Bryan	Professor & Head	Agricultural Engr. Dept.
W. P. Waite	Associate Professor	Electrical Engr. Dept.

The program was conducted by:

R. D. Mayo	Research Assistant	Dept. of Agricultural Engr. Agricultural Experiment Station
W. H. Stiles	Grad. Res. Assistant	Electrical Engineering Dept.
L. G. Collier	Grad. Res. Assistant	Electrical Engineering Dept.
C. H. Turner	Grad. Res. Assistant	Electrical Engineering Dept.
J. A. Rich	Grad. Res. Assistant	Electrical Engineering Dept.
F. T. Robinson	Grad. Res. Assistant	Electrical Engineering Dept.

TABLE OF CONTENTS

Page

LIST OF FIGURES

LIST OF TABLES

1. INTRODUCTION

Water plays a vital role in any ecosystem. The quantity and quality of water available to any system directly affects its gross ecological efficiency. If the ecologist is to impose synthetic constraints regarding water, he must have spatial and temporal inventory of soil moisture content to optimize his control. Present day techniques for measuring soil moisture content are essentially in situ measurements and represent a major problem in studies of large ecosystems (Hoskyn and Bryan, 1969).

It has long been established that the microwave emission and radar cross section of terrain surfaces are strongly influenced by the moisture content of the soil (Peake, 1959; Lundien, 1966). This has led to considerable conjecture regarding the potential of air (satellite) borne microwave remote sensors for monitoring the spatial distribution of soil moisture content over broad areas (Davis et al., 1966; Poe et al., 1971).

Soil moisture content influences the microwave reflection or emission characteristics of soil surfaces through changes in the complex dielectric constant. Due to the large disparity in the dielectric constant of dry soils (in the range of 2 to 5) and water (near 80) a measure of the dielectric constant of the soil-water mixture gives an excellent estimate of the moisture content. If the surface is smooth, the power reflection coefficient or emissivity of the surface measured with an active or passive microwave sensor is directly related to the complex dielectric constant and in turn the moisture content of the surface.

Unfortunately other parameters of both the terrain and the sensing system likewise produce significant effects on the measured signal. In general, the microwave emission and radar cross section of terrain surfaces are dependent

upon the following parameters:

1. Composition (complex dielectric constant)
2. Structure (target roughness)
3. Temperature
4. Frequency
5. Incidence angle
6. Polarization

The functional dependence of the passive and active measurements is not precisely the same for these parameters, however, there are a number of general observations which may be made that are equally appropriate for either type of measurement system. First, it should be noted that only the first three parameters are characteristics of the terrain surface, while the last three are system parameters which are to some extent controllable by the investigator. The obvious strategy in any attempt to measure one of the target parameters is to select the system parameters to enhance the contribution to the measured signal of the desired target parameter. If it is not possible to select an operating region in which the return is dominantly controlled by a single terrain parameter, then diversity of the controllable parameters must be employed in an attempt to separate the relative contributions to the signal of each of the terrain parameters. Whichever method is used the functional dependence of the measurement of the terrain and system parameters must be known to make an intelligent selection of either operating region or diversity techniques.

The objective of this study is to define the functional dependence of the parameters affecting the microwave return from soil surfaces and to recommend the design of a system capable of remotely monitoring soil moisture content.

The study is a three-part effort involving the investigation of analytical models to represent the terrain-sensor interaction, the development of a measurement system capable of measurement diversity with the three system parameters (frequency, incidence angle, polarization), and the conduct of laboratory and field measurements of soil surfaces under a variety of closely controlled conditions.

Section 2 covers the analytical models appropriate for representing soil surfaces in the microwave spectrum. The behavior of the dielectric constant of water across the microwave spectrum and its effect on the reflection characteristics of smooth soil-water mixtures is examined. This study is extended to the investigation of electromagnetic scattering from rough surfaces of arbitrary dielectric constant using both physical optics and small perturbation models. Finally, the reflectivity of layered media which may be used to represent inhomogeneous vertical moisture profiles is presented.

Section 3 covers the design and development of the microwave measurement system. This system is capable of performing absolute measurements of power reflectivity for a wide range of system parameters. Incidence angle may be varied from 10^{o} to approximately 70^{o}, both horizontal and vertical polarization may be used, and all measurements may be recorded across a continuous frequency range of 4 - 26.5 GHz.

Section 4 covers the measurement program conducted with the above system. Laboratory measurements of soil surfaces are presented for a wide range of system and surface parameters. The effects of surface roughness are examined in detail for rough surfaces for which the statistics are known and which conform to the restrictions on height and slope dictated by the analytical models. These measurements are compared with measurements

of surfaces deliberately violating the continuity requirements of inhomogeneous media are likewise presented. The results obtained from the theoretical and laboratory programs are verified by a series of field measurements taken at the University of Arkansas Agricultural Experiment Station under realistic although accurately monitored conditions.

The data analysis of Section 5 compares the results of the laboratory and field measurement programs with the predictions obtained from the analytical models. It is demonstrated that the effects of naturally occurring, discontinuous roughness are considerably more severe than predicted from the continuous surfaces used in the analytical models. This implies that simply using longer wavelengths to decrease the signal response due to roughness may well be impractical and the only means of measuring the moisture content of unknown surfaces will require frequency diversity measurements to separate the effects of roughness and composition.

2. THEORETICAL BACKGROUND

2.1 Introduction

Before launching into a detailed description of the surface-sensor interaction let us consider in a very general fashion the variations one might expect in the parameters affecting the microwave signal. These parameters are again:

1. Composition (complex dielectric constant)
2. Structure (surface roughness)
3. Temperature
4. Frequency
5. Incidence angle
6. Polarization

The general effect on the measurement of the three surface parameters and their dependence on the system parameters is briefly summarized in the following discussions.

Composition (complex dielectric constant)

The complex dielectric constant has two major effects on the microwave measurement of terrain surfaces. First, the microwave reflectivity of the terrain surface is directly dependent on the magnitude of the complex dielectric constant and is given by the Fresnel reflection coefficient formulas (Stratton, 1941). The possibility of measuring soil moisture rests upon the large disparity in dielectric constant of water and soil. In the microwave region of the spectrum the dielectric constant of water is quite large, as much as 80, while that of dry soil is typically less than 5. The resulting

dielectric constant of a soil-water mixture is thus seen to be dominantly influenced by tne percent water in the mixture.

The effect of changes in the surface dielectric constant is opposite for active and passive microwave measurement systems. That is, the radar cross section is directly dependent on the surface reflectivity and in turn the dielectric constant of the surface mixture. Thus, an increase in moisture causes an increase in reflectivity and a corresponding increase in radar cross section. However, the emissivity of a smooth surface is given by one minus the power reflection coefficient (magnitude squared of Fresnel reflection coefficient) hence, an increase in moisture causes a decrease in emissivity and a corresponding decrease in the measured brightness temperature.

The second major effect of the complex dielectric constant is related to the conductivity of the material. That is, the loss or attenuation of the microwave energy is a function of the material conductivity and the frequency of the radiation. In general, the higher the conductivity or the frequency, the greater the attenuation in the material, hence the effective penetration is less. It should be noted that the effective conductivity contains components of loss involved in polarization of the material as well as normal conduction currents and that the effective conductivity of soil or vegetation containing water is likewise dominantly influenced by the percent water content. Thus, for increased moistures the depth of material to which the signal responds to decreased.

This may have a significant effect on the return from vegetated surfaces, as at the higher frequencies the return is essentially from the vegetation canopy while at lower frequencies, with greater penetration capability, the return may be primarily from the surface beneath the vegetation.

At still lower frequencies significant penetration of the surface material is possible and response to subsurface layers or objects becomes a possibility. Note, that this analysis assumes a simple two-layer (three media) model with the upper layer comprised of vegetation which is assumed to have an effective dielectric constant lower than that of the surface.

Structure (terrain roughness)

Electromagnetic energy incident on a terrain surface is partially reflected in either a "specular" or "diffuse" manner depending upon the roughness of the terrain. Specular, or mirror-like, reflection takes place when points on the surface have a linear phase relationship, which occurs when both the incident wave front and the surface are planar. Under these conditions the reflection obeys Snell's law of reflection (angle of incidence equals angle of reflection) and virtually all of the reflected energy is contained in a small angular region about the Snell's law angle. If the surface has irregularities that are a significant portion of a wavelength it is possible to get phase interference effects between points on the surface and energy may be reflected at angles other than the specular. The general practice is to separate the reflected energy into specular (coherent) and diffuse (scattered) components.

Several interesting observations regarding the effect of roughness on active and passive microwave measurement systems may be made. Since roughness, or diffuse reflection, is a function of phase, it is seen that the roughness must be spoken of in terms of the wavelength of the radiation. That is, a given surface may be essentially smooth at a wavelength of one meter, while the same surface may appear quite rough at a wavelength of one millimeter. As a surface becomes rougher, it will reflect less energy at

the specular angle (the coherent component will decrease) and correspondingly more energy will be scattered at the non-specular angles (the diffuse, or incoherent component will increase). For a conventional monostatic radar system operating at other than normal incidence, it is seen that some roughness is necessary to obtain a backscattered signal. In addition, it is seen that increased roughness will give an increased scattering cross section and thus give the indication of an increased reflectivity or moisture content. On the other hand, a passive measurement system always monitors the specular component, thus increased roughness will appear as decreased reflectivity (increased emissivity) and give increased brightness temperature and the appearance of decreased moisture content.

The important point to note is that the effect of roughness on the active and passive measurement systems is reversed because they are measuring differing portions of the angular scattering pattern. If the radar (active) system is operated bistatically at the specular angle, or if monostatically at normal incidence, the effect of roughness is similar to that indicated by the passive system.

Temperature

The measured signal is much more sensitive to thermometric temperature for the passive (radiometric) system, however, this effect is usually accounted for by independent measurement permitting separation of effects due to thermometric temperature and emissivity. For the active system the effects of temperature in dielectric dispersion are normally negligible in compari son with other effects.

From the preceeding discussion it is clear that the basic problem in the microwave measurement of soil moisture is the separation of the effects

of structure and composition. To relate the measurement to complex dielectric constant and in turn to soil moisture it is necessary to make an estimate of the surface reflectivity or emissivity. While this measurement is quite straight forward for a surface consisting of a plane homogeneous half-space, this is not usually a representative model for natural surfaces.

From the preceeding discussion, two basic approaches to the measurement of soil moisture may be formulated. One, since the effect of surface roughness decreases with increasing wavelength, simply increase the wavelength until roughness effects may be considered negligible. Two, use diversity in the system parameters such as frequency and incidence angle to estimate the roughness of the surface and permit, through the use of an analytical model, correction of the measured reflectivity (emissivity) to an effective smooth surface reflectivity (emissivity).

Both approaches will require definition of the surface roughness ranges encountered in agricultural and hydrological applications (in itself, a formidable problem). The frequency, or frequency and angular range, must then be selected for compatibility with this roughness range.

In summary, one may see that the most critical question to be answered in the development of microwave soil moisture measurement systems is the effect of roughness on the measurement at a variety of wavelengths. The theoretical and experimental program described herein is designed to answer this question for a range of roughness and soil moisture content compatible with agricultural and hydrologic applications.

2.2 The Effect of Water on the Reflection of Electromagnetic Waves by Smooth Surfaces.

Consider a smooth surface of infinite extent illuminated by a plane wave as shown in Figure 2.2-1. If medium 1 is taken as the atmosphere with dielectric constant and permeability approximately that of free space (ε_o and μ_o) and medium two is taken as an arbitrary dielectric surface, evaluation of the boundary conditions leads to the Fresnel reflection coefficients (Γ)

$$\Gamma_h = \frac{\mu_r \cos\theta - \sqrt{\epsilon_r \mu_r - \sin^2\theta}}{\mu_r \cos\theta + \sqrt{\epsilon_r \mu_r - \sin^2\theta}}$$

$$\Gamma_v = \frac{\epsilon_r \cos\theta - \sqrt{\epsilon_r \mu_r - \sin^2\theta}}{\epsilon_r \cos\theta + \sqrt{\epsilon_r \mu_r - \sin^2\theta}} \qquad (2.2\text{-}1)$$

where θ is the angle of incidence (and by Snell's law the angle of reflection as well), ε_r and μ_r are respectively the dielectric constant and permeability relative to freespace. These relations express the ratio of reflected to incident electric field intensity for both horizontal (h) and vertical (v) polarizations. For nonmagnetic materials such as soil and water the relative permeability differs negligibly from one (Von Hipple, 1954). Thus the above expressions reduce to

$$\Gamma_h = \frac{\cos\theta - \sqrt{\epsilon_r - \sin^2\theta}}{\cos\theta + \sqrt{\epsilon_r - \sin^2\theta}} \qquad (2.2\text{-}2)$$

$$\Gamma_v = \frac{\epsilon_r \cos\theta - \sqrt{\epsilon_r - \sin^2\theta}}{\epsilon_r \cos\theta + \sqrt{\epsilon_r - \sin^2\theta}}$$

and it may be seen that the complex relative dielectric constant may be determined from the complex reflection coefficient.

If the loss tangent (ratio of the imaginary and real components of the

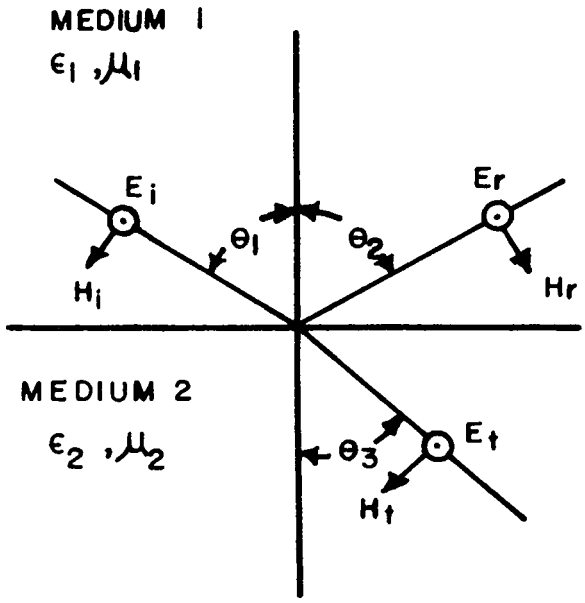

(a) Horizontal (perpendicular) polarization

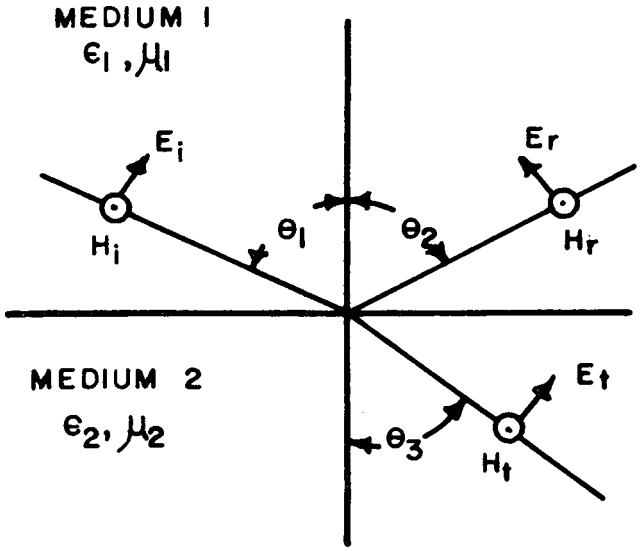

(b) Vertical (parallel) polarization

REFLECTION AND REFRACTION AT A PLATE INTERFACE

Figure 2.2-1

complex dielectric constant) is assumed to be small, then the complex dielectric constant may be adequately represented by its magnitude instead of its magnitude and phase. The reflection coefficient may then be represented by its magnitude alone. Since the available equipment only measured the magnitude of the reflection coefficient, the above assumption was necessary. Magnitudes are implied in the remaining text.

The relative dielectric constants for some dry soils are given in Table 2.2-1 (Von Hipple, 1954).

TABLE 2.2-1

Type	ε_r
Sandy soil	2.53
Loamy soil	2.44
Clay soil	2.16
Magnetite soil	3.50

These values are essentially constant and the loss tangents are negligibly small over the frequency range of interest.

The complex relative dielectric constant of fresh water may be adequately represented by an equation of the Debye form with a single relaxation time

$$\epsilon_c = \epsilon_\infty + \frac{\epsilon_o - \epsilon_\infty}{1 - j 2\pi \tau f} \qquad (2.2\text{-}3)$$

where ε_o = static dielectric constant

ε_∞ = optical dielectric constant

τ = rela ation time

f = frequency

Determinations of ε_o, ε_∞ and τ as functions of temperature have appeared frequently in the literature. Malmberg and Margott (1956), in a careful series of measurements, found that ε_o could be represented by the equation

$$\epsilon_o = 87.740 - 0.40008T + 9.398\times10^{-4}T^2 + 1.410\times10^{-6}T^3 \quad (2.2\text{-}4)$$

for temperatures in the range $0 \leq T \leq 100°C$.

A least squares fit of the data of Grant, Buchanan, and Cook (1957) yields an expression for the relaxation time given by (Edgerton et al, 1971)

$$2\pi\tau = 1.1109\times10^{-10} - 3.824\times10^{-12}T + 6.938\times10^{-14}T^2 - 5.096\times10^{-16}T^3 \quad (2.2\text{-}5)$$

over the temperature range $0 \leq T \leq 40°C$.

There remains considerable disagreement over both the precise value and the temperature variation of ε_∞. However, the value of ε_c is not sensitive to the precise value of ε_∞ for frequencies below approximately 60 GHz. Thus, a temperature independent value of

$$\varepsilon_\infty = 4.9 \quad (2.2\text{-}6)$$

is assumed adequate for the calculations performed here.

Figure 2.2-2 shows the variation of the complex dielectric constant with frequency, at a temperature of 20°C and based on the above equations for the constants in the Debye expression. Figures 2.2-3 and 2.2-4 illustrate the temperature variation of the complex relative dielectric constant over the frequency range of interest.

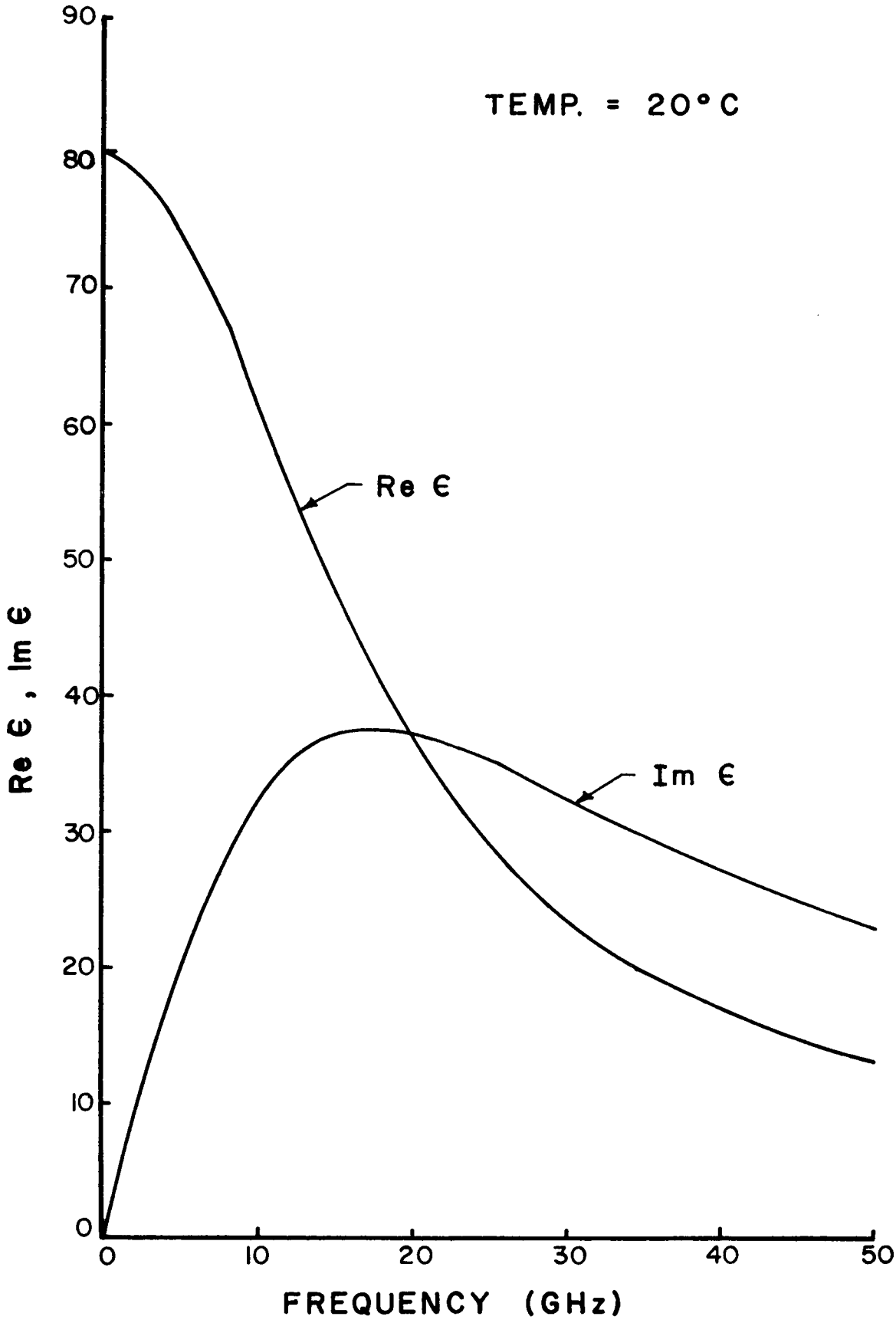

THE COMPLEX DIELECTRIC CONSTANT OF FRESH WATER

Figure 2.2-2

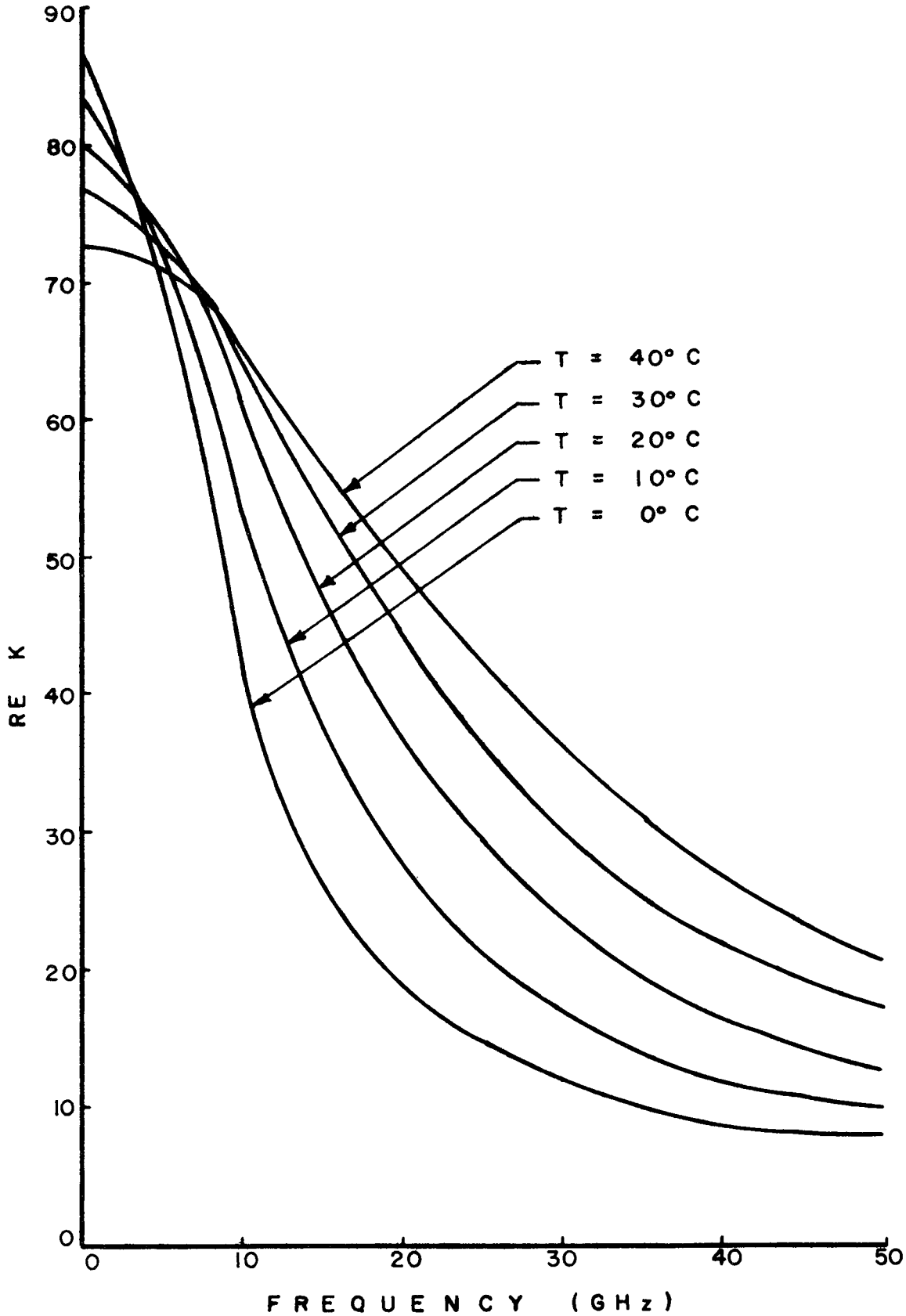

TEMPERATURE VARIATION OF THE REAL PORTION OF THE COMPLEX DIELECTRIC CONSTANT OF FRESH WATER

Figure 2.2-3

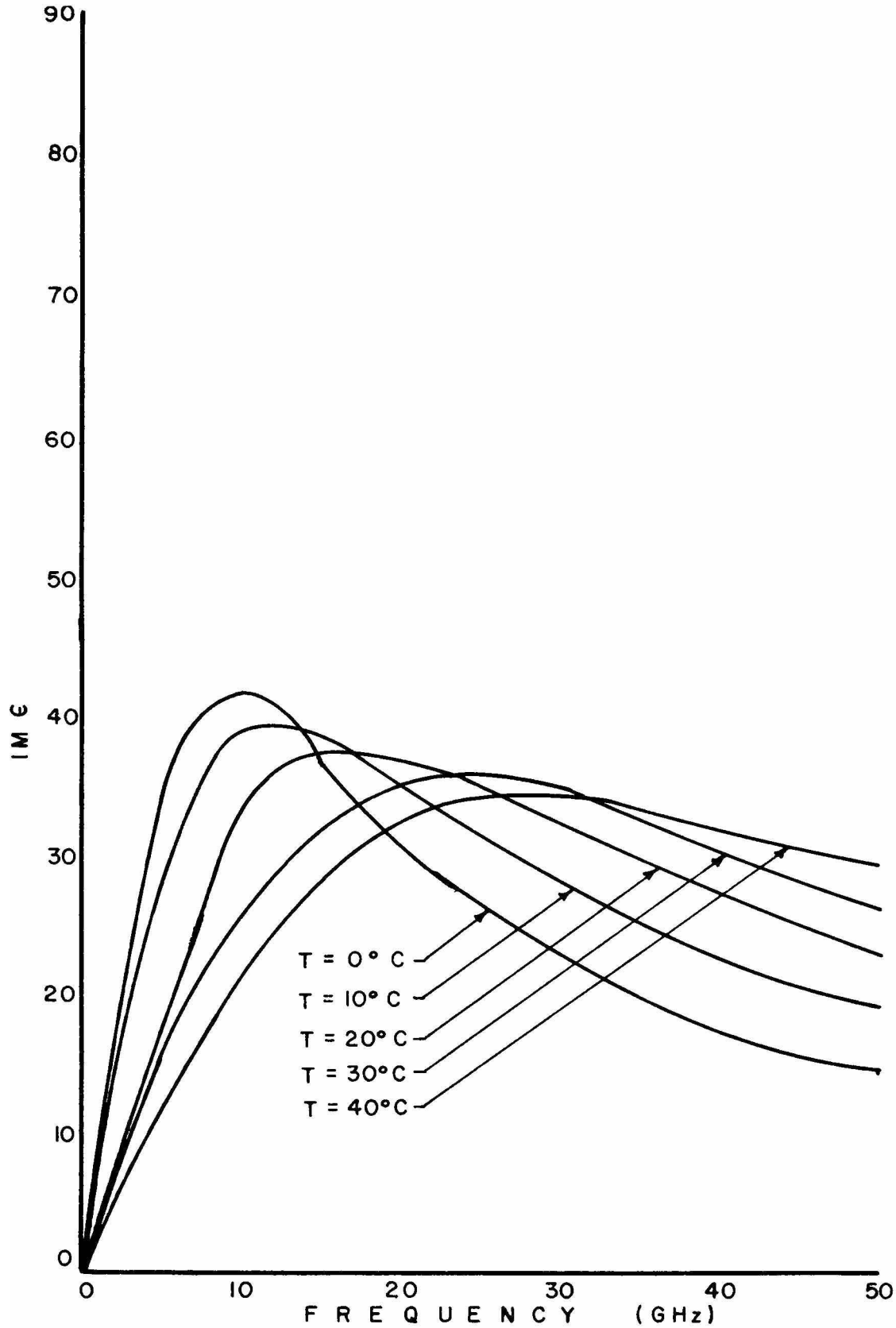

TEMPERATURE VARIATION OF THE IMAGINARY PORTION OF THE COMPLEX DIELECTRIC CONSTANT OF FRESH WATER

Figure 2.2-4

A magnitude plot of the complex dielectric constant is shown in Figure 2.2-5. From this curve and Table 2.2-1 the large disparity in the relative dielectric constants of dry soil and water is apparent. This large difference makes possible the moisture determination of wet soils by microwave measurement.

Figure 2.2-6 illustrates the frequency variation of the theoretical reflection coefficient of a water surface resulting from the dispersive nature of water in this frequency range. The points shown on this curve are calibration measurements taken over an 18 month time span. No attempt was made to correct for temperature, however, the agreement between theory and measurement is an excellent indication of the absolute accuracy of the measurement system.

Assuming no dielectric interaction between water and soil, the relative dielectric constant for a soil-water mixture may be given by

$$\epsilon_r = \alpha \epsilon_w + (1-\alpha)\epsilon_s \qquad (2.2\text{-}7)$$

where α is the fraction of water in the mixture and ϵ_s is the relative dielectric constant for the soil. For soil with a relative dielectric constant of three, a plot of reflection coefficient at normal incidence versus per cent moisture, parameterized by frequency, is shown in Figure 2.2-7. Reflection coefficient versus frequency, parameterized by per cent moisture, is plotted in Figure 2.2-8. This Figure shows a slight frequency dependence for wet soils as a result of the dispersion of water.

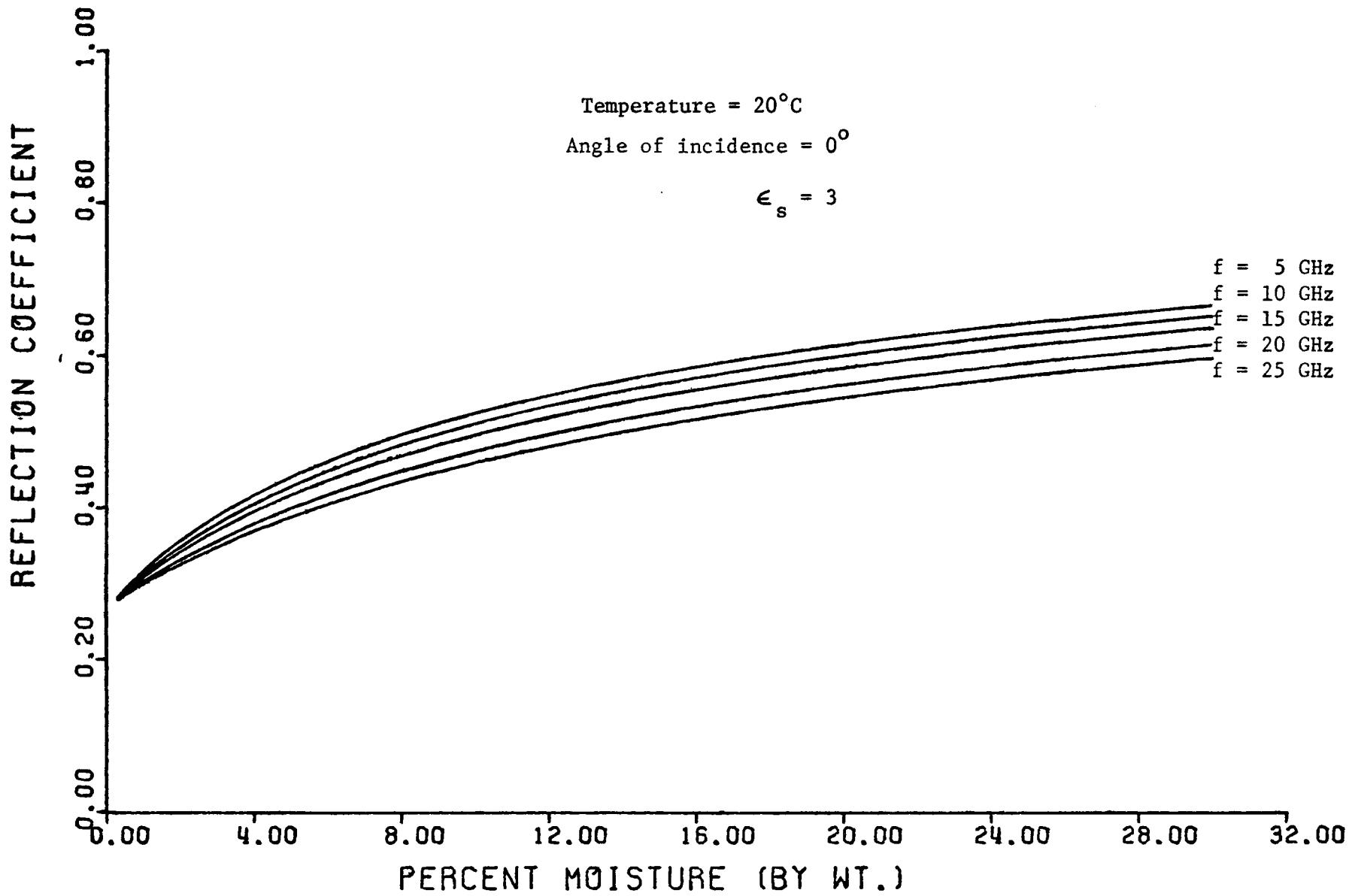

Figure 2.2-7 Theoretical reflection coefficient from wet soil

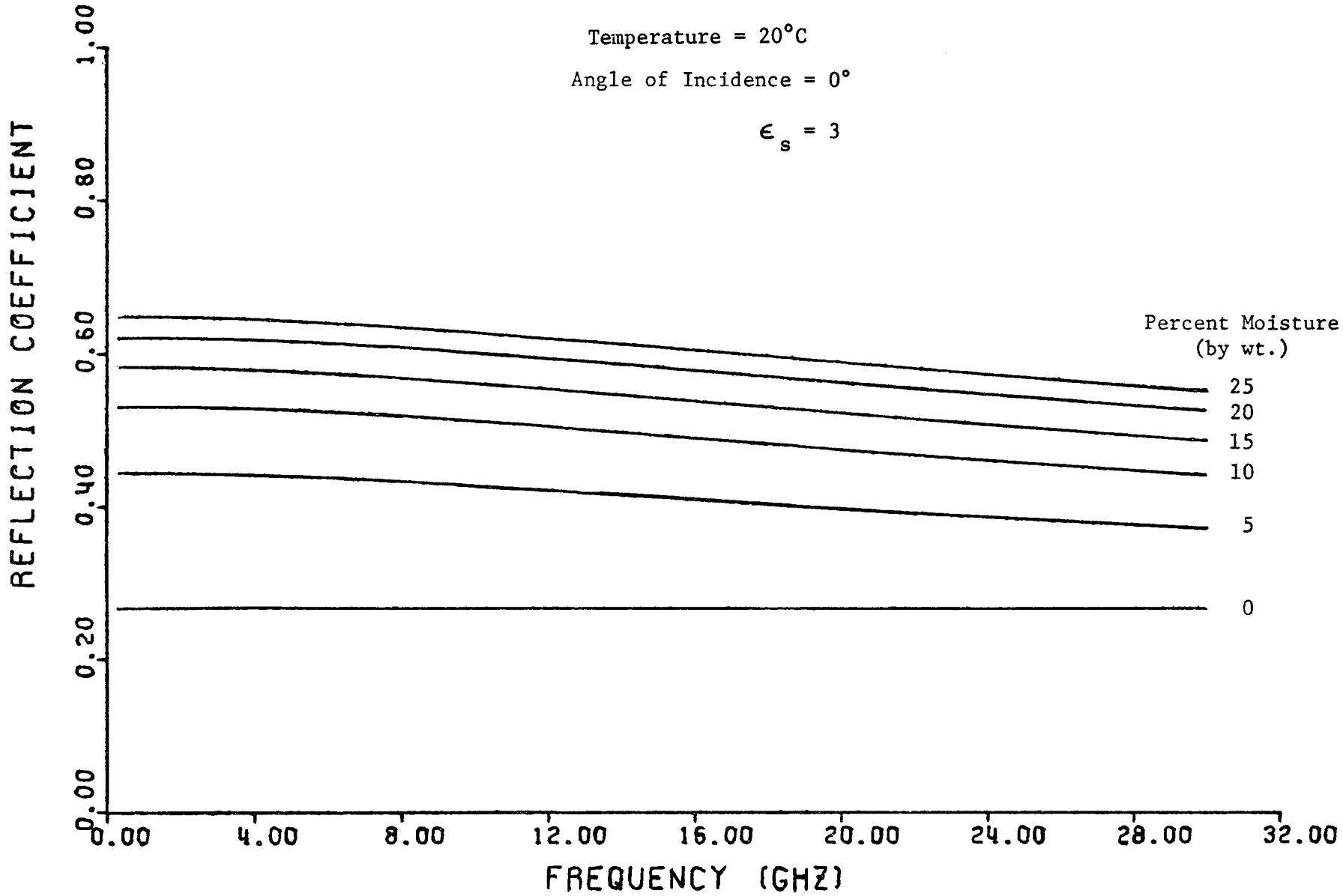

Figure 2.2-8 Theoretical reflection coefficient from wet soil

2.3 The Scattering of Electromagnetic Waves from Rough Surfaces of Arbitrary Dielectric Constant

For an infinite plane surface illuminated by a plane wave, all power is reflected in the specular direction (direction of the Snell's law angle). If the area illuminated is finite, diffraction effects are observed and a lobe structure appears distributed about the specular angle. This effect is predicted from physical optics (Ruck et al., 1970). This pattern, due to the diffraction of the finite surface, is called the "coherent component" of the scattered field. For slight height variations with position on the surface, the fields are nearly coherent, that is, the phase change along the surface remains essentially linear. Thus, calculation of the total coherent power requires a vectoral summation over the elementary scattering areas of the surface.

The introduction of surface roughness with appreciable height deviations with respect to the wavelength effectively reduces the coherent field. Roughness of this scale produces phase changes between scattering elements of the surface which in turn may result in cancellation of the field at the specular angle and reinforcement at angles appreciably removed from the specular. In effect, the power removed from the coherent component is redistributed over the remainder of the scattering half-space. Where the height deviations are random and of significant size (with respect to wavelength) the phase distribution of the elemental wavelets combining at non-specular angles is random and this portion of the return is dubbed the "incoherent component" of the scattered field. Due to the random phase distribution and the fact that for significant phase shifts the distribution of phase will be essentially uniform over the basic phase cycle of 2π radians, the total incoherent power is

the power return due to each scattering element (Beckmann and Spizzichino, 1963).

Since the scattered power is separable into coherent and incoherent components, it follows that scattering cross section may also be separated into these components.

For the investigation of electromagnetic scattering a term is needed to express the effects of the target on the scattered or reflected wave. For a smooth surface, the reflection coefficient is sufficient to describe the surface effects. For slightly rough surfaces, an effective reflection coefficient (Γ_{eff}) may be developed (Peake, 1968). In general for a rough surface, the term used is radar scattering cross section (σ). Radar scattering cross section is a measure of the size and roughness of the target as seen by the radar. "Given the target echo at the receiving system, scattering cross section is the area which would intercept sufficient power out of the transmitted field to produce the given echo by isotropic reradiation" (Ruck, et al., 1970). A defining equation (Skolnik, 1962) is

$$\sigma = \frac{\text{Power scattered toward receiver/unit solid angle}}{\text{Incident power density}/4\pi} \qquad (2.3\text{-}1)$$

For comparison between targets of different size, the scattering cross section is normalized by dividing by the total illuminated area (A). This produces a differential scattering cross section (σ_o). With the assumptions that the transmitting and receiving apertures have the same gain (G), range (R) is constant across the illuminated area (A), a "square beam" of uniform gain exists across the illuminated area, differential scattering cross section is uniform across the illuminated area, and the range to the transmitting and receiving apertures is the same, the expression for differential

radar scattering cross section reduces to

$$\sigma_o = \frac{(4\pi)^3 R^4 P_r}{G^2 \lambda^2 A P_t} \qquad (2.3\text{-}2)$$

where λ is the wavelength of the incide t radiation, P_t is the transmitted power and P_r is the received power. A relationship between differential radar scattering cross sectionaand effective reflection coefficient is derived in Appendix A for convenience in relating these two parameters.

$$\sigma_o = \frac{\pi R^2}{A} \left|\Gamma_{eff}\right|^2 \qquad (2.3\text{-}3)$$

2.3.1 Kirchoff (Physical Optics) Model of Rough Surface

The generalized Kirchhoff method for solution of the scattered field from a rough surface consists of approximating the boundary conditions at the surface in a manner for which the Hemholtz integral may be evaluated. This method is demonstrated by a scalar solution to the problem with the understanding that a vector solution follows the same procedure. The scattered electric field intensity ($E_s(P)$) at a point P in the far field is the result of the Helmholtz integral (Beckmann and Spizzichino, 1963)

$$E_s(P) = \frac{1}{4\pi} \iint_s \left[E_{surf} \left(\frac{\partial \psi}{\partial n}\right) - \psi \left(\frac{\partial E_{surf}}{\partial n}\right) \right] dS$$

$$\psi = \frac{e^{jk_2 R'}}{R'} \qquad (2.3.1\text{-}1)$$

where S is the surface, ψ is the Green's function, $\overline{k_2}$ is the scattering direction and R' is the range from the surface to the point P.

The geometry for the problem is illustrated in Figure 2.3.1-1. E_{surf} and $\frac{\partial E_{surf}}{\partial n}$ are the value of the field and its normal derivative at the surface.

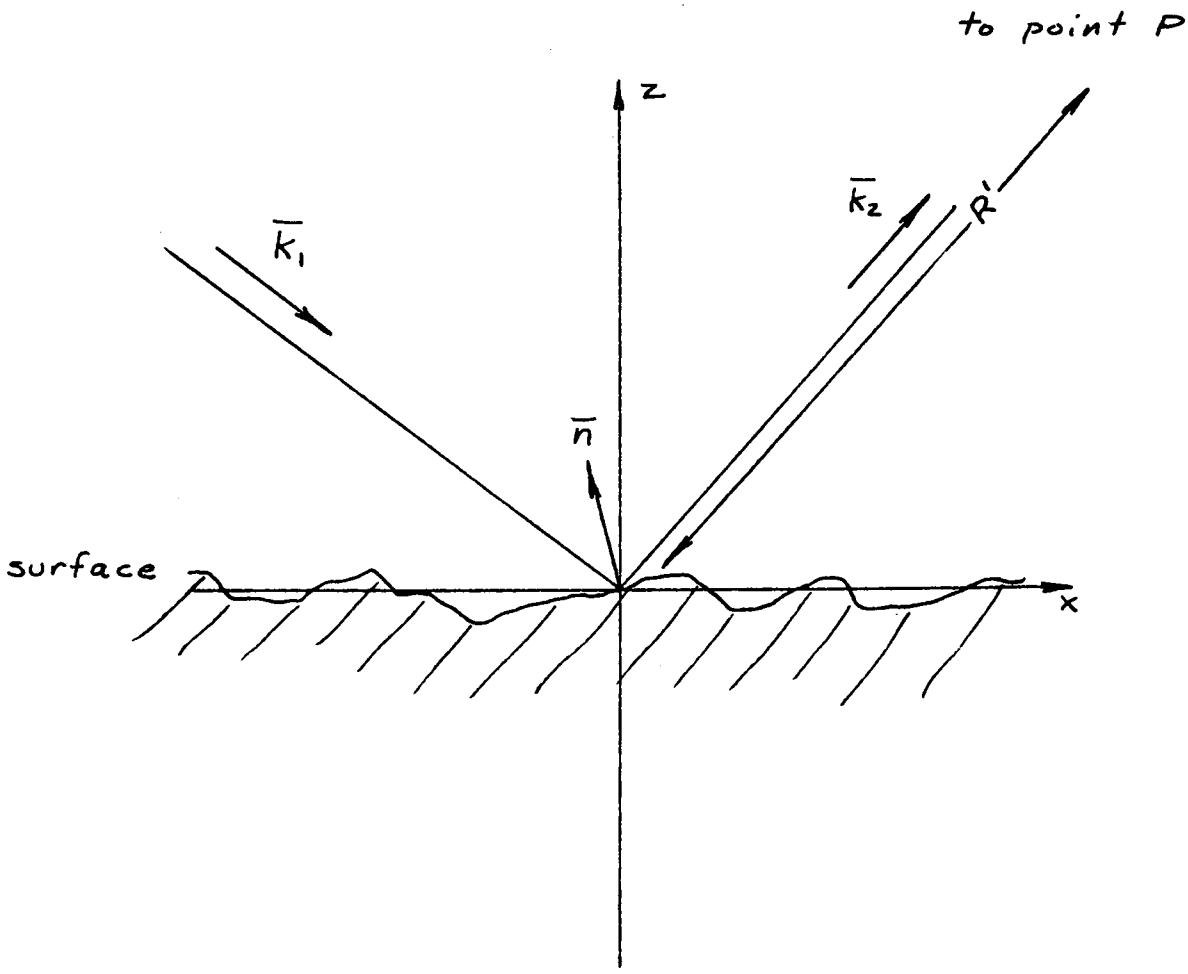

Figure 2.3.1-1 Geometry for Kirchhoff model

The field at any point on the surface is approximated by the field that would appear on a plane tangent to that point. The resulting boundary conditions may then be approximated by

$$E_{surf} = (1+\Gamma)\, E_i$$
$$\frac{\partial E_{surf}}{\partial n} = j\,(1+\Gamma)\, E_i\, \bar{k}_1 \cdot \bar{n} \qquad (2.3.1\text{-}2)$$

where E is the incident field intensity, $\bar{k_1}$ is the incident direction and $\bar{n}$ is the local normal at the point. Γ is the Fresnel reflection coefficient evaluated at the angle between the incident direction and the normal. By applying these boundary conditions and estimating an average reflection coefficient over the surface, the integral may be evaluated and the scattered field determined. The assumption that the surface fields could be approximated by fields on a tangent plane requires that the slopes of the surface be small or the radius of curvature be large. This is the main condition restricting the validity of the Kirchhoff method.

For a rough surface, the coherent energy exists in the pattern about the specular angle due to a combination of surface roughness and diffraction of the surface (Barrick et al., 1970). The coherent scattered field is proportional to the square of the average of $E_s(P)$. Proceeding as in the general Kirchhoff method except with a vector formulation, assumptions are made that surface slopes are again much less than unity, the surface height is Gaussian distributed, and the area is uniformly illuminated. Using the tangent plane approximation, the differential coherent scattering cross section according to (Barrick et al., 1970) is

$$\sigma_{0pq} = \frac{\beta^2 A}{\pi} \left(\frac{\sin \frac{\beta S_x L_x}{2}}{\frac{\beta S_x L_x}{2}} \right)^2 |\alpha_{pq}|^2 \exp\left[-\beta^2 \bar{z}^2 S_z^2\right] \qquad (2.3.1\text{-}3)$$

where p and q are arbitrary polarizations of transmit and recieve

$$\mathcal{S}_x = \sin\theta_i - \sin\theta_s \cos\theta_s$$

$$\mathcal{S}_z = -\cos\theta_1 - \cos\theta_s$$

$$\alpha_{hh} = \cos\theta_i \Gamma_h$$

$$\alpha_{vv} = -\cos\theta_s \Gamma_v$$

and scattering is restricted to the plane of incidence. Here, A is the illuminated area, β is the propagation constant, L_x is the major axis of the illuminated area, and $\overline{z^2}$ is the mean square height of the surface.

2.3.2 Rayleigh Model of Rough Surface

The generalized Rayleigh method for solution of the scattered field from a rough surface consists of postulating the scattered field an an infinite sum of plane waves and then solving for the unknown waves by satisfying the exact boundary conditions at the surface (Beckmann and Spizzichino, 1963).

$$\sum_{m\,n} E(m,n) \qquad (2.3.2\text{-}1)$$

where E is plane wave whose direction is determined by the integers m and n. Each of the fields is then represented in series form. Then by satisfying the boundary conditions at the surface, the scattered fields may be determined. However, unless the roughness on the surface is small enough such that the series representations converge rapidly, the exact solution to the fields requires the solution to an infinite number of equations. Therefore, practically, the Rayleigh method is restricted to surfaces with small mean square height.

2.3.3 Small Perturbation Model of Rough Surface

The small perturbation theory is the name chosen for an electromagnetic scattering theory originally developed by S. O. Rice (1951). This theory is a development of the Rayleight method and is valid for surfaces which are essentially flat but may have small variations (perturbations) from the mean plane. The geometry for the problem is shown in Figure 2.3.3-1.

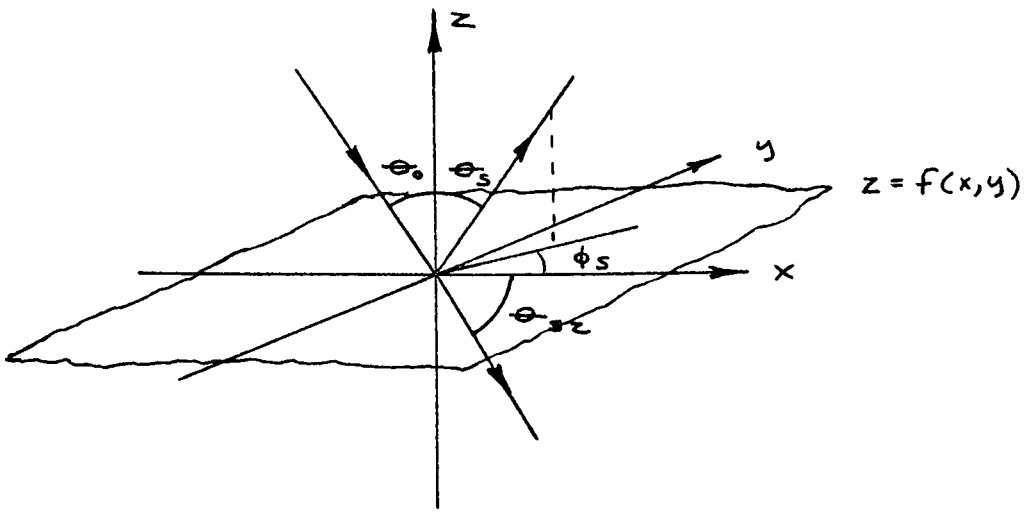

Figure 2.3.3-1 Geometry for small perturbation model

The surface z = f (x,y) may vary a small amount from z = 0. The surface is defined as a random function to ensure generality of formulation. First the surface is expanded as a two-dimensional Fourier series with random coefficients for application of the Rayleigh method of solution to the scattering problem. The statistics of these coefficients may then be used to determine the frequency spectrum or roughness distribution function of the surface. The complete development of the representation of the surface is included in Appendix B.

The general scattered electric fields are defined as:

$$E_{x,y,or\,z} = \sum_{m\,n} N_{mn}\, E(m,n,z) \qquad (2.3.3\text{-}1)$$

where N_{mn} is the magnitude of the electric field (E (m,n,z)). n and m are integers summed from $-\infty$ to $+\infty$ and determine the different directions of propagation of an infinite set of plane waves. Then boundary conditions and the divergence condition are applied at the surface. Assuming that the surface height variations are much less than a wave length and that the surface slopes are small, then making the series approximations resulting from the assumptions, the scattering coefficients N_{mn} are obtained. The use of series expansions suggests separation of the coefficients according to their smallness.

$$N_{mn} = N_{mn}^{(1)} + N_{mn}^{(2)} + \cdots \qquad (2.3.3\text{-}2)$$

Third and higher order terms are neglected due to increased complexity (Rice, 1951). The derivation of the first and second order coefficients is given in Appendix B.

From this point, two different methods of analysis are investigated in the following sections. The continuation of the Rice (1951) development yields a coherent rough surface effective reflection coefficient. The development of Peake (1959) yields expressions for incoherent scattering cross section.

Coherent Effective Reflection Coefficient

The geometry for this problem is identical to Figure 2.3.3-1. Only the horizontally polarized case is developed. The statistical average of the E_x and E_z electric fields can be shown to be zero for horizontal

polarization (Rice, 1951). As a result, the total electric field consists of only the y-component. The y-component of the specularly reflected electric field (E_y^R) is

$$E_y^R = \Gamma_h \, e^{-j\beta(\alpha x + \gamma z)} + \sum_{m\,n} \left(B_{mn}^{(1)} + B_{mn}^{(2)}\right) E(m,n,z) \qquad (2.3.3\text{-}3)$$

where Γ_h = Fresnel reflection coefficient

β = Propagation constant

α = $\sin(\theta_o)$

γ = $\cos(\theta_o)$

P(m-v,n) = random variable rep esentation of the surface

L = period of the surface

a = $2\pi/L$

ε_r = relative dielectric constant

$B_{mn}^{(1)}, B_{mn}^{(2)}$ = coefficients of the y-component of the scattered electric field

b(m,n), c(m,n), d(m,n)
Dmn, h_1, h_2, h_3, h_4, U } - defined in Appendix B

Substitution of the coefficients from equations 41, 50, and 51 of Appendix B yields

$$E_y^R = \Gamma_h \, e^{-j\beta(\alpha x + \gamma z)} + \sum_{m\,n} \left[\frac{j2U\,P(m-v,n)}{d(m,n)} \left(\frac{a^2 n^2}{D_{mn}} - 1 \right) \right.$$

$$+ \frac{a^2 n^2 \, b(m,n)}{d(m,n)\, D_{m,n}} h_2 + \frac{D_{mn} - a^2 n^2}{d(m,n)\, D_{mn}} \left[c(m,n) h_2 - h_3 \right] \qquad (2.3.3\text{-}4)$$

$$\left. + \frac{a^2 m n}{d(m,n)\, D_{mn}} \left[b(m,n) h_1 - c(m,n) h_1 + h_4 \right] \right] E(m,n,z)$$

Computation of the statistical average of the field requires m = v and n = 0. Therefore, the statistical average of the electric field in the specular

direction is

$$\langle E_y^R \rangle = \Gamma_h e^{-j\beta(\alpha x+\gamma z)} + \frac{1}{d(\nu,o)} [c(\nu,o) \langle h_2(\nu,o,k,\ell)\rangle - \langle h_3(\nu,o,k,\ell)\rangle] \cdot E(\nu,o,z) \tag{2.3.3-5}$$

$$= \Gamma_h e^{-j\beta(\alpha x+\gamma z)} \left[1 - 2\beta\gamma \sum_{k\ell} \left(\sqrt{\epsilon_r-\alpha^2} + \frac{\beta(\epsilon_r-1)}{d(k,\ell)} \left(\frac{q^2\ell^2}{D_{k\ell}} - 1\right)\right] \frac{\pi^2}{L^2} W(ak-q\nu, q\ell)$$

Here W(ak-aν,al) is the surface spectral distribution function and represents the frequency components of the surface. The spectral distribution function is the Fourier transform of the mean square height times the correlation function. A complete description is in Appendix B. If r = ak and s = al and the period L approaches infinity, the summation may be replaced by an integral.

$$\langle E_y^R \rangle = \Gamma_h e^{-j\beta(\alpha x+\gamma z)} \left[1 - 2\beta\gamma \int_{-\infty}^{\infty}\int \left(\sqrt{\epsilon_r-\alpha^2} + \frac{\beta^2(\epsilon_r-1)}{d} \left(\frac{s^2}{D} - 1\right) \frac{W(r-\beta,\alpha,s)}{4} dr\, ds\right. \tag{2.3.3-6}$$

where

$$d = (\beta^2 - r^2 - s^2)^{1/2} + (\beta^2\epsilon_r - r^2 - s^2)^{1/2}$$

$$D = r^2 + s^2 + (\beta^2 - r^2 - s^2)^{1/2} (\beta^2\epsilon_r - r^2 - s^2)^{1/2}$$

The surface is defined to have small height variation and slowly varying slopes. With the additional restriction that the distances between the perturbations be large (no shadowing due to the perturbations), the surface distribution function W(p,q) will be composed of low frequency components. The result is that W(p,q) is appreciably different from zero only near p = q = 0. Thus, the approximate value of the coefficient of W(r-βα,s) is

its value evaluated at r = βα and s = 0.

$$\langle E_y^R \rangle = \Gamma_h e^{-j\beta(\alpha x + \gamma z)} \left[1 - 2\beta^2 \gamma^2 \iint_{-\infty}^{\infty} \frac{W(t-\beta\alpha, s)}{4} \, dt \, ds \right] \tag{2.3.3-7}$$

From the definition of the surface,

$$\langle f^2(x,y) \rangle = \sum_{m\,n} \langle P(m,n) \, P(-m,n) \rangle \tag{2.3.3-8}$$

Letting L approach infinity and replacing the summation by an integral, the mean square height of the surface is

$$\begin{aligned} \bar{\bar{z}}^2 = \langle f^2(x,y) \rangle &= \iint_{-\infty}^{\infty} \frac{\pi^2}{L^2} W(p,q) \, dm \, dn \\ &\qquad p = qm \quad q = qn \\ &= \iint_{-\infty}^{\infty} \frac{W(p,q)}{4} \, dp \, dq \end{aligned} \tag{2.3.3-9}$$

The average reflected field is then

$$\langle E_y^R \rangle = \Gamma_h \, e^{-j\beta(x \sin\theta_0 + \bar{z} \cos\theta_0)} \left[1 - 2\beta^2 \bar{\bar{z}}^2 \cos^2\theta_0 \right] \tag{2.3.3-10}$$

The effective rough surface specular reflection coefficient (Γ_h^R) at the surface is

$$\Gamma_h^R = \frac{E_y^R}{E_y^i} = \Gamma_h \left[1 - 2\beta^2 \bar{\bar{z}}^2 \cos^2\theta_0 \right] \tag{2.3.3-11}$$

where h designates horizontal polarization. Since small order series representations were used to derive the coefficients and since $\bar{\bar{z}}^2$ is small, the form of the roughness factor suggests

$$1 - 2\beta^2 \bar{z}^2 \cos^2\theta_o \approx e^{-2\beta^2 \bar{z}^2 \cos^2\theta_o} \tag{2.3.3-12}$$

Therefore, exp $(-2\beta^2 \bar{z}^2 \cos^2\theta_o)$ is probably a better approximation to the surface roughness factor.

$$\Gamma_h^R = \Gamma_h e^{-2\beta^2 \bar{z}^2 \cos^2\theta_o} \tag{2.3.3-13}$$

From Appendix A the specular coherent scattering cross section is

$$\sigma_o = \frac{\pi R^2}{A} |\Gamma_h|^2 e^{-4\beta^2 \bar{z}^2 \cos^2\theta_o} \tag{2.3.3-14}$$

where R is the range and A is the illuminated area

It can be shown that the same reflection coefficient modification also applies for a vertically polarized wave (Rice, 1951).

$$\Gamma_v^R = \Gamma_v e^{-2\beta^2 \bar{z}^2 \cos^2\theta} \tag{2.3.3-15}$$

Incoherent Scattering Cross Section

The incoherent scattering cross section terms are developed following the method of Peake (1959). For simplicity only the first order terms are used. The geometry is that of Figure 2.3.3-1. The specularly reflected term is dropped, therefore, the results give only the incoherent component of the scattered field. Only the horizontally polarized case is developed.

The direction corresponding to m,n is first represented in spherical coordinates by

$$\begin{aligned} q_m &= \beta \sin\theta_s \cos\phi_s \\ q_n &= \beta \sin\theta_s \sin\phi_s \end{aligned} \tag{2.3.3-16}$$

The scattered field (E^s) for horizontal polarization is, therefore,

$$E_h^s(m,n) = \left| A_{mn}^{(i)} \sin\phi_s \cos\theta_s + B_{mn}^{(i)} \cos\phi_s + C_{mn}^{(i)} \sin\phi_s \right| E(m,n,z) \tag{2.3.3-17}$$

To evaluate the differential radar scattering cross section, the average power over a small range of solid angle must be determined. In spherical coordinates the differential element of solid angle (Ω) is

$$d\Omega = \sin\theta_s \, d\theta_s \, d\phi_s \tag{2.3.3-18}$$

Evaluation of the Jacobian of the transformation to cartesian coordinates gives

$$d\theta_s \, d\phi_s = \frac{1}{\cos\theta_s \sin\theta_s} \left(\frac{a}{\beta}\right)^2 \left[\cos\phi_s \sin\phi_s (dn^2 - dm^2) + (\cos^2\phi_s - \sin^2\phi_s) \, dm \, dn\right] \tag{2.3.3-19}$$

The average power scattered over a unit solid angle is, therefore, the average power density times the effective area of the radiator. Since the surface has area L^2 and the scattering direction is θ_s, 0_s, the effective area is $L^2 \cos\theta_s$. The power density over a small range of scattered angle about the direction determined by m and n is approximated by its mean times the differential element. Therefore, the scattered power over an element of scattered angle is

$$P_s = \frac{\eta}{2} \left[|E_h^s(m,n)|^2 \, dm \, dn \right] L^2 \cos^2\theta_s \tag{2.3.3-20}$$

The incident field was defined to have unit intensity at the surface. Therefore, the incident power at the surface is

$$P_i = \frac{\eta}{2} |1|^2 L^2$$

From the definition of differential radar scattering cross section in equation 2.3-1,

$$\sigma_o = \frac{\frac{\eta}{2} |E_h^s(m,n)|^2 \, dm \, dn \, L^2 \cos\theta_s / d\Omega}{\frac{\eta}{2} |1|^2 L^2 / 4\pi} \tag{2.3.3-21}$$

$$= \frac{4\pi \cos\theta_s \left| A_{mn}^{(1)} \sin\phi_s \cos\phi_s + B_{mn}^{(1)} \cos\phi_s + C_{mn}^{(1)} \sin\phi_s \right|^2 dm\, dn}{d\Omega}$$

Restriction to the plane of incidence $\phi_s = 0$, n = 0 dictates

$$d\Omega = \left(\frac{a}{\beta}\right)^2 \frac{1}{\cos\theta_s} \, dm \, dn$$

$$\sigma_o = 4\pi \left(\frac{\beta}{a}\right)^2 \left| B_{m0}^{(1)} \right|^2 \cos^2\theta_s \tag{2.3.3-22}$$

Substitution of $\beta_{mo}^{(1)}$ from equation B41 of Appendix B gives

$$\sigma_o = \frac{4L^2\beta^2}{\pi} \cos^2\theta_o \cos^2\theta_s \, T_h \, |P(m-v, 0)|^2 \tag{2.3.3-24}$$

where

$$T_h = \left| \frac{\epsilon_r - 1}{(\cos\theta_o + \sqrt{\epsilon_r - \sin^2\theta_o})(\cos\theta_s + \sqrt{\epsilon_r - \sin^2\theta_s})} \right|^2$$

From equations B6 and B11 of Appendix B,

$$\sigma_o = 4\pi\beta^4 \cos^2\theta_o \cos^2\theta_s \, T_h \, W(am - av, 0)$$

$$= \frac{4}{\pi} \beta^4 \cos^2\theta_o \cos^2\theta_s \, T_h \iint_{-\infty}^{\infty} \bar{z}^2 \rho(\xi, \eta) \, e^{jq} \, d\xi \, d\eta \tag{2.3.3-25}$$

where

$$q = j\xi(am - av)$$

$$= j\xi(\sin\theta_s \cos\phi_s - \sin\theta_o)$$

Converting to cylindrical coordinates and assuming that the correlation function is radially symmetric,

$$\xi = r\cos\phi$$

$$\eta = r\sin\phi$$

$$\rho(\xi,\eta) = \rho\left(\sqrt{\xi^2+\eta^2}\right) = \rho(r) \tag{2.3.3-26}$$

$$\sigma_o = \frac{4}{\pi}\beta^4\cos^2\theta_o\cos^2\theta_s\,T_h\,\bar{z}^2\int_0^{2\pi}\int_0^{\infty}\rho(r)\,e^{j\beta(\sin\theta_s\cos\phi_s-\sin\theta_o)\cos\psi}\,r\,dr\,d\psi$$

Performing the integral as in Appendix C yields

$$\sigma_o = 4\beta^4\bar{z}^2V^2\cos^2\theta_o\cos^2\theta_s\,T_h\,e^{-\frac{V^2\beta^2}{4}(\sin\theta_s\cos\phi_s-\sin\theta_o)^2} \tag{2.3.3-27}$$

if a Gaussian correlation function

$$\rho(r) = e^{-r^2/V^2} \tag{2.3.3-28}$$

is assumed where V is the correlation distance. Equation 2.3.3-27 gives the incoherent differential scattering cross section for any combination of incident and scattered angles in the plane of incidence. Three different angular configurations are considered. First, for scattering at specular angles, $\theta = \theta_o = \theta_s$, $\phi = 0$ and

$$\sigma_{o\,spec} = 4\beta^4\cos^4\theta\,T_h\,\bar{z}^2V^2 \tag{2.3.3-29}$$

where

$$T_h = \left|\frac{\epsilon_r - 1}{(\cos\theta + \sqrt{\epsilon_r - \sin^2\theta})^2}\right|^2 = |\Gamma_h|^2 \tag{2.3.3-30}$$

For backscattering cross section, $\theta = \theta_o = \theta_s$, $\phi_s = \pi$ and

$$\sigma_{o\,back} = 4\beta^4\cos^4\theta\,T_h\,\bar{z}^2V^2\,e^{-V^2\beta^2\sin^2\theta} \tag{2.3.3-31}$$

where $T_h = |\Gamma_h|^2$

And for calculation of the scattering pattern for a given incidence angle, $\phi_s = 0$ and equation 2.3.3-27 is used.

For vertical polarization, the resulting expressions for scattering cross section are identical except for the T factor. Peake (1959) derived the value for vertical polarization

$$T_v = \left| \frac{(\epsilon_r - 1)\left[\epsilon_r \sin\theta_0 \sin\theta_s - \cos\phi_s \sqrt{\epsilon_r - \sin^2\theta_0}\ \sqrt{\epsilon_r - \sin^2\theta_s}\right]}{\left[\epsilon_r \cos\theta_0 + \sqrt{\epsilon_r - \sin^2\theta_0}\right]\left[\epsilon_r \cos\theta_s + \sqrt{\epsilon_r - \sin^2\theta_s}\right]} \right|^2 \quad (2.3.3\text{-}32)$$

2.4 The Reflection of Electromagnetic Waves from Inhomogeneous Media

Consider the reflection coefficient from a smooth layered media as shown in Figure 2.3.4-1.

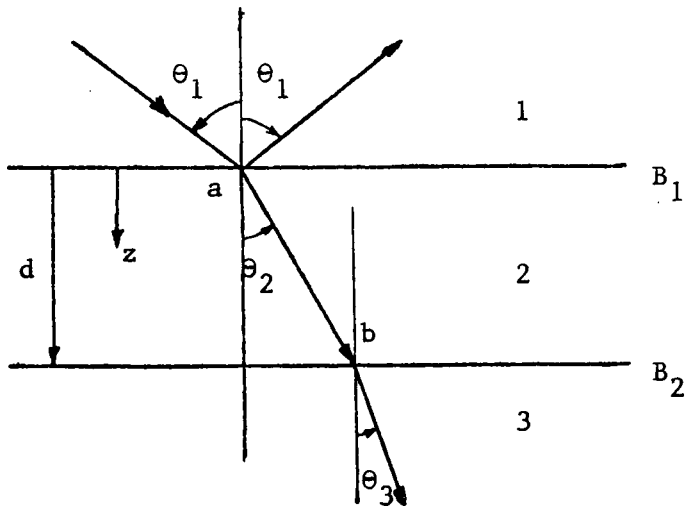

Figure 2.3.4-1 Layered media model

As indicated, medium 1 is the uppermost, medium 3 is the lowermost, with medium 2 the center layer. All parameters of medium 1 will be subscripted with a 1, parameters of medium 2 will be subscripted with a 2, etc.

The approach used to determine the total reflection coefficient at boundary one, B_1, will be the transmission line analogy. The characteristic wave impedance of medium 3 will be transferred through medium 2 to B_1, where the total reflection coefficient, R_{total}, will be calculated. The problem will be subdivided by considering separately horizontal (electric field perpendicular to the plane of incidence) and vertical (electric field in the plane of incidence) polarization. First horizontal polarization will be considered.

Horizontal Polarization

To make more efficient use of the transmission line analogy the characteristic wave impedances will be referred to the Z-direction. Therefore, the characteristic wave impedance of medium 3 referred to the z-direction is (Ramo, Whinnery, Van Duzer, 1967)

$$(Z_3)_H = \eta_3 \sec(\Theta_3), \tag{2.3.4-1}$$

where η is the intrinsic impedance of the medium. Using the transmission line formula this impedance is then transferred to B_1 giving the load impedance at that boundary as

$$(Z_L)_H = \eta_2 \sec(\Theta_2) \frac{\eta_3 \sec(\Theta_3)\cos(k_2 d \cos\Theta_2) + j\eta_2 \sec(\Theta_2)\sin(k_2 d \cos\Theta_2)}{\eta_2 \sec(\Theta_2)\cos(k_2 d \cos\Theta_2) + j\eta_3 \sec(\Theta_3)\sin(k_2 d \cos\Theta_2)} \tag{2.3.4-2}$$

where $\eta_2 \sec(\Theta_2)$ is the impedance of medium 2 referred to the Z-direction and k_2 is the wave number in medium 2. The total reflection coefficient is then calculated at B_1 as

$$R_{total} = \frac{Z_L - Z_1}{Z_L + Z_1} \tag{2.3.4-3}$$

with $(Z_1)_H = \eta_1 \sec(\Theta_1)$.

The angle Θ_1 is determined by the user, while the angles Θ_2 and Θ_3 are determined by the application of Snell's Law to the boundaries B_1 and B_2. The following equations result:

$$\begin{aligned} k_1 \sin(\Theta_1) &= k_2 \sin(\Theta_2) \\ k_2 \sin(\Theta_2) &= k_3 \sin(\Theta_3). \end{aligned} \tag{2.3.4-4}$$

The k's are determined by the properties of the media and the frequency of the illumination thus allowing the solution for Θ_2 and Θ_3.

Vertical Polarization

The solution for vertical polarization is exactly the same as for horizontal polarization, except

$$(Z_3)_V = \eta_3 \cos(\Theta_3), \tag{2.3.4-5}$$

$$(Z_L)_V = {}_2\cos(\eta_2)\ \frac{\eta_3\cos(\Theta_3)\cos\ (k_2 d\ \cos\ \Theta_2)\ + j\eta_2\cos(\Theta_2)\sin(k_2 d\ \cos\ \Theta_2)}{\eta_2\cos(\Theta_2)\cos\ (k_2 d\ \cos\ \Theta_2)\ + j\eta_3\cos(\Theta_3)\sin(k_2 d\ \cos\ \Theta_2)} \tag{2.3.4-6}$$

and

$$(Z_1)_V = \eta_1 \cos(\Theta_1). \tag{2.3.4-7}$$

3. EXPERIMENTAL INSTRUMENTATION

The system used for obtaining data was a bistatic broad spectrum reflectometer-scatterometer. Power measurements were taken for both horizontal and vertical polarizations with incident and receiving angles from 10° to 60° and frequencies from 4.0 to 26.5 GHz. The power return data were converted first to either reflectivity or scattering cross section, and then to dielectric constant or percent moisture. The operation, components, measurement procedure, and data reduction methods are discussed in the following sections.

3.1 System Operation

A reflectometer or scatterometer is a device for measuring the power returned from a target surface. The distinction between a reflectometer and a scatterometer is a matter of terminology as both use the same instrumentation. A reflectometer measures specularly "reflected" power while the scatterometer measures non-specularly "scattered" power.

A block diagram of a reflectometer-scatterometer is shown in Figure 3.1-1. The sweep oscillator supplies electromagnetic power to the transmitting aperture and this power is radiated toward the target. The power reflected or scattered from the target in the direction of the receiving aperture is then direct detected with a crystal detector. A directional coupler is inserted in the transmitting path to provide a reference to the transmitter power. The coupler also provides power leveling feedback to the sweep oscillator. The detectors are operated in the square law region, that is, where the DC output voltage is proportional to the input rf power.

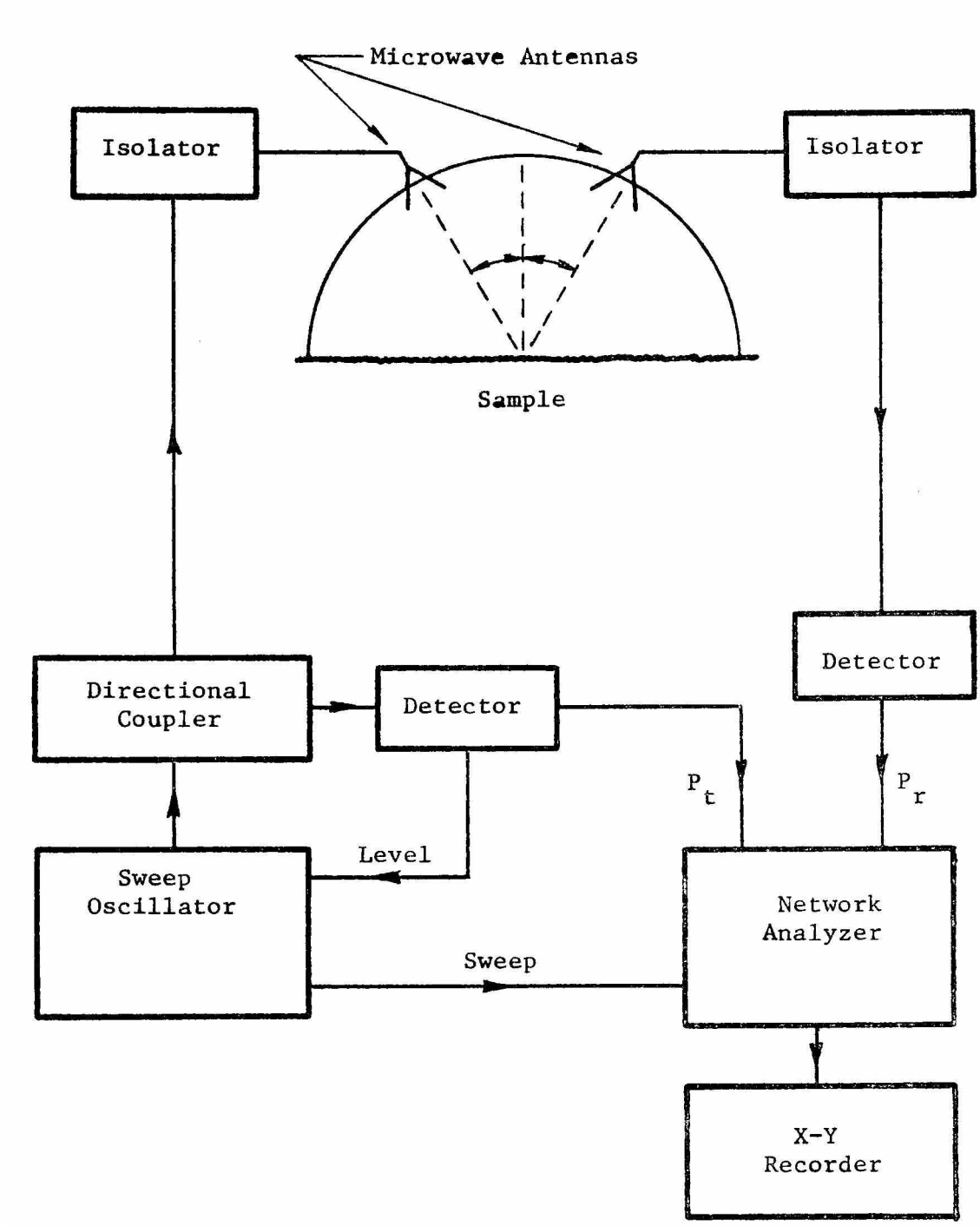

Figure 3.1-1 Block Diagram of the Dual Aperture Reflectometer-Scatterometer

In the network analyzer the voltages proportional to the transmitted and received powers are ratioed and expressed in db. This ratio is then output to an X-Y recorder.

This specific system was operated CW with frequency swept across a 4.75-26.5 GHz range. This broad spectrum capability enabled a study of the frequency dependence of the target characteristics.

3.2 Component Description

With the exception of the support apparatus, the equipment used in this experiment was commercially available. The sweep oscillator was an Alfred Model 650. With four BWO plug in units, the oscillator could be swept in frequency from 4.0 - 8.0, 8.0 - 12.4, 12.4 - 18.0, and 18.0 - 26.5 GHz. The network analyzer used was an Alfred Model 7051 mounted in an Alfred Model 8000 oscilloscope main frame. The logarithmic amplifiers of the network analyzer allowed absolute or relative power level measurements over a theoretical 60 db dynamic range. However, this range was limited by the performance of the crystal detectors. The directional couplers used were Hewlett-Packard or Alfred units with 10 db coupling. The transmitting and receiving apertures were identical and were standard gain waveguide horns. The manufacturers were Scientific Atlanta and Microlab/FXR. Isolators were inserted to reduce antenna to waveguide impedence mismatch. These were manufactured by PRD and E and M Laboratories. The X-Y recorder was a Hewlett-Packard Model 7005. Two different arches were constructed with a six-foot radius for the 4.0 - 8.0 GHz frequency range. These arches were constructed to allow angular change in antenna position with a constant range. The antenna mounts were constructed to allow easy

change of polarization. The system in various configurations, both laboratory and field, is shown in Figure 3.2-1.

3.3 System Calibration

Each target had returned power measured for incident and receiving angles from 10° - 60°, both polarizations, and several frequency bands. For each configuration of the system, the frequency of the sweep oscillator was swept and the ratioed power recorded on an X-Y recorder. The recorded value was the ratio of the input and output powers of the system as measured at the network analyzer. This ratio contains many system parameters including line loss in the rf cable, loss in the isolators, antenna gain, and spreading loss due to the beamwidths of the antennas.

If the surface is smooth, the transmitting and receiving antennas have the same characteristics and are at the same range from the target surface, then simple image theory predicts the return ratio to be

$$\frac{P_r}{P_t} = \frac{G^2\lambda^2}{(8\pi R)^2} \left| R_{v,h} \right|^2 \qquad (3.3\text{-}1)$$

where

P_r = received power
P_t = transmitted power
G = antenna gain
R = range
λ = wavelength
$R_{v,h}$ = appropriate Fresnel reflection coefficient for vertical or horizontal polarization.

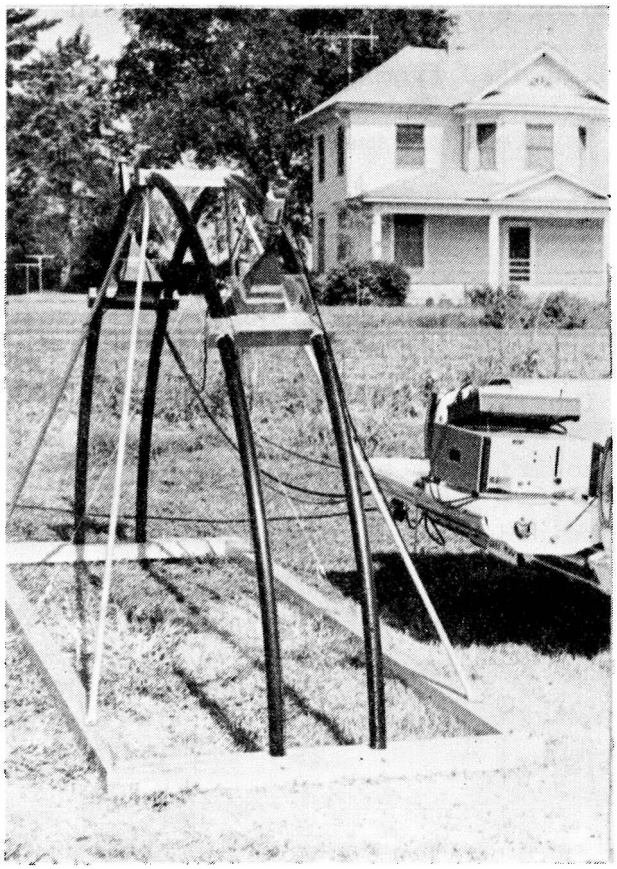

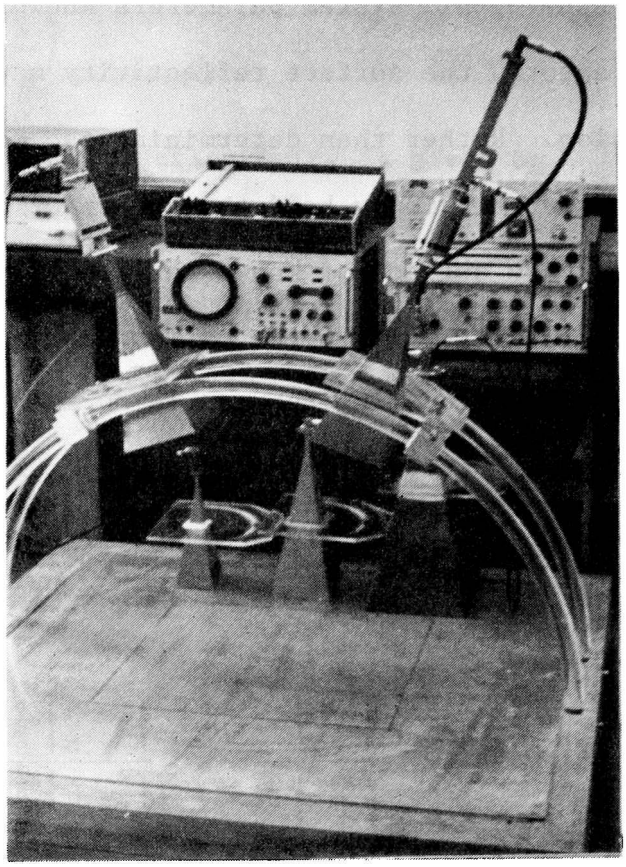

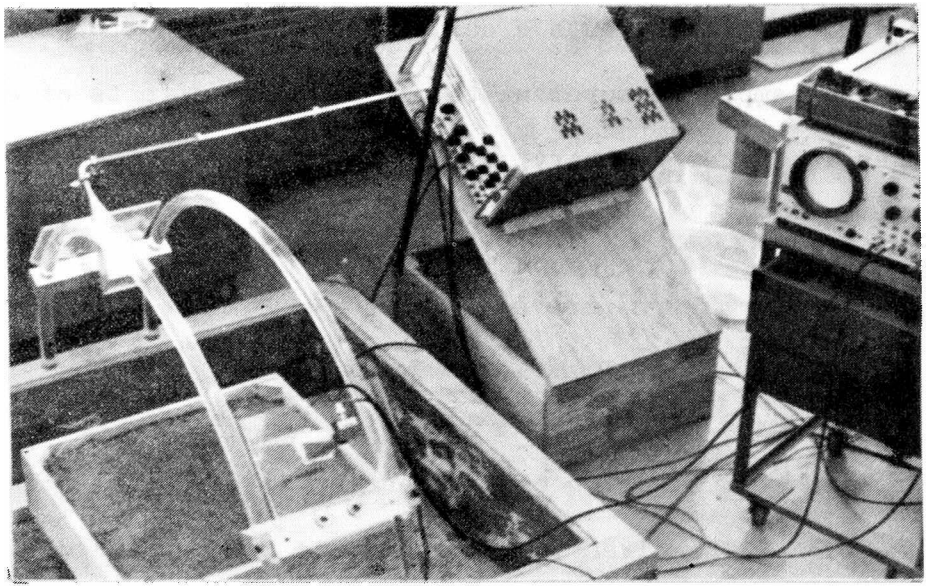

Figure 3.2-1 System Configuration

Assuming all system parameters known, including any multiplicative pattern factors, the surface reflectivity may be calculated from the above expression. Rather than determining the absolute systems parameters, it is far easier to simply hold them constant and repeat the measurement for a calibration surface of known reflectivity.

In actual use the calibration measurement is made on a thin sheet of aluminum covering the sample surface and which is assumed to have perfect conductivity and hence, a power reflection coefficient of one. The reflectivity of the sample surface may then be obtained by performing another ratio

$$\frac{\left(\frac{P_r}{P_t}\right)_s}{\left(\frac{P_r}{P_t}\right)_c} = \frac{\left|R_{v,h}\right|_s^2}{\left|R_{v,h}\right|_c^2} = \left|R_{v,h}\right|^2 \qquad (3.3\text{-}2)$$

where the subscripts s and c refer to sample and calibration measurements respectively. In all measurements a calibration run is performed immediately prior to the sample measurement to minimize any effects of equipment drift or changes in system geometry or surface characteristics.

3.4 Data Reduction

The recorded curves of (P_r/P_t) measured at the network analyzer must be converted to either reflection coefficient or differential radar scattering cross section. The directional coupler in the reference channel inserts 10 db loss. If coax and isolator losses are neglected, 0.1 (P_r/P_t) measured may be substituted for P_r/P_t in the radar equation. Therefore,

$$\sigma_o = \frac{(4\pi)^3 R^4}{10 G^2 \lambda^2 A} \left(\frac{P_r}{P_t}\right)_{measured} \tag{3.4-1}$$

The relationship of scattering cross-section to reflectivity is given by

$$\sigma_o = \frac{\pi R^2}{A} |\Gamma_{eff}|^2 \tag{3.4-2}$$

For calculation of reflection coefficient using the calibration against the aluminum plate,

$$|\Gamma_{eff}|^2 = \frac{|\Gamma_{eff}|^2}{|\Gamma_{plate}|^2} = \frac{\sigma_o}{\sigma_{o\,plate}} = \frac{\left(\frac{P_r}{P_t}\right)_{sample}}{\left(\frac{P_r}{P_t}\right)_{plate}} \tag{3.4-3}$$

Since the (P_r/P_t) measurements are in decibels,

$$|\Gamma_{eff}|^2_{db} = \left(\frac{P_r}{P_t}\right)_{sample\ db} - \left(\frac{P_r}{P_t}\right)_{plate\ db}$$

The above equation is exact since the reflection coefficient is known for the plate and all system parameters are eliminated. If a calibration curve was not taken, scattering cross-section could be calibrated from Equation 3.4-1.

A reproduction of an actual data plot is shown in Figure 3.4-1. These curves were taken using a network analyzer with a variable offset. Thus, the curves are not in absolute relation to each other, but must be modified by the offset numbers in db which are shown as codes PH, PV, SH, and SV. In these codes P means plate, S means sample surface, H means horizontal polarization, and V means vertical polarization. The four curves shown represent the P_r/P_t of the sample and the aluminum plate perfect conductor at both polarizations.

Incorporating the offsets into Equation 3.4-4 results in,

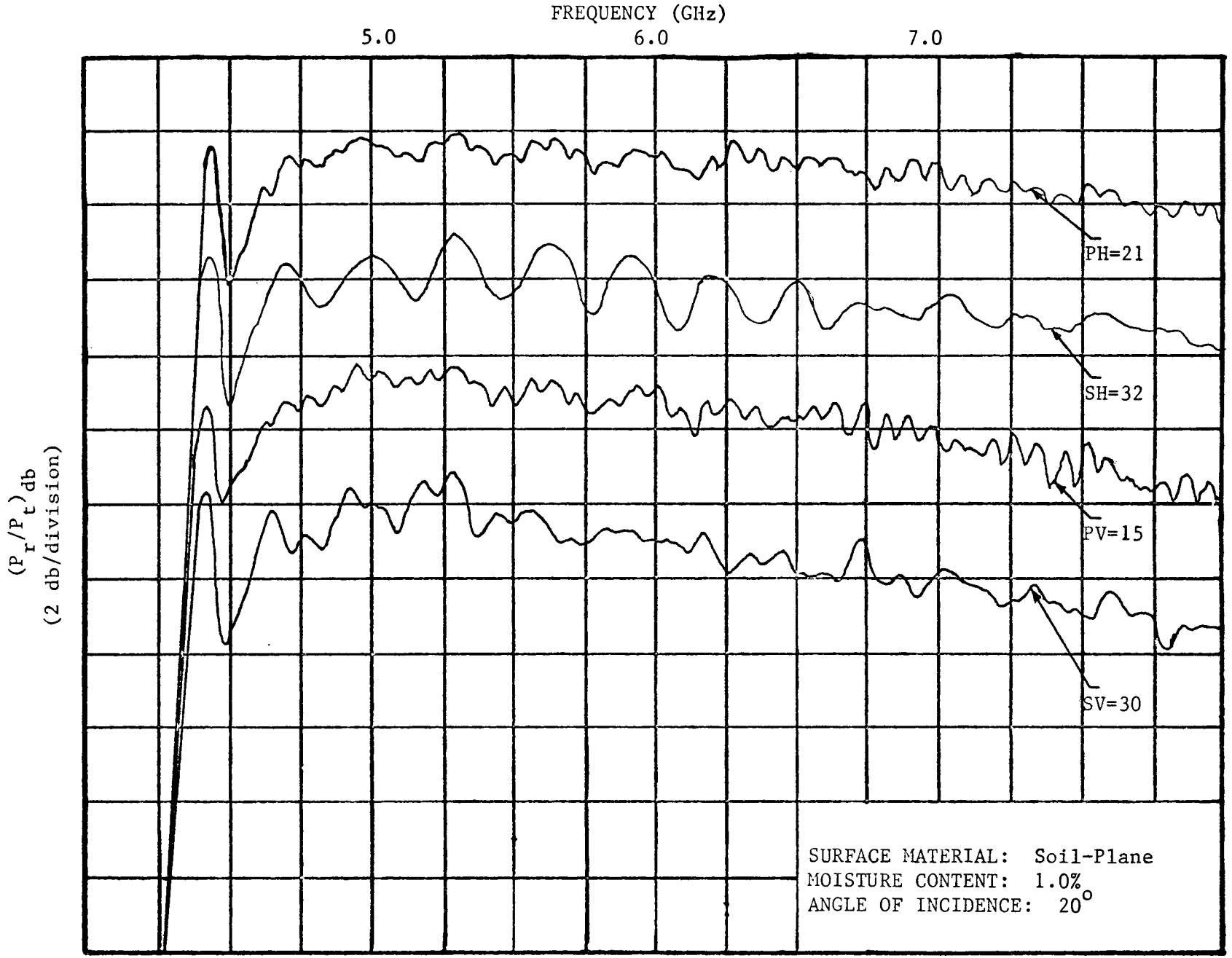

Figure 3.4-1 Example of Raw Data for the Plane Earth Problem

$$|\Gamma_{eff}|^2 = \left(\frac{P_r}{P_t}\right)_{sample\ db} - \left(\frac{P_r}{P_t}\right)_{plate\ db} - (SH - PH) \qquad (3.4\text{-}5)$$

As an example from Figure 3.4-1 at 6.0 GHz and for horizontal polarization,

$$|\Gamma_{eff}|^2_{db} = -3.4 - 32.0 + 21.0 = 14.4\ db$$

which leads to an effective reflectivity of,

$$|\Gamma_{eff}| = 0.191$$

3.5 System Limitations

As stated earlier in Section 3.2, the system had a dynamic range of approximately 60 db. This covered power levels from -40dbm to + 20dbm. With this limitation the low frequency band was only able to effectively measure surfaces with a mean-square height of 4.0 mm or less. As would be expected, this effect was even more pronounced in the higher frequency bands. This resulted in a rather severe limitation when attempts were made to investigate the effects of surface roughness and low level vegetation cover.

Within the system itself analysis of equipment sensitivity lead to an error tolerance of $\pm$ 0.6 db. About 0.2 db of this tolerance was attributed to data reduction technique with the remaining 0.4 db attributed to equipment accuracy. These bounds are graphically displayed in Figure 3.5-1. For example, for a true moisture content of 9.0% (by weight) the system may

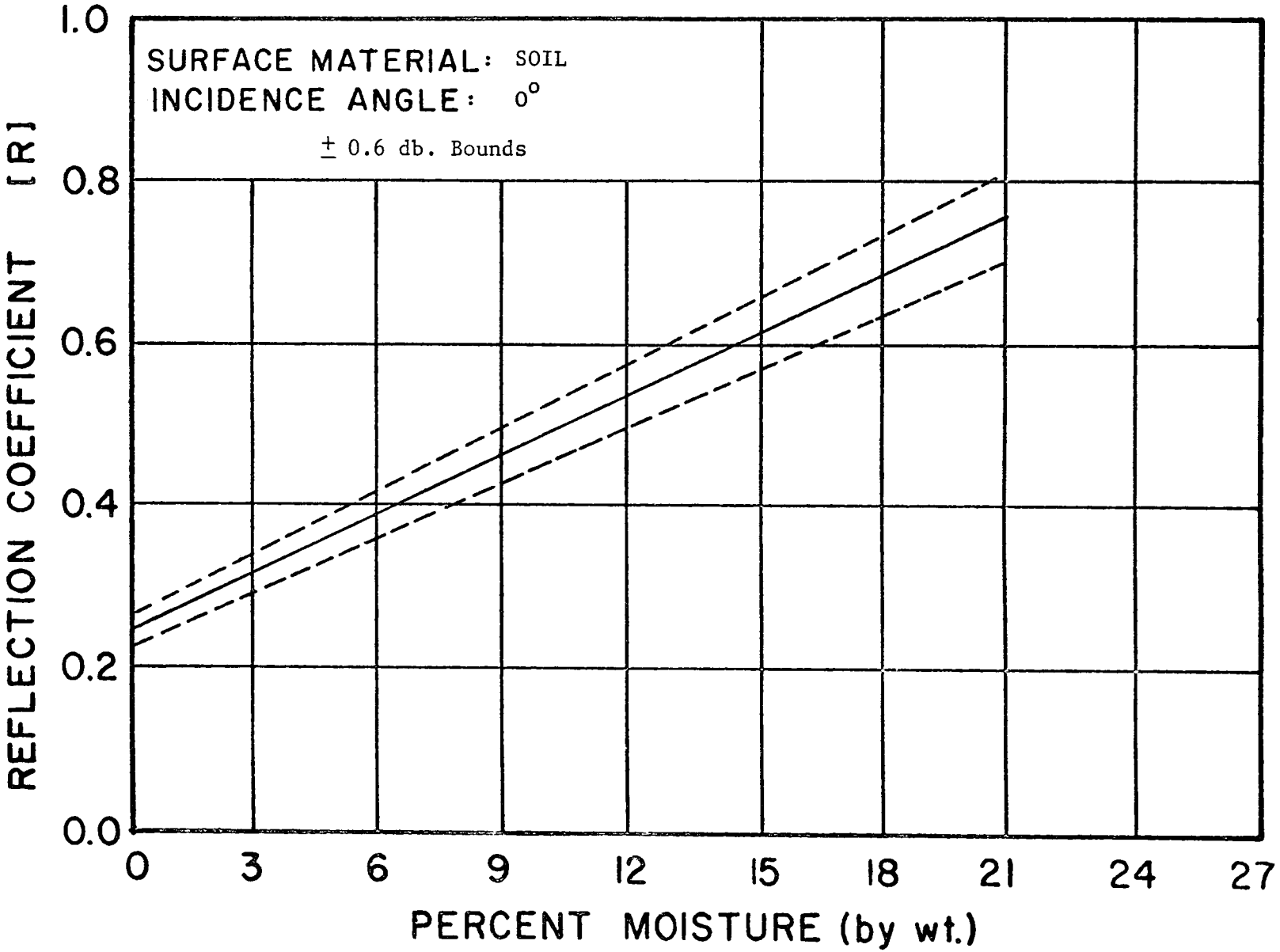

Figure 3.5-1 Overall System Error Bounds

predict between 7.5% and 0.5% moisture.

Despite the limitations noted this system measures soil-moisture content comparably or superior to existing methods without the necessity of direct contact with target measured.

4. EXPERIMENTAL DATA

4.1 Introduction

Using the system design described previously, a multiplicity of target types and structures were investigated. These included laboratory measurements of smooth surfaces with varying moisture conente, discontinuous rough surfaces with varying moisture content, layered media and surfaces with low vegetation cover. Field measurements were conducted on natural terrain surfaces both with and without vegetation cover.

The original research proposal describing this program called for the measurements to be conducted across a frequency range of 4-12.4 GHz. Subsequent to the approval of this grant an associated research program was funded by the National Science Foundation (Grant NSF GK 31515) to investigate microwave terrain signatures in a higher frequency range (12.4 - 26.5 GHz). With the additional equipment available from these programs many of the measurements were extended to cover the combined frequency range of 4-26.5 GHz. These additional data points were particularly valuable in the effort to use frequency diversity to correct for roughness effects which is discussed in detail in Section 5.

4.2 Laboratory Measurements

4.2.1 Smooth Surfaces

The targets used were made from various types of sand, soil, and water mixtures. Different moisture contents were prepared by controlling the amount of water added to the dry soil. A homogeneous sample was obtained

by mixing the combination in a concrete mixer. The surface of the sample was then made as smooth as possible. In some cases a smooth surface was not attainable due to cohesion of the soil particles.

Measurements were made of the specular power reflection at a variety of incidence angles and moisture contents. For each angular configuration and moisture content, the ratio of received to transmitted power was recorded as frequency was swept across a band. This procedure was then repeated for all four frequency bands for both the target and the aluminum calibration plate for both polarizations. An example of the data for horizontal and vertical polarizations for a smooth surface and the aluminum calibration plate is shown in Figure 4.2.1-1. The offsets must be added to the distances between the curves to obtain the power reflection coefficient. These reflection coefficients were then plotted as Fresnel curves for a variety of discrete frequencies and sample moisture contents as illustrated in Figures 4.2.1-2 through 4.2.1-7. These figures represent only a small sample of over 300 Fresnel plots generated during the course of this program. To conserve space these data are presented in tabular form as Appendix D.

By extrapolation back to 0^{o}, which is approximated by the average of horizontal and vertical polarization reflectivities for both 10^{o} and 20^{o}, a plot of reflectivity versus percent moisture may be obtained as shown in Figure 4.2.1-8. Reflectivities at several frequencies are shown in this figure. From the zero incidence reflectivity values the apparent dielectric constant (ignoring losses) may also be calculated. Figures 4.2.1-9 through 4.2.1-12 show samples of the variation of dielectric constant with percent moisture content for smooth soil at a variety of frequencies. As was predicted from the large disparity in the dielectric constant of the constituent materials,

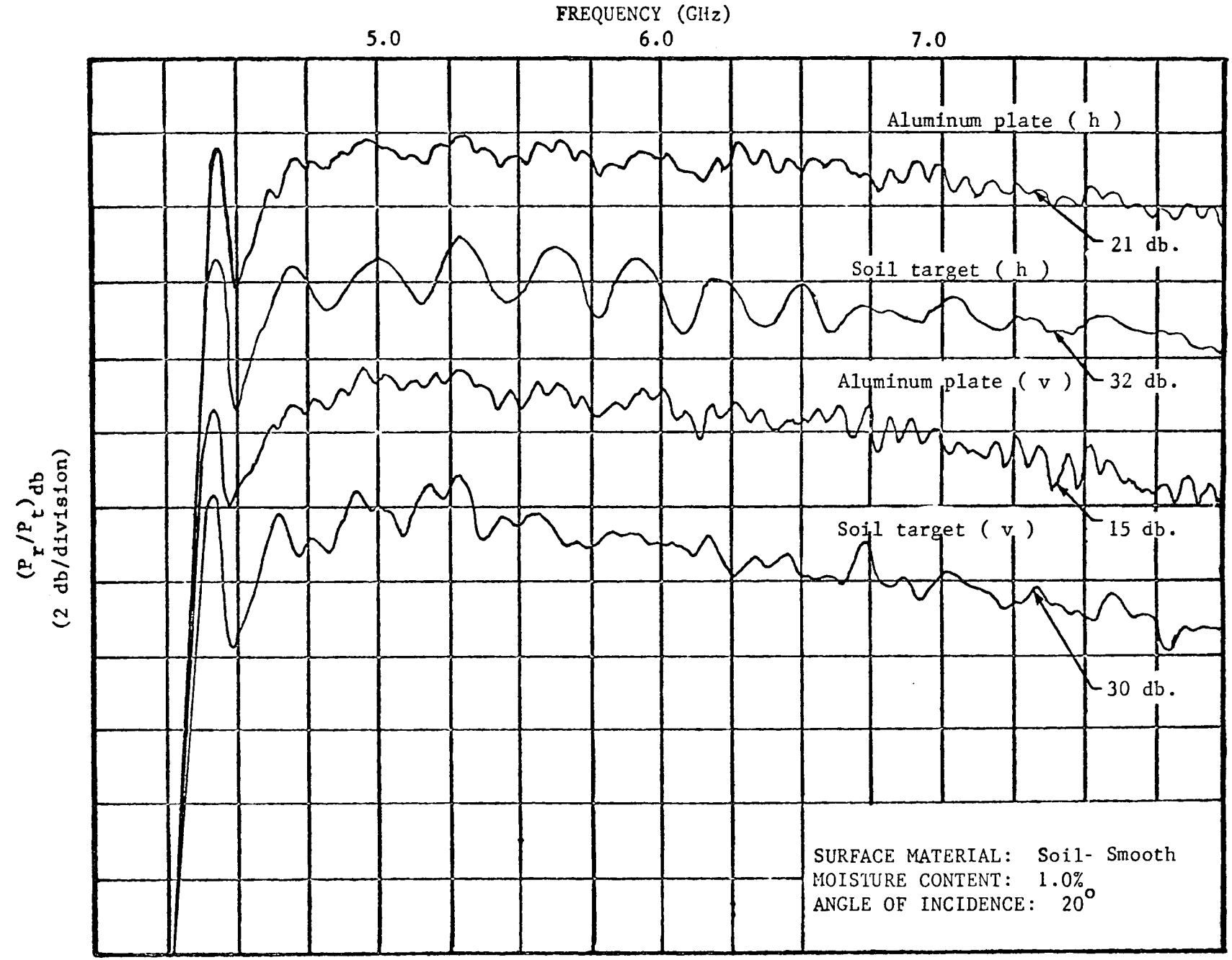

Figure 4.2.1-1 Example of data for determination of smooth surface reflectivity

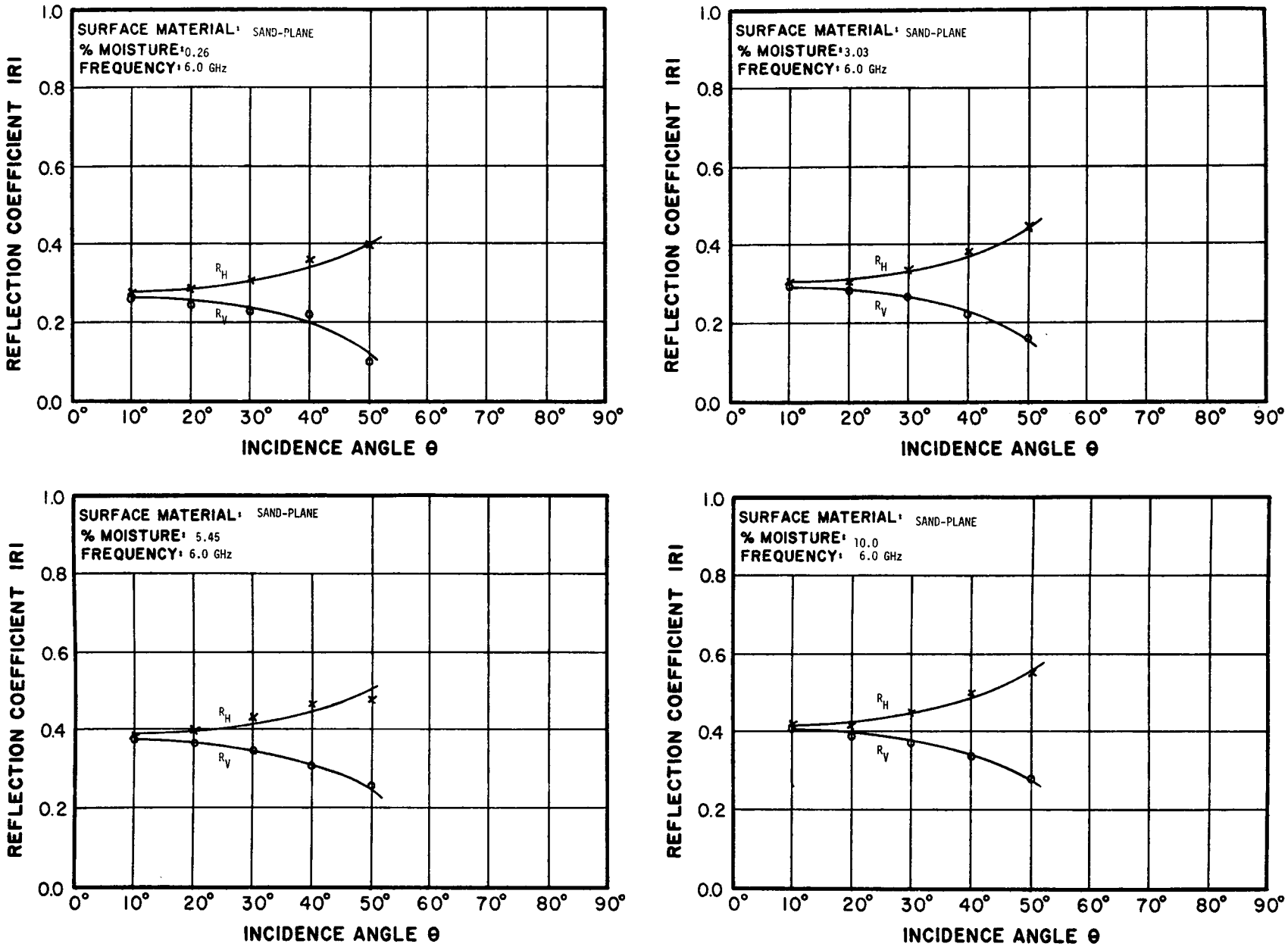

Figure 4.2.1-2 Reflectivity of smooth sand with various moisture contents - 6 GHz

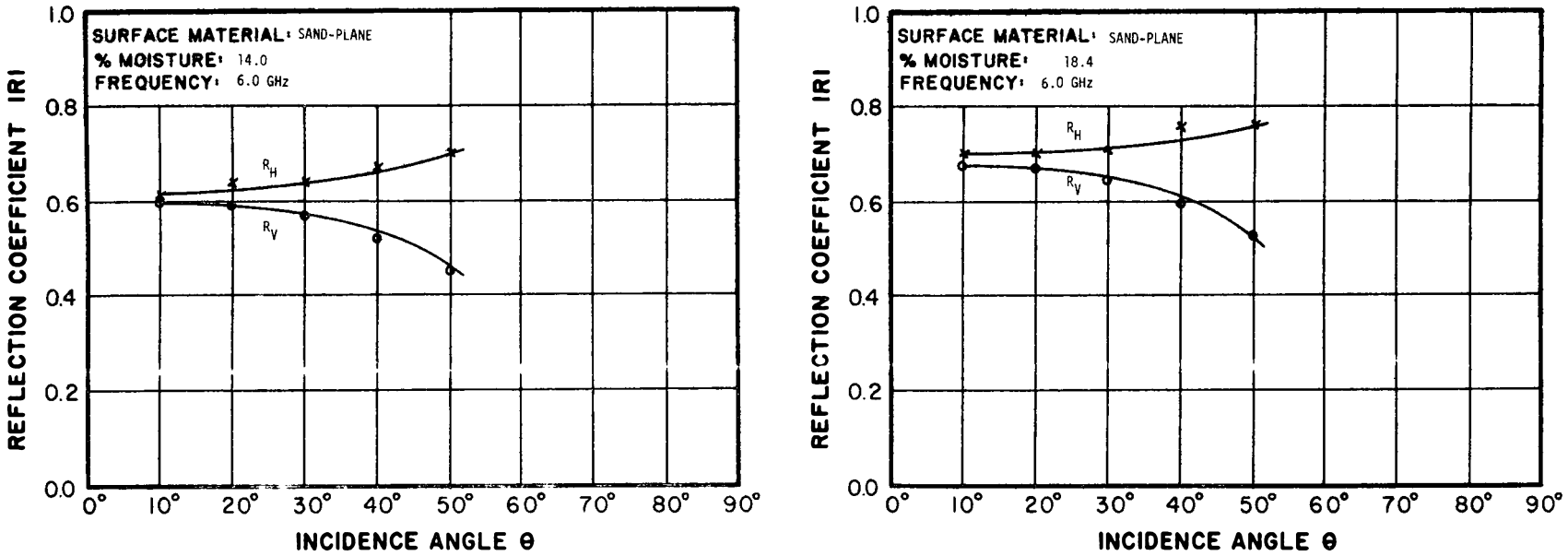

Figure 4.2.1-3 Reflectivity of smooth sand with various moisture contents - 6 GHz

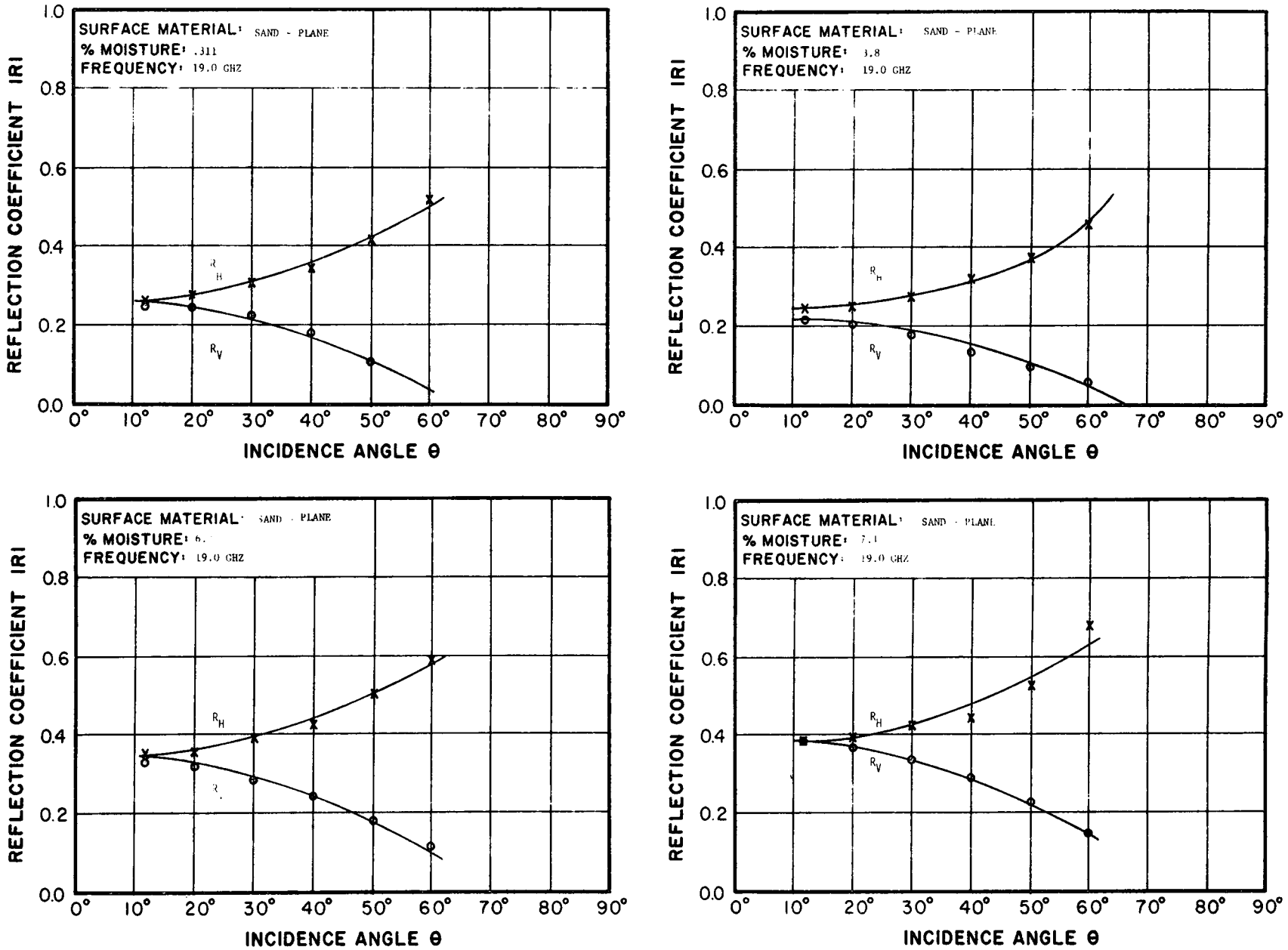

Figure 4.2.1-4 Reflectivity of smooth sand with various moisture contents - 19 GHz

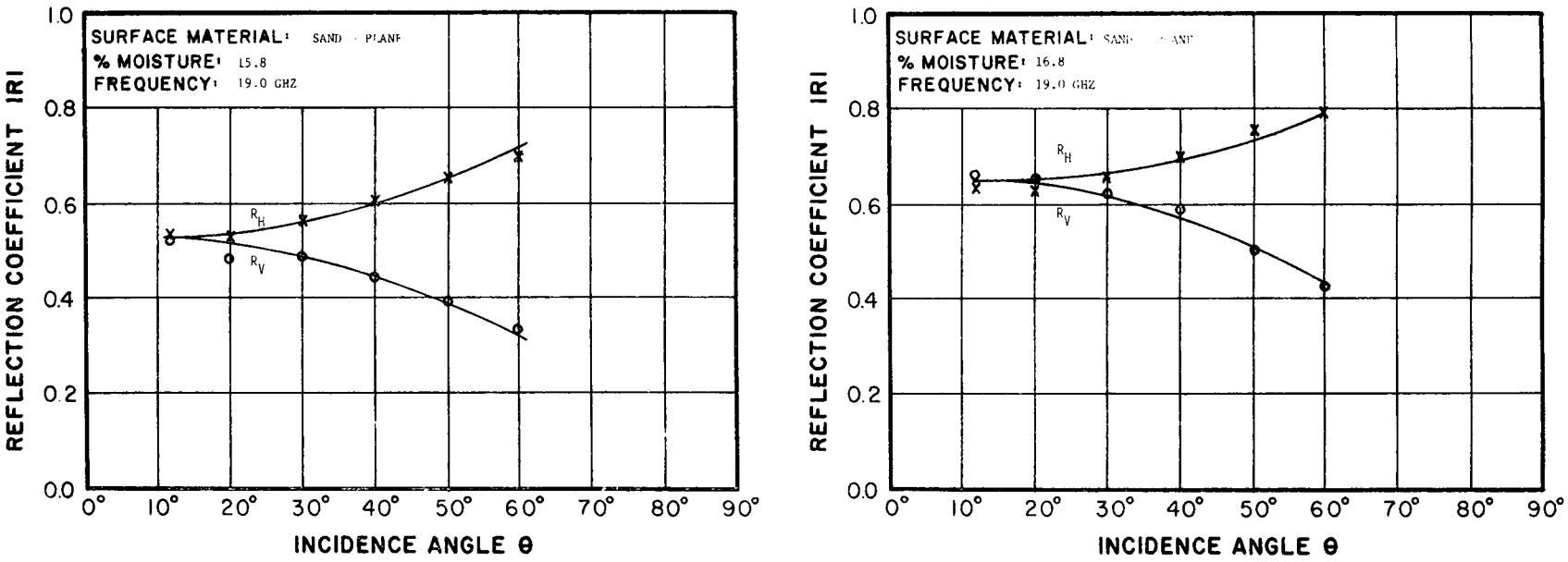

Figure 4.2.1-5 Reflectivity of smooth sand with various moisture contents - 19 GHz

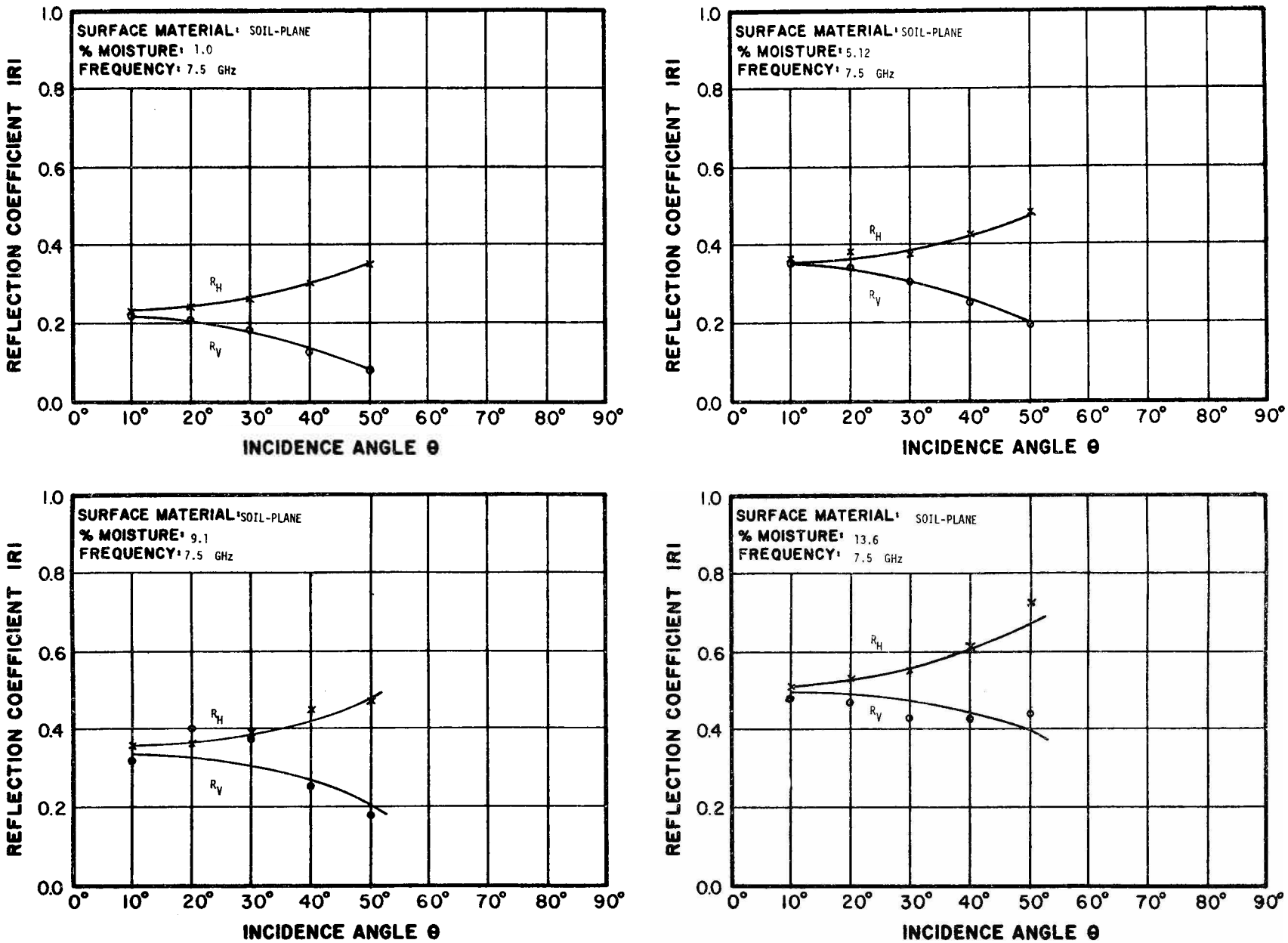

Figure 4.2.1-6 Reflectivity of smooth soil with various moisture contents - 7.5 GHz

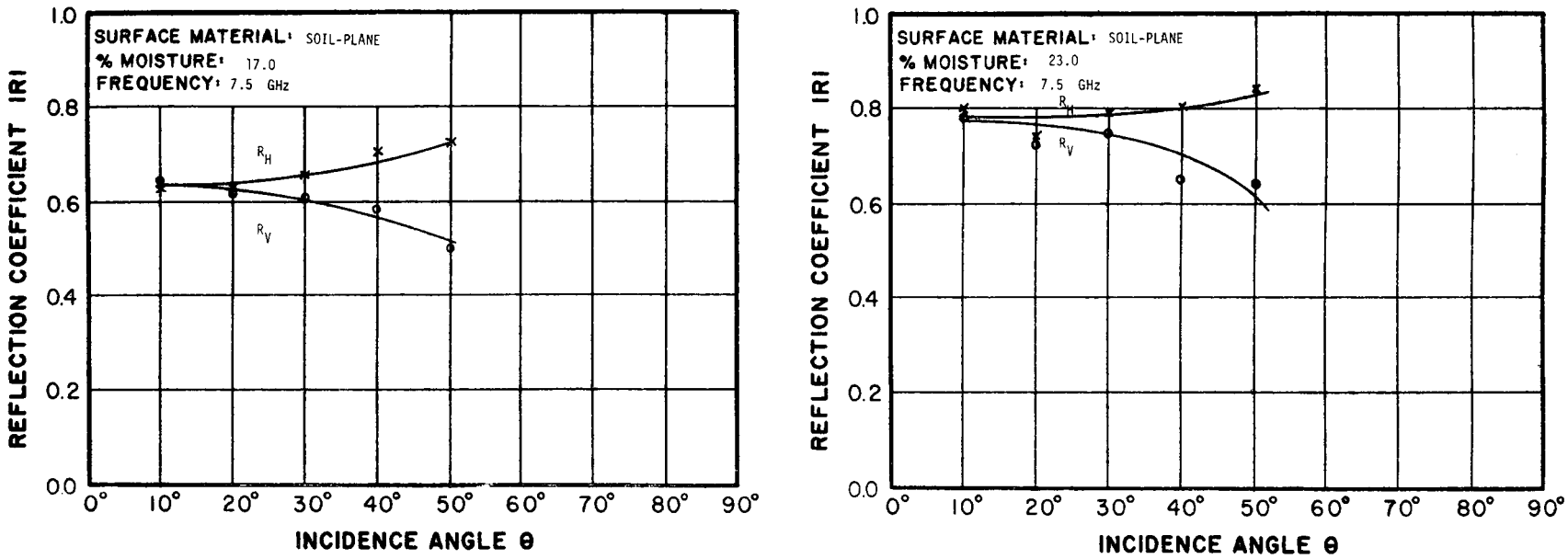

Figure 4.2.1-7 Reflectivity of smooth soil with various moisture contents - 7.5 GHz

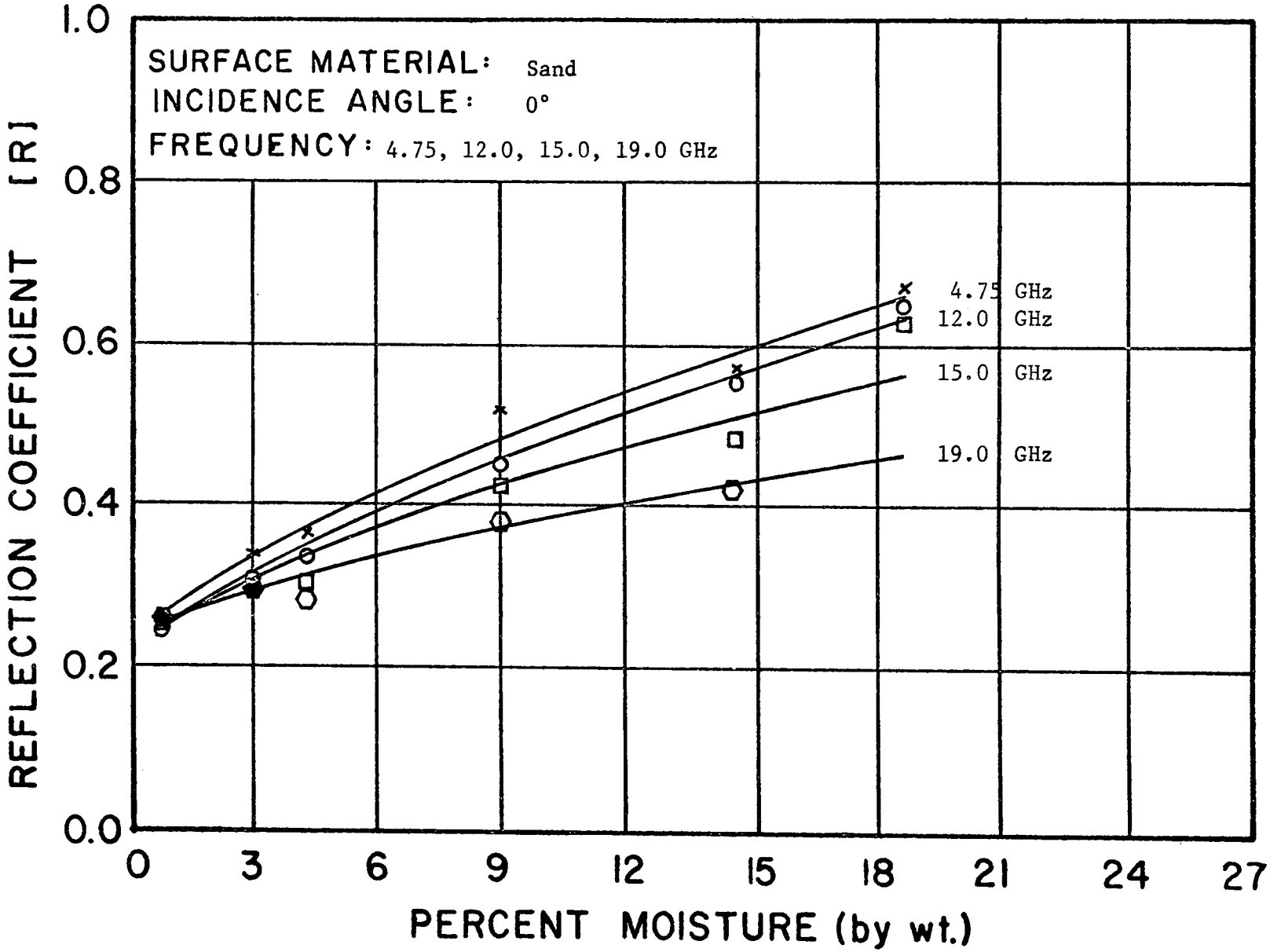

Figure 4.2.1-8 Reflectivity of sand versus percent moisture

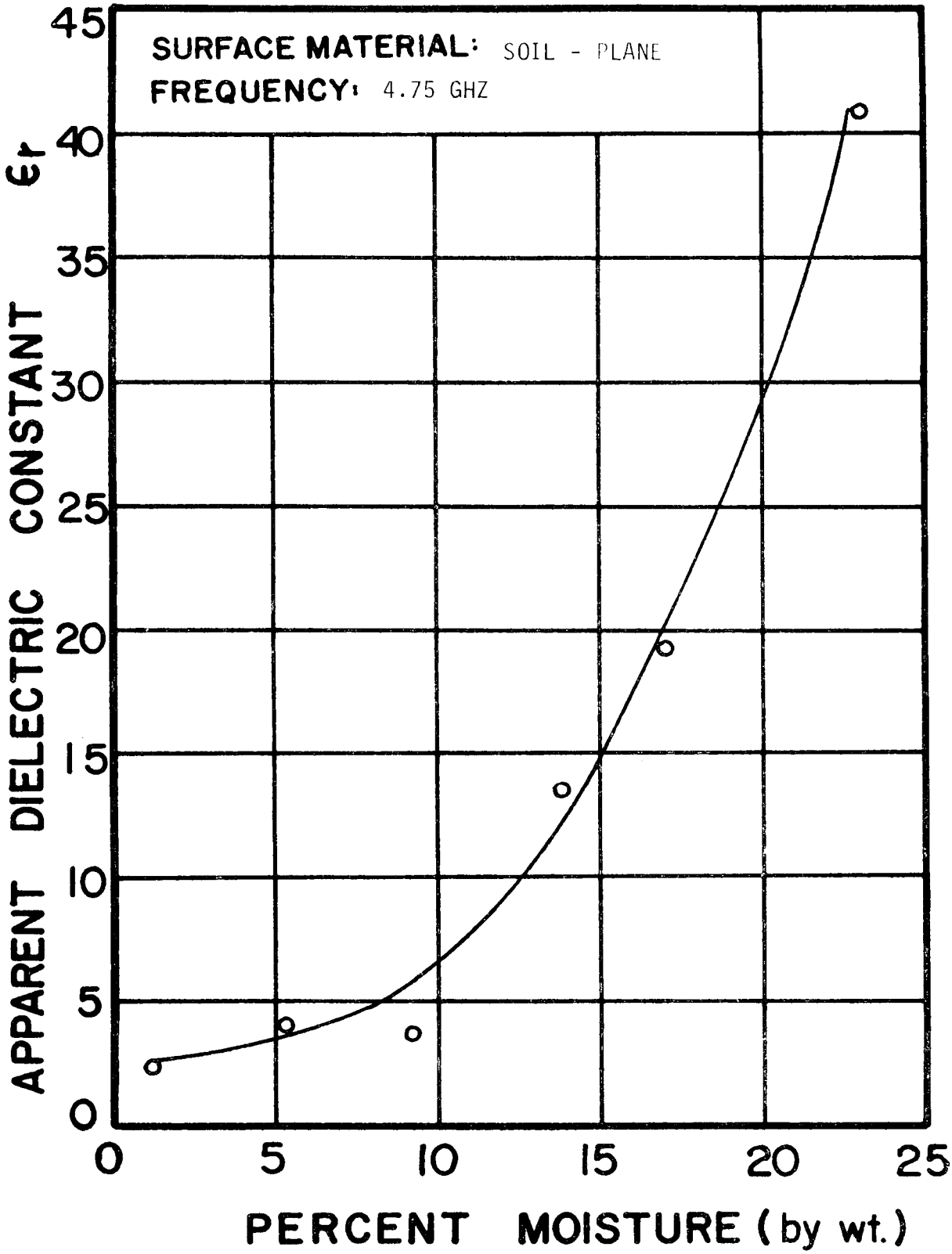

Figure 4.2.1-9 Apparent dielectric constant of smooth soil versus percent moisture content - 4.75 GHz

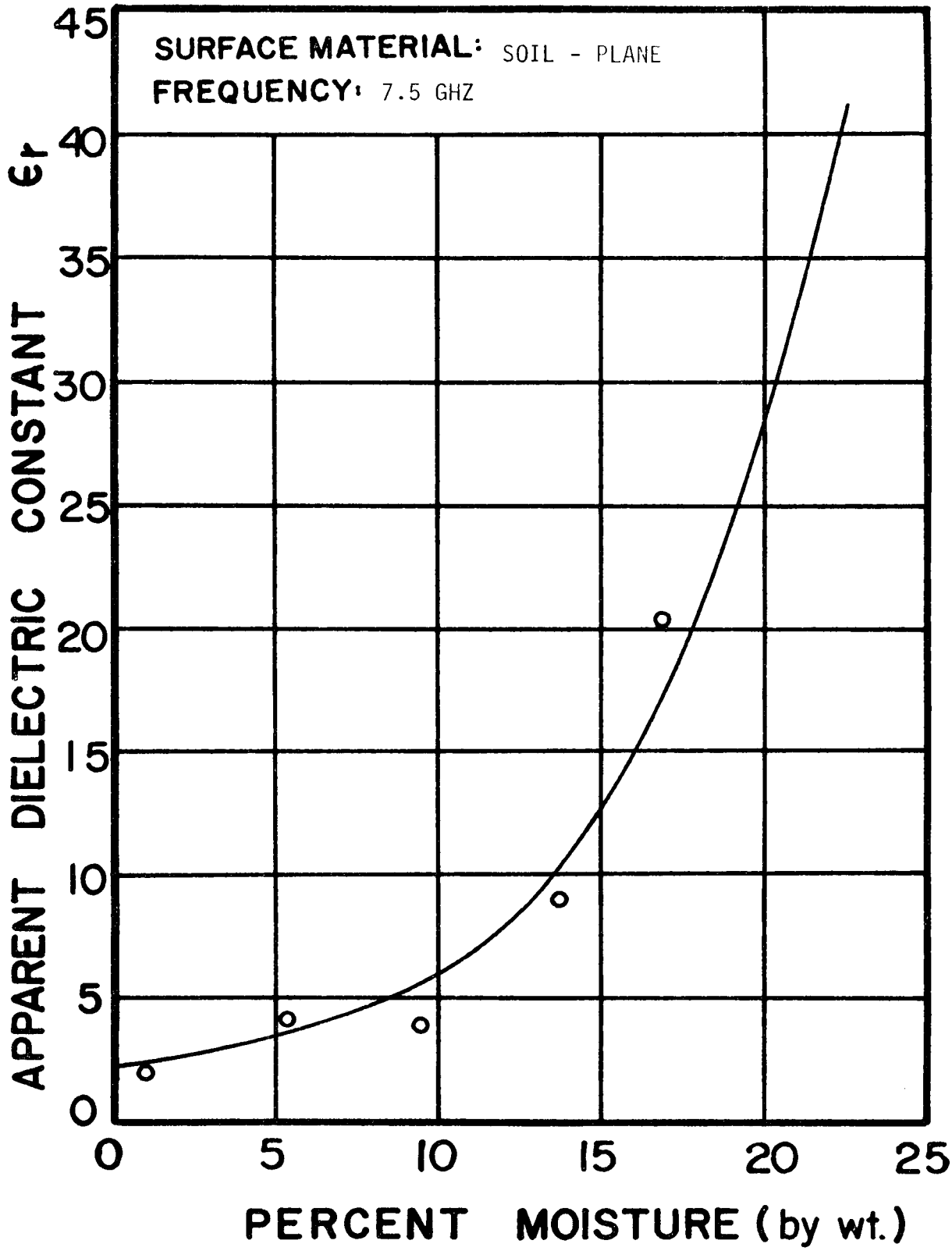

Figure 4.2.1-10 Apparent dielectric constant of smooth soil versus percent moisture content - 7.5 GHz

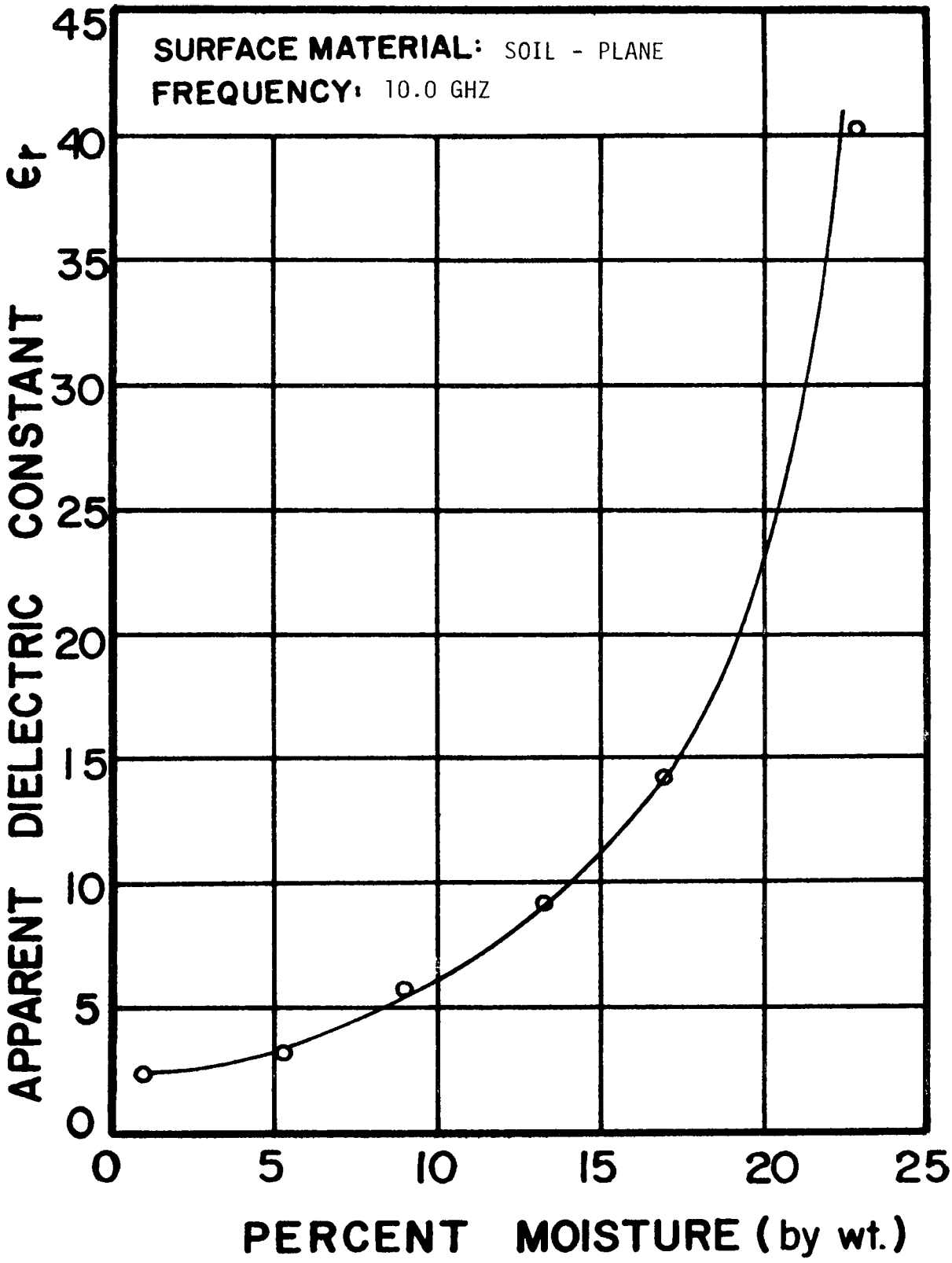

Figure 4.2.1-11 Apparent dielectric constant of smooth soil versus percent moisture content - 10 GHz

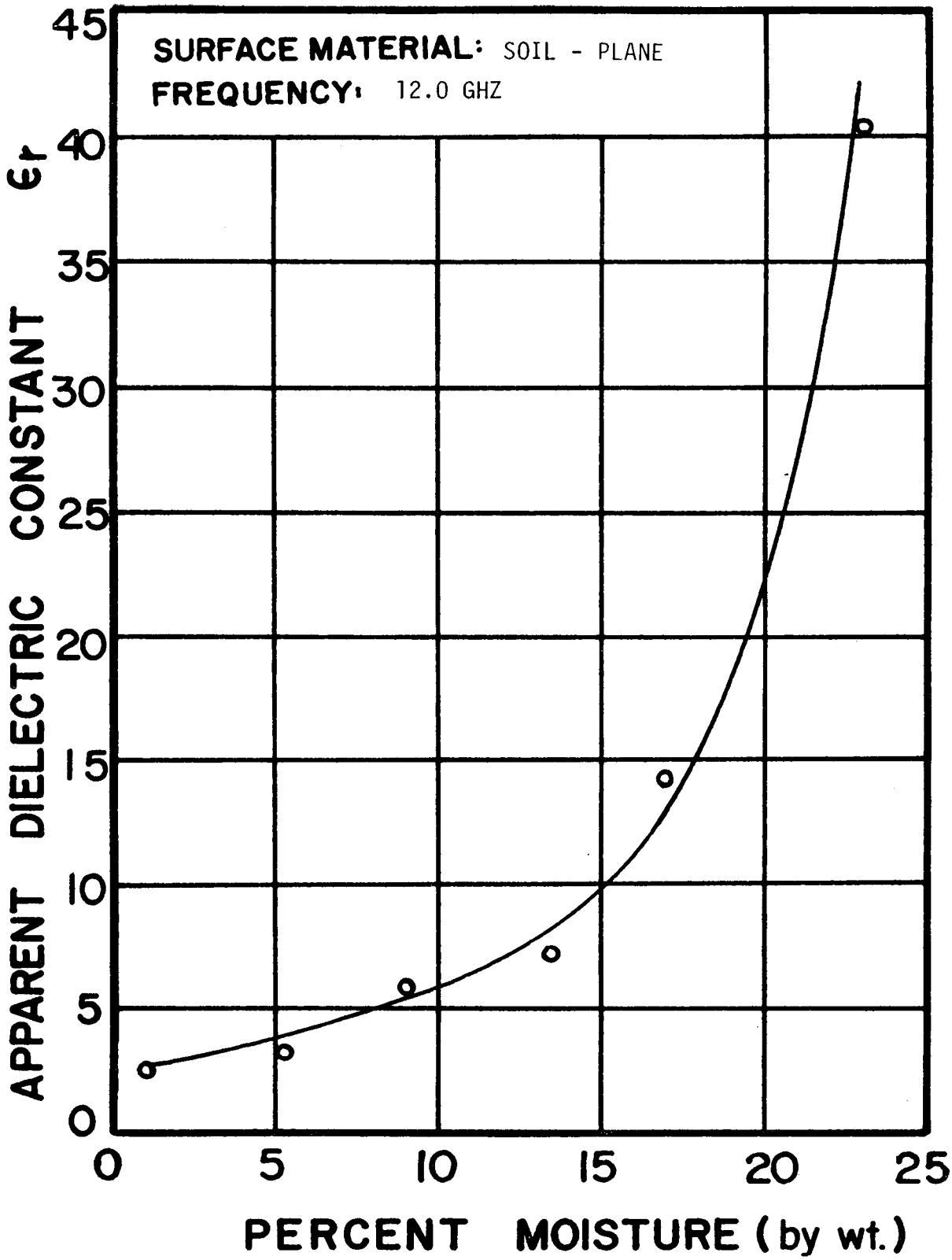

Figure 4.2.1-12 Apparent dielectric constant of smooth soil versus percent moisture content - 12 GHz

the dielectric constant of the mixture is dominantly influenced by the percent moisture content.

Data were taken with the surface made as smooth as possible for sand (Figure 4.2.1-13) and soil (Figure 4.2.1-14) for various moisture contents. When the moisture content of the sand or soil target was either very dry or saturated with water, the cohesion between the particles was small and the surface appeared smooth. For these moisture contents, the frequency dependence of the reflection coefficient matched the theoretical frequency dependence of Figure 2.2-8. However, for moisture contents between the two extremes, the cohesion of the particles made smoothing difficult. As a result the curves exhibited a greatly increased frequency dependence indicating the surface actually appeared rough to the measurement system. These curves were originally to be the basis for the correlation of surface reflectivity and moisture content for each soil type investigated. Since the surface appeared rough for some moisture contents, the effects of roughness had to be eliminated before the data set could be used in the prediction of moisture content. This correction is performed in section 5.3.

4.2.2 Continuous Rough Surfaces

To investigate the effects of surface roughness, a mold was constructed with known statistical characteristics. The mold was used to ensure repeatability of the surface characteristics for different target compositions. The design satisfied the limitations of the two investigated scattering theories. Specifically, the mold was constructed with smooth slopes and small height variations with respect to the wavelength of the incident radiation.

A photograph of the mold is shown in Figure 4.2.2-1 and the roughness impressed on a sand target is shown in Figure 4.2.2-2. This mold was con-

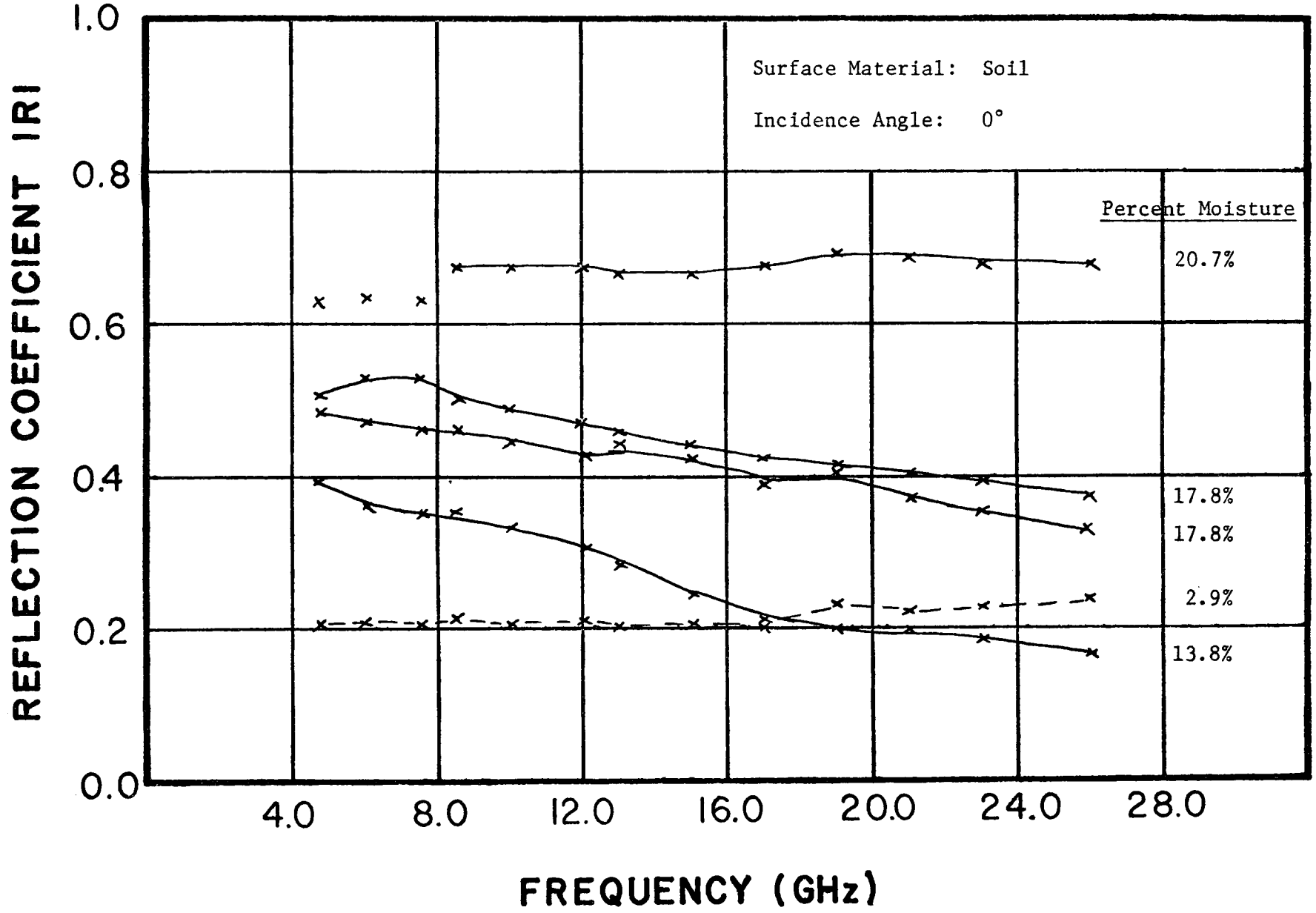

Figure 4.2.1-13 Soil moisture content calibration data

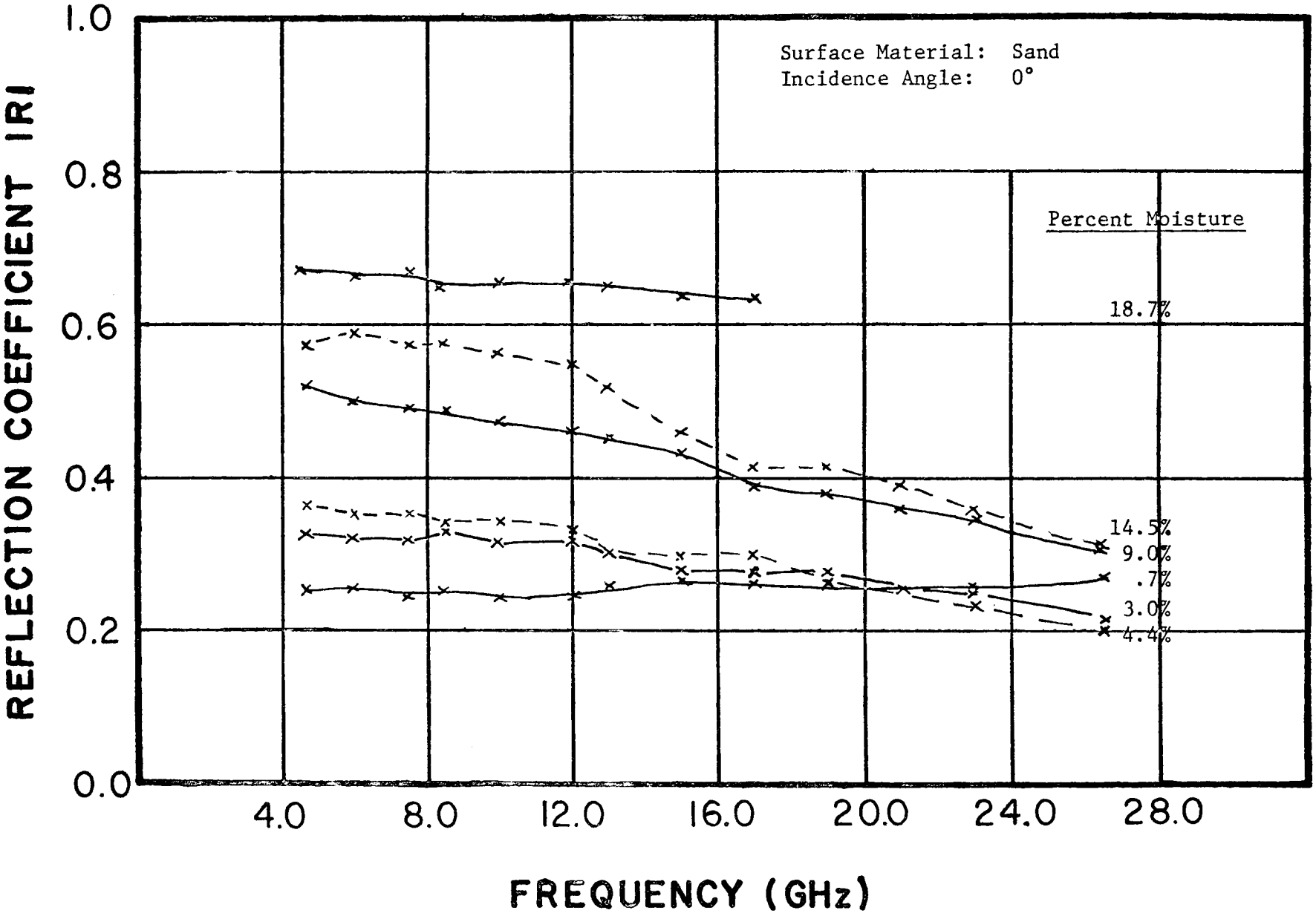

Figure 4.2.1-14 Sand moisture content calibration data

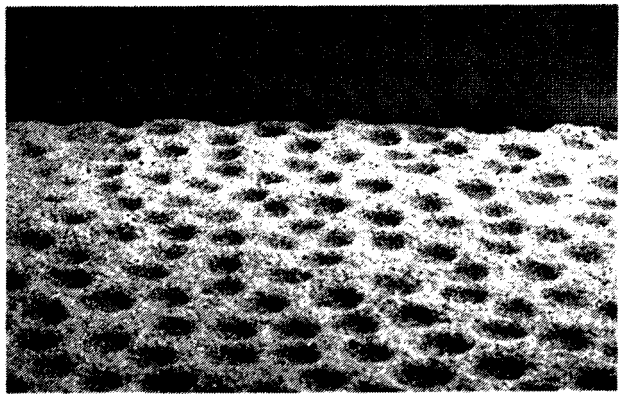

Figure 4.2.2-2 Rough surface from impression of the mold

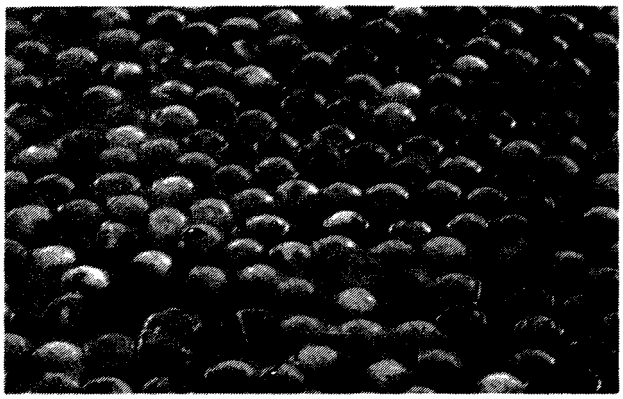

Figure 4.2.2-1 Mold used for impressing known roughness on a target

structed by adhering marbles to a metal plate and then filling in the discontinuities between marbles with fiberglass resin.

The statistics of the surface were calculated using the method of Rouse (1968). Measurements of sampled height were taken for two passes across the surface. These measurements were taken with a dial indicator at spacings of .020 inch.

An estimation of the correlation function was calculated from

$$C(r) = C(\ell \Delta x) = \frac{\frac{1}{N-\ell} \sum_{i=1}^{N-\ell} (h_i - \bar{m})(h_{i+1} - \bar{m})}{\frac{1}{N} \sum_{i=1}^{N} (h_i - \bar{m})^2} \qquad (4.2.2\text{-}1)$$

where h_i = height of i^{th} point of N points

ℓ = lag

Δx = .020 inch-sampling interval

$\bar{m} = \frac{1}{N} \sum_{i=1}^{N} h_i$ - sample mean

For application to the scattering theories, these measurements were approximated by a Gaussian correlation function

$$C(r) = e^{-\frac{r^2}{V^2}} \qquad (4.2.2\text{-}2)$$

with V the correlation distance (distance at which $C(r) = e^{-1}$). The sample correlation function and the Gaussian approximation are shown in Figure 4.2.2-3. The close agreement is obvious.

The probability distribution function of the surface height was also calculated and plotted in Figure 4.2.2-4. For use in the scattering theories, the data points were approximated by a Gaussian distribution function

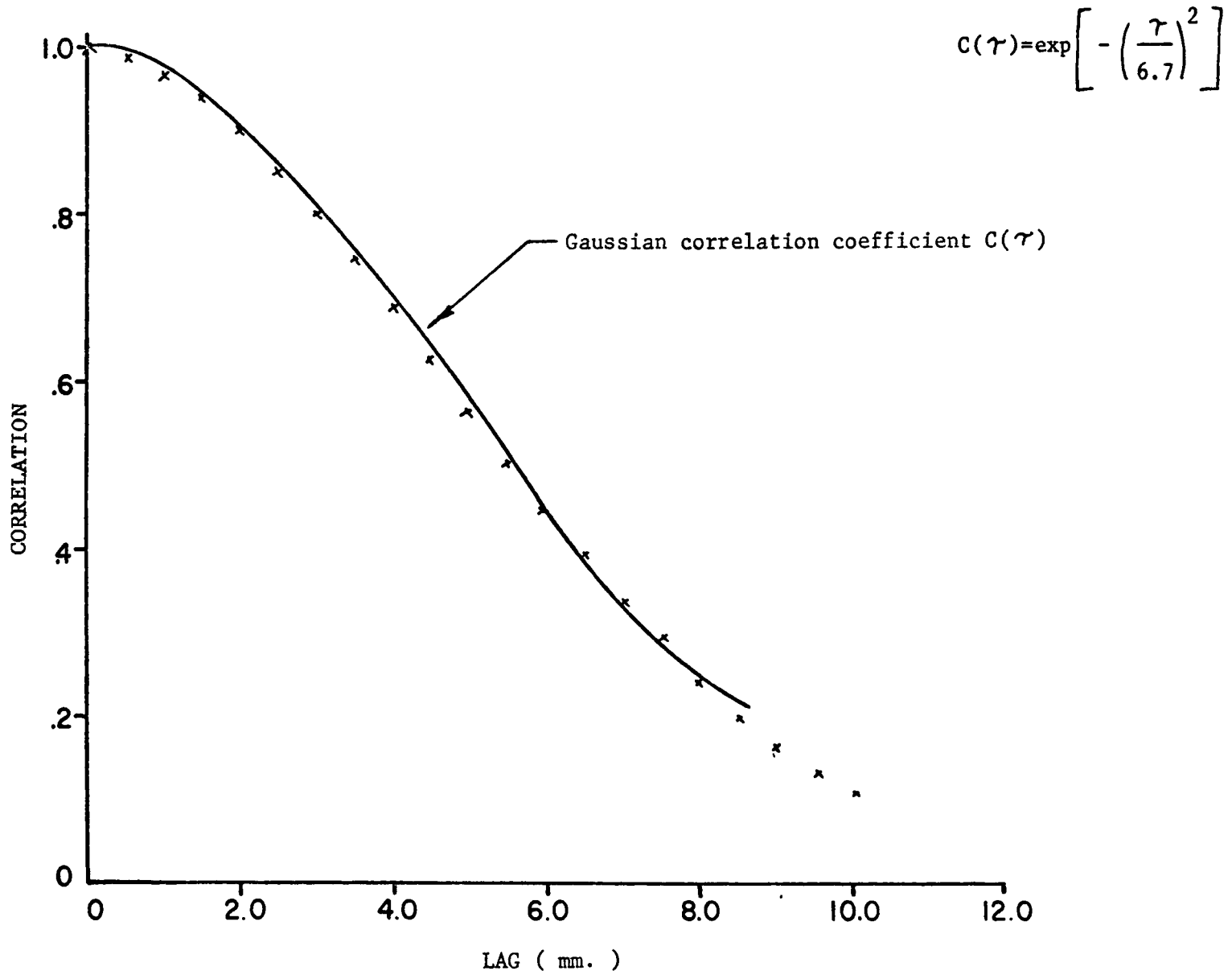

Figure 4.2.2-3 Experimental and Theoretical Correlation Function for the Rough Surface

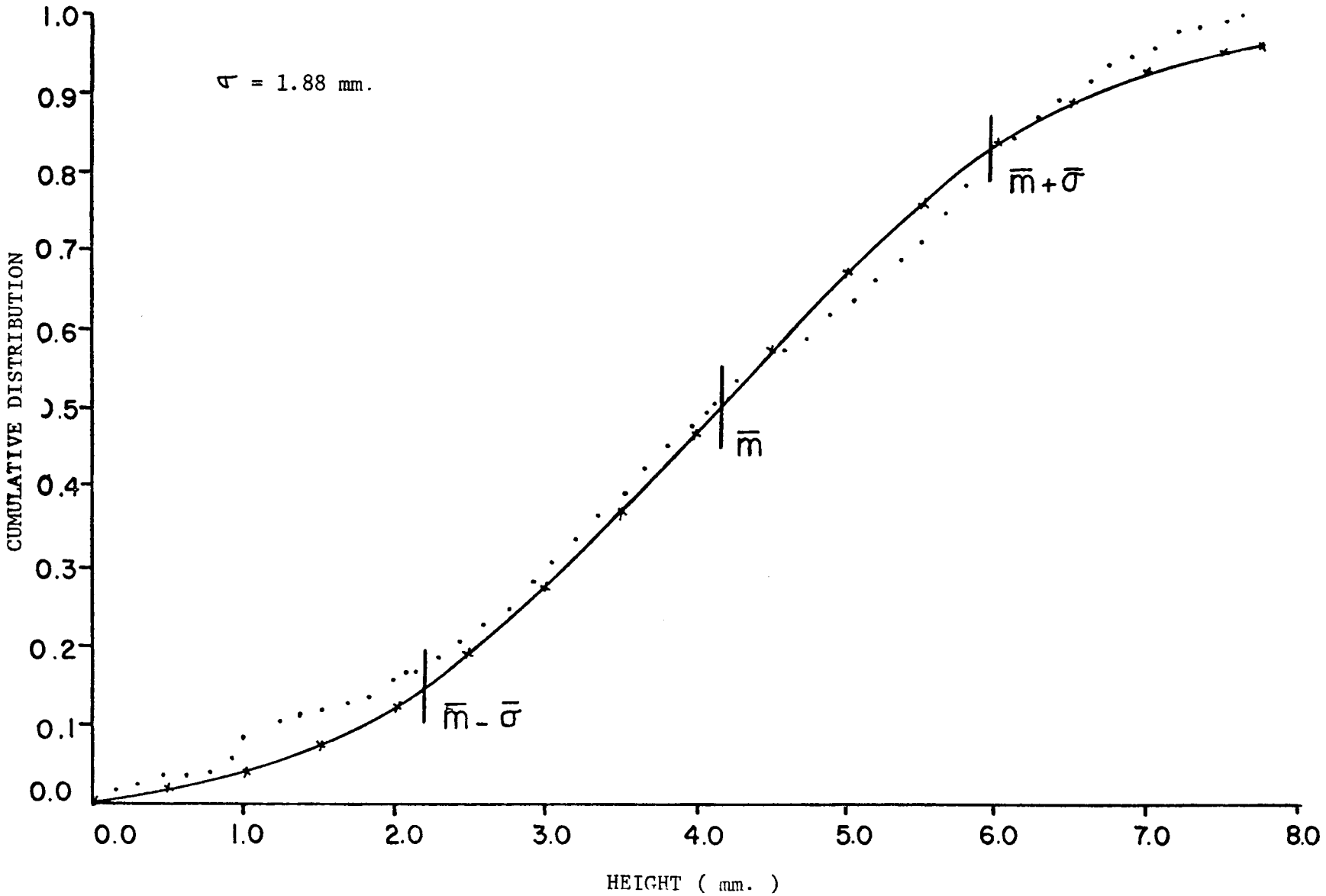

Figure 4.2.2-4 Experimental and Theoretical Cumulative Distribution for the Rough Surface

$$\psi(z) = \int_{-\infty}^{\text{max. height}} \frac{1}{\sqrt{2\pi\sigma^2}} \exp\left[\frac{(z-\bar{z})^2}{2\sigma^2}\right] \qquad (4.2.2\text{-}3)$$

with $\bar{Z}$ the mean and σ^2 the variance of the surface. The match with the data is also shown in Figure 4.2.2-4.

The smooth surface measurements described in the preceding section were repeated for each sample composition and moisture after impressing on the surface the known roughness of the mold just described. The effects of roughness may be seen from a comparison of the raw data for the roughened surface (Figure 4.2.2-5) and that of the smooth surface shown in Figure 4.2.1-1. This comparison shows the rough surface to have a decreased reflectivity at even the lowest measurement frequency and also exhibits a more pronounced frequency sensitivity.

In order to extrapolate to the 0^o incidence angle reflectivity the rough surface data were also plotted as Fresnel curves as shown in Figures 4.2.2-6 through 4.2.2-11. Comparison of these data with the corresponding smooth surface data shows the expected decrease in reflectivity, however, the shape of the curve does not give any indication that the surface measured is actually rough. Thus, in the absence of roughness information the estimate of moisture content will be erroneously low even at the lowest frequency (4.5 GHz). Rough surface data of all compositions and moisture contents is likewise tabulated in Appendix D.

Utilizing frequency diversity correction of roughness prediction of moisture content is possible. The method is described and carried out elsewhere in section 5 of this report.

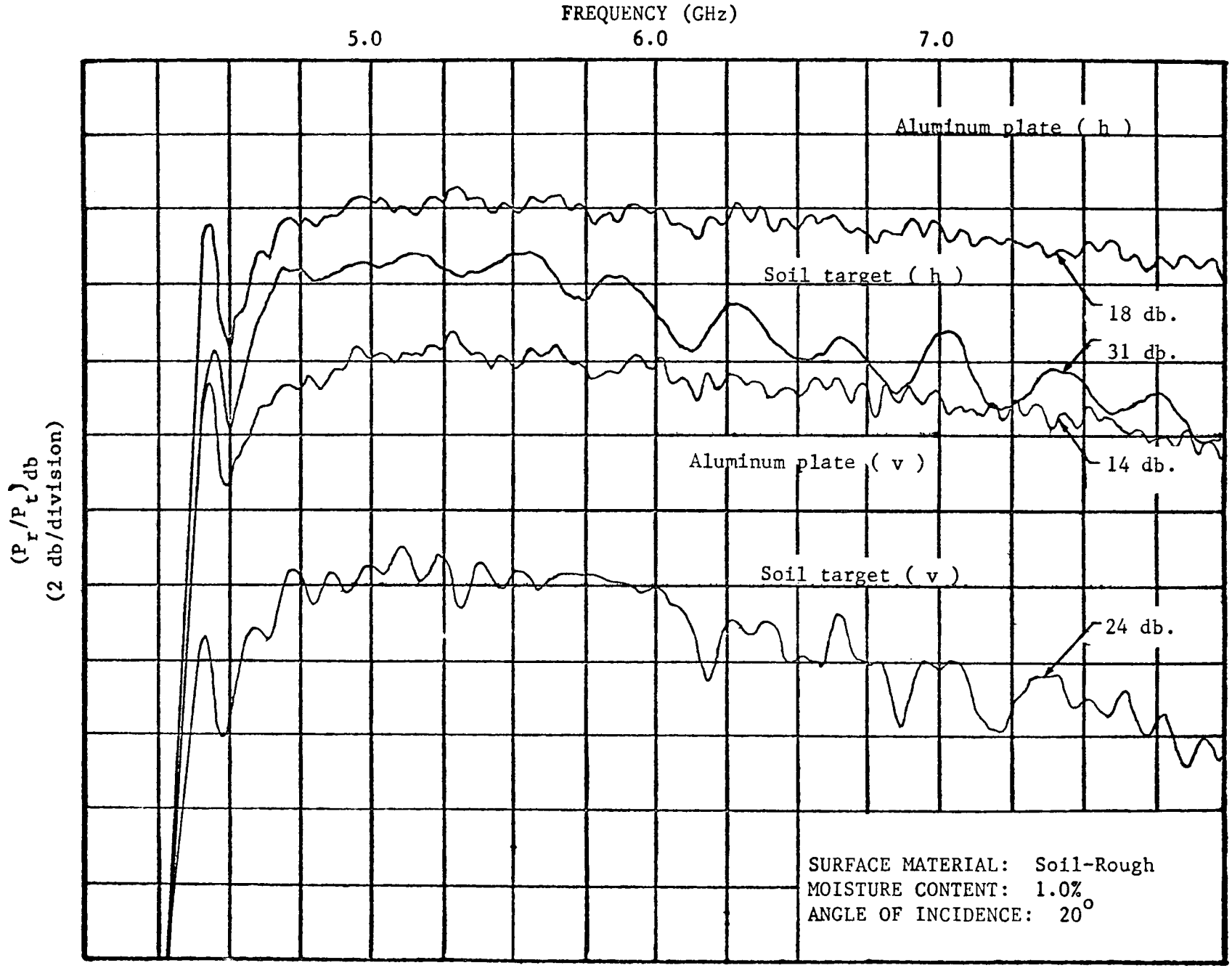

Figure 4.2.2-5 Example of data for determination of rough surface reflectivity

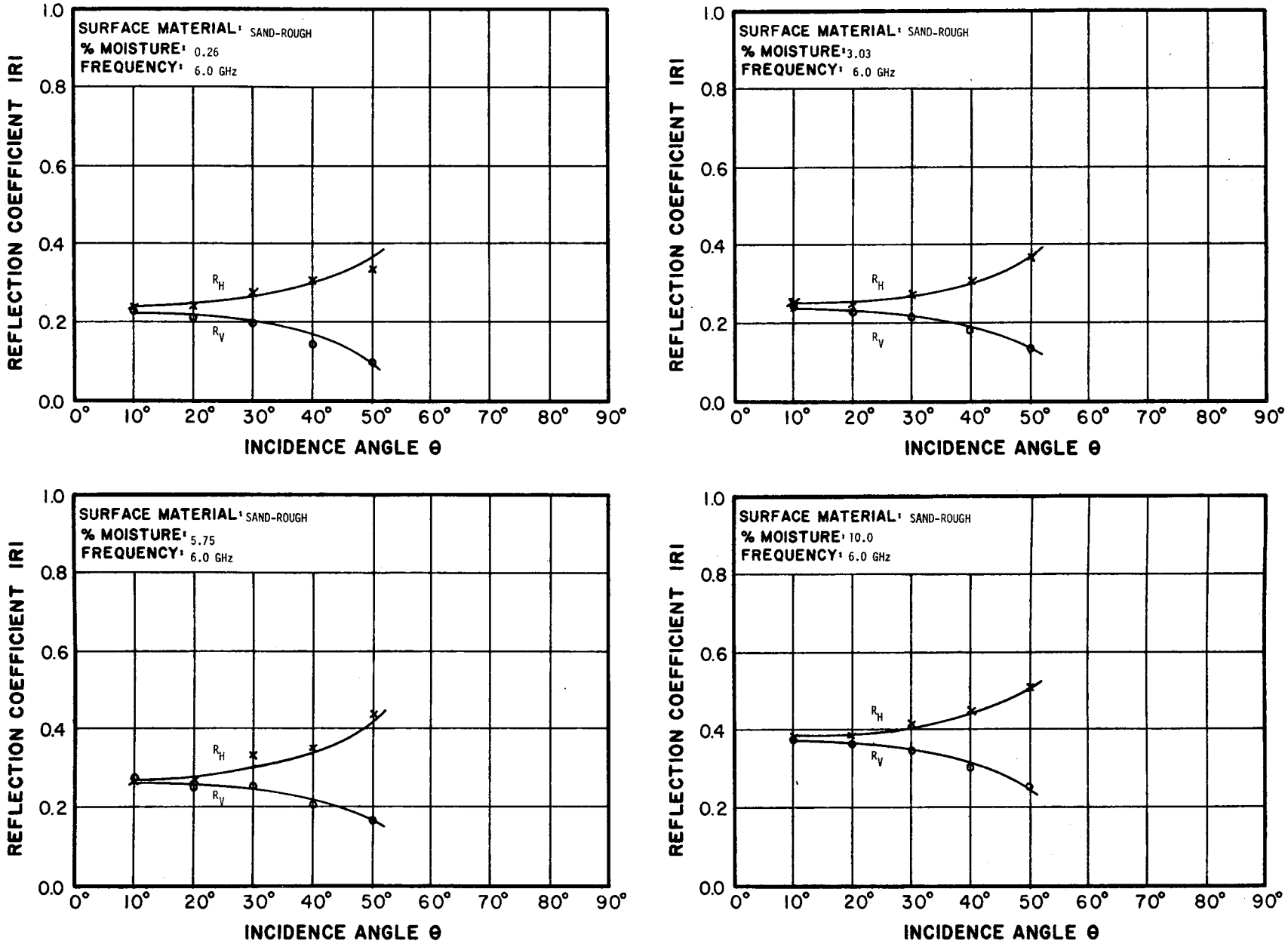

Figure 4.2.2-6 Reflectivity of rough sand with various moisture contents - 6 GHz

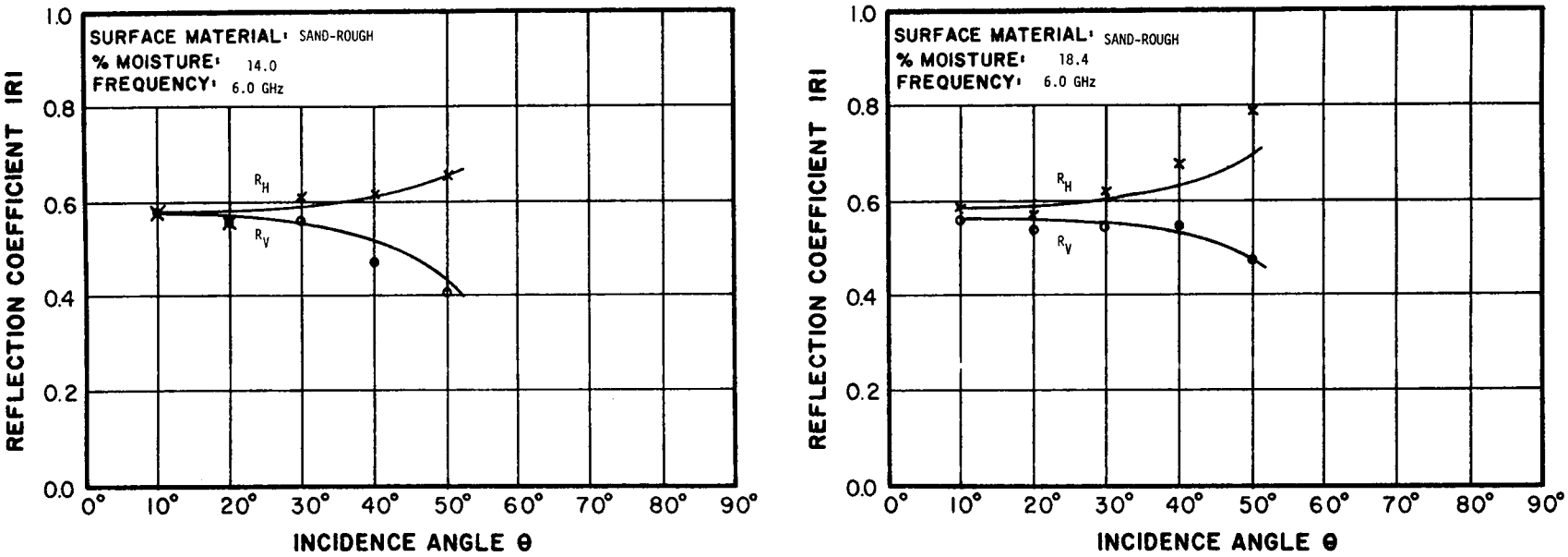

Figure 4.2.2-7 Reflectivity of rough sand with various moisture contents - 6 GHz

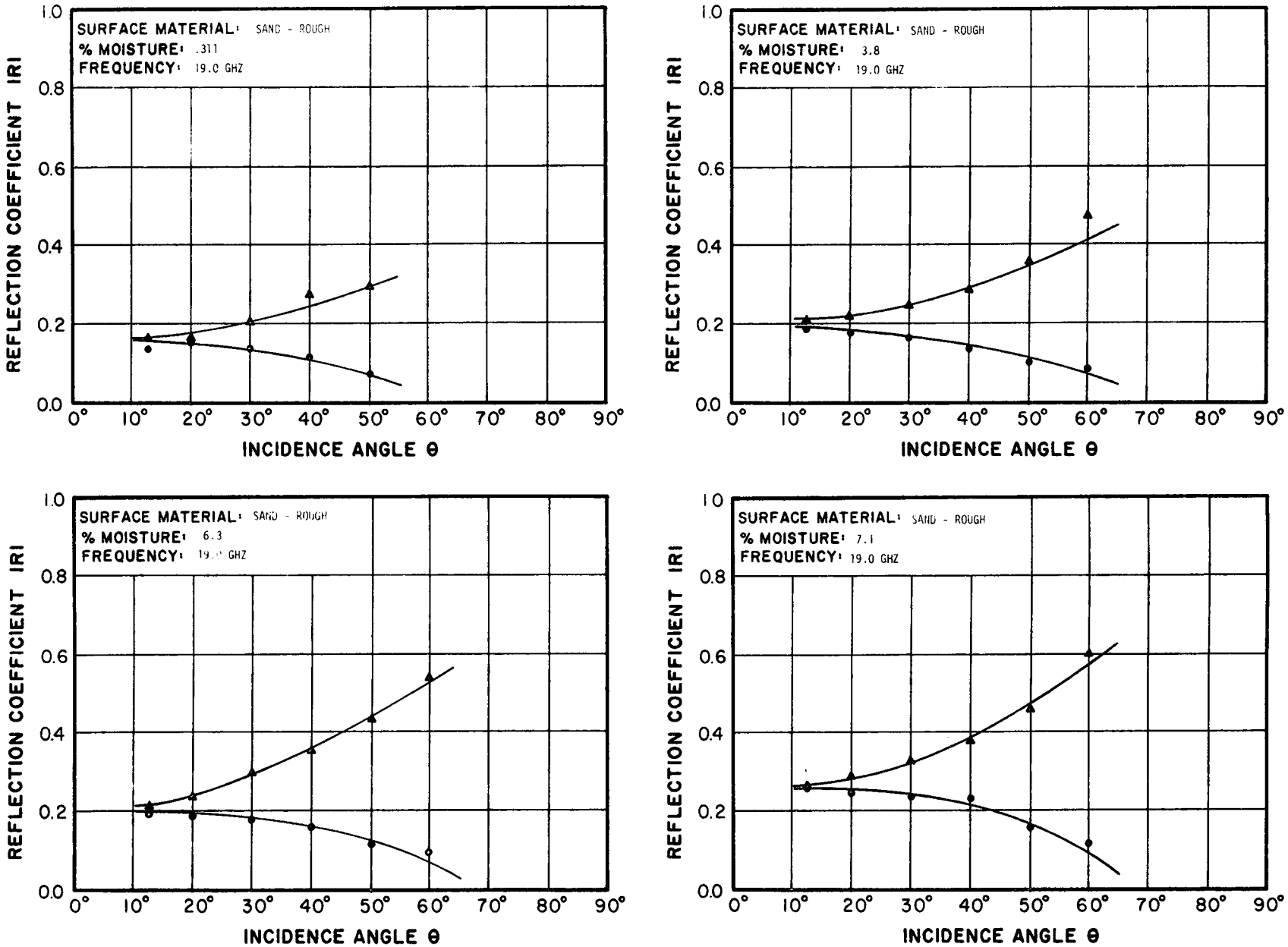

Figure 4.2.2-8 Reflectivity of rough sand with various moisture contents - 19 GHz

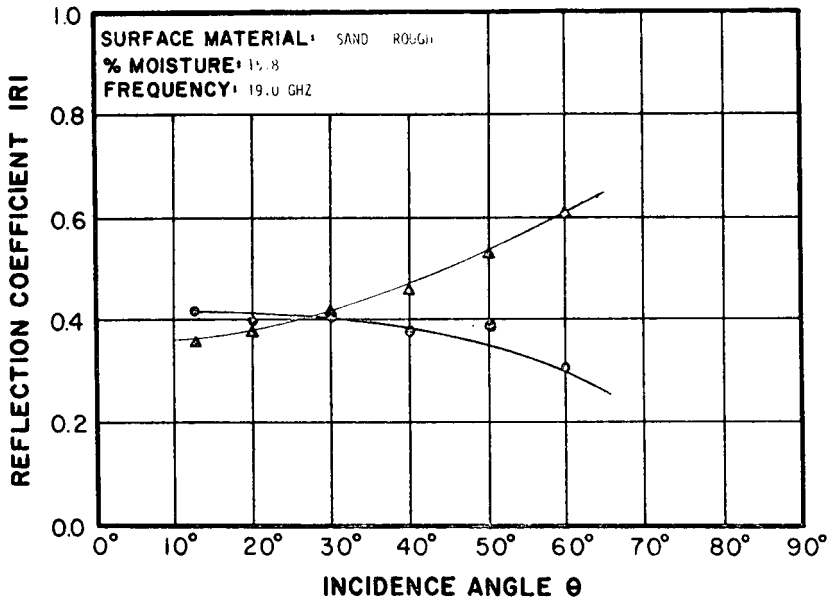

Figure 4.2.2-9 Reflectivity of rough sand with various moisture contents - 19 GHz

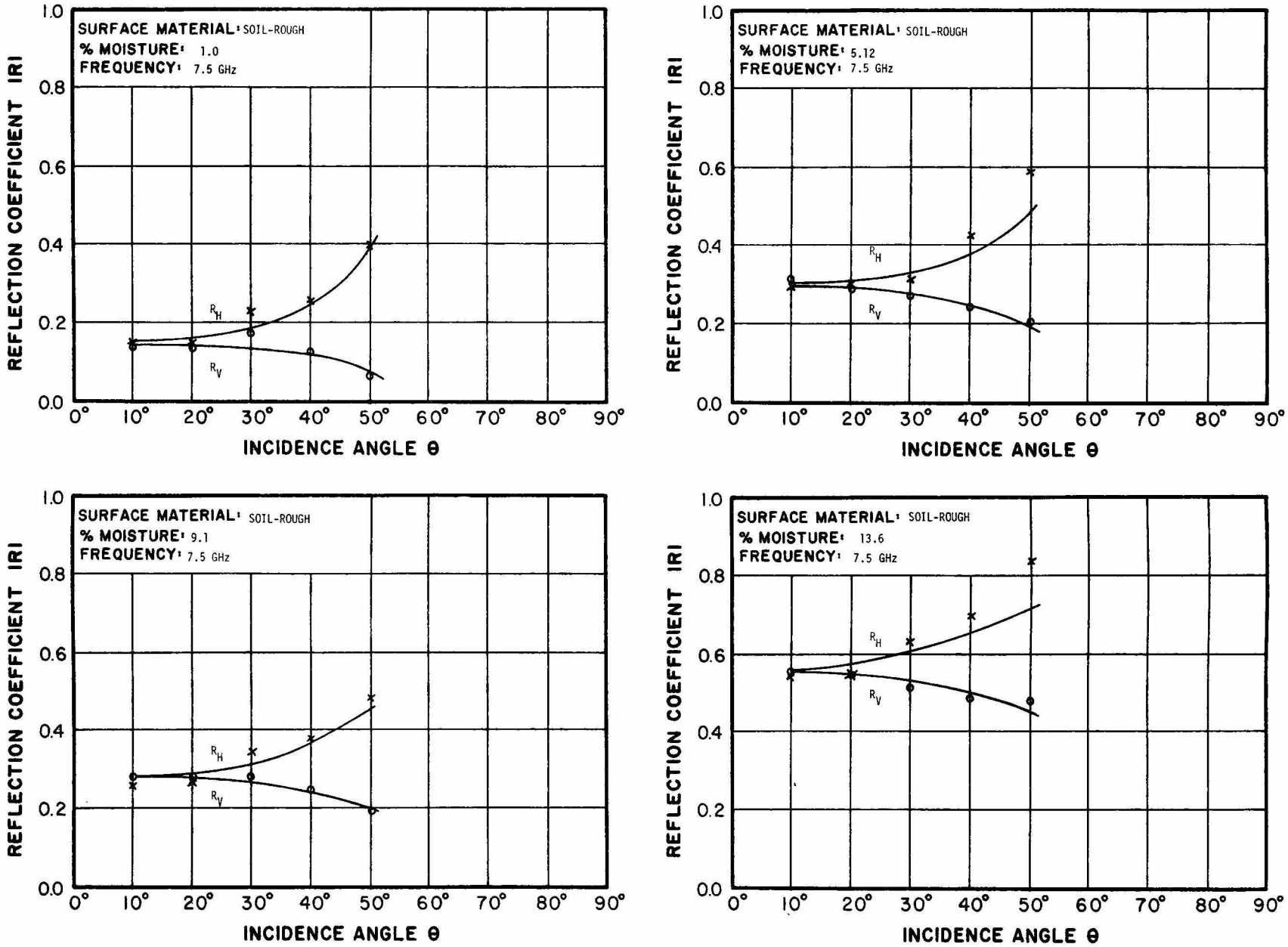

Figure 4.2.2-10 Reflectivity of rough soil with various moisture contents - 7.5 GHz

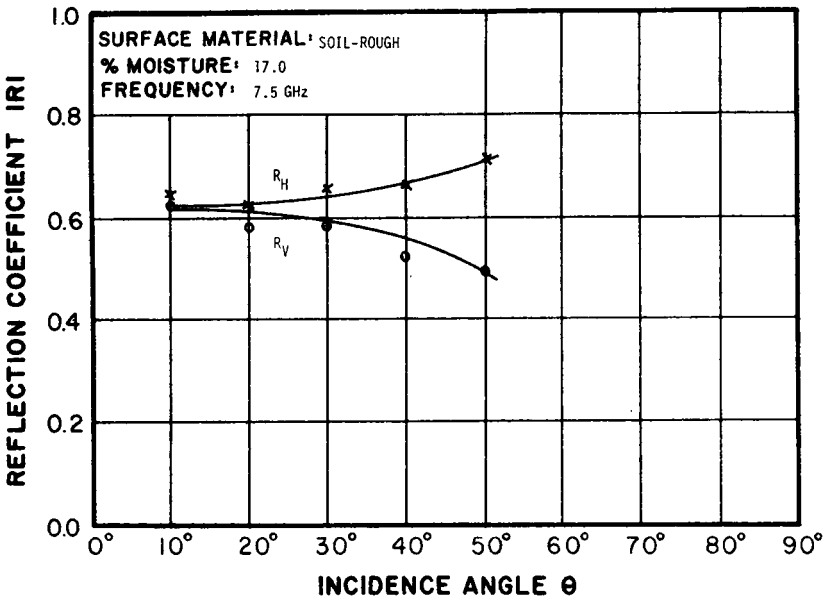

Figure 4.2.2-11 Reflectivity of rough soil with various moisture contents - 7.5 GHz

4.2.3 Discontinuous Rough Surfaces

Examination of the data of the prior two sections indicates (for mid-range moisture contents) a frequency dependence greater than that predicted by the theoretical models. A probable cause for this appeared to be the surface discontinuities (much smaller than a wavelength) caused by the particle cohesion and resultant clumping mentioned earlier. Close examination of these surfaces revealed a significant departure from the continuity and slope assumptions required to develop the theoretical models.

Based upon this assumption an investigation of two randomly discontinuous surfaces was performed. These surfaces are shown in Figures 4.2.3-1 and 4.2.3-2. Figure 4.2.3-3 shows the molded surface of section 4.2.2 for comparison. No feasible way existed to determine the statistics of the discontinuous surfaces, however, visual comparison with the molded surface indicates that the mean height of these surfaces was comparable to or less than that of the molded surface. Comparative measurements of the three rough surfaces are shown in Figure 4.2.3-4. The increased frequency dependence of the discontinuous surfaces is obvious and indicates that surfaces of this nature have an "effective" roughness greater than predicted from the mean surface height.

As no theories currently exist to account for this phenomenon, this line of research was not pursued. However, application of the existing theories using the measured "effective" roughness did result in significant improvement in moisture content estimates as shown in section 5.

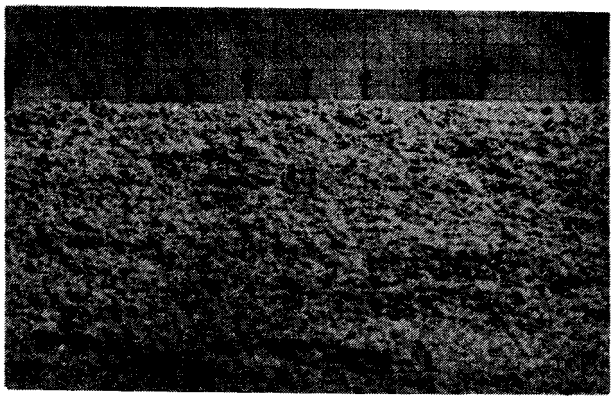

Figure 4.2.3-1 Randomly discontinuous surface 1

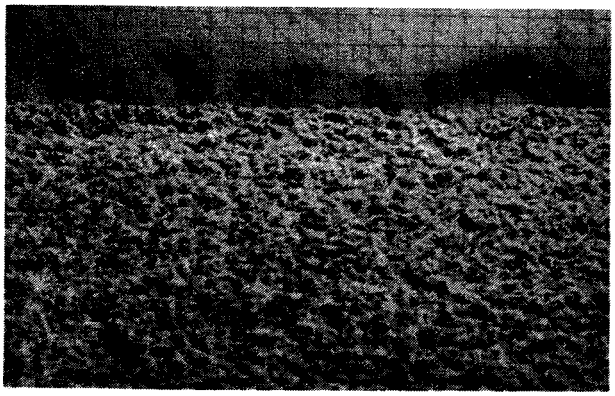

Figure 4.2.3-2 Randomly discontinuous surface 2

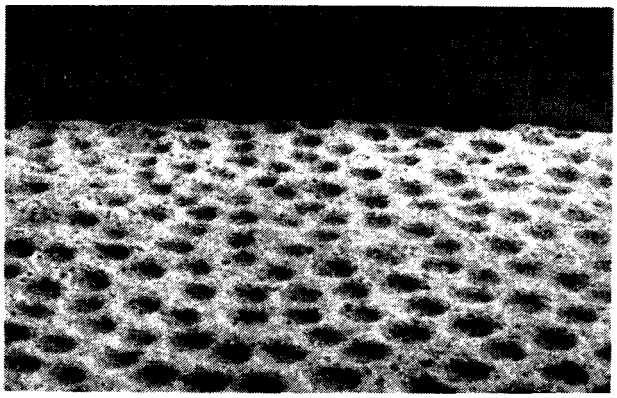

Figure 4.2.3-3 Molded rough surface

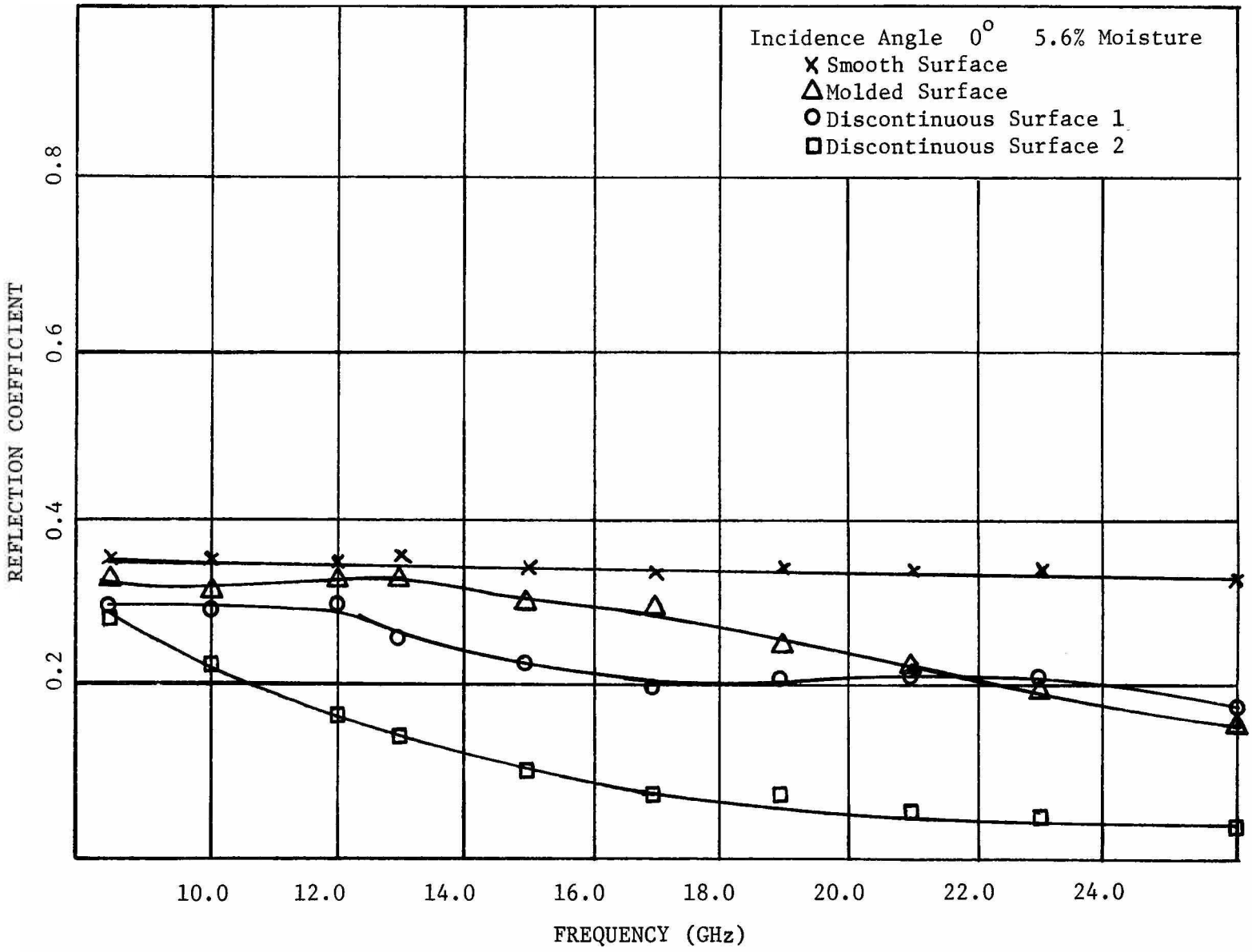

Figure 4.2.3-4 Reflection Coefficient Measured for a Target with Known and Unknown Roughness

4.2.4 Inhomogeneous Media

A layered model for laboratory measurements was constructed by burying a styrofoam block at various depths within the soil-moisture mixture. The block measured 30.8 x 27.9 x 6.4 cm with a dielectric constant of approximately 1.2 and negligible loss tangent.

Figure 4.2.4-1 depicts the altered return signature resulting from the presence of the subsurface layer. Comparison of this figure with either Figure 4.2.1-1 or 4.2.2-5 illustrates the extent of the layer effect. The null pattern observed is basically a result of phase interference between the reflections from the surface and subsurface boundaries. As the relative magnitude of the dielectric constant and conductivity is altered the return smooths out to a reasonable estimate of either the upper or lower layer. Obviously the detection of this effect necessitates use of frequency diversity to determine if a layer is present. Once this is determined an estimate of the layer composition (moisture content) is possible by comparison with theoretical models. This, however, adds another dimension to the selection of the appropriate frequency range for detection and estimation of the layer require a frequency sweep compatible with the electrical depth of the layer.

The measurement results and model predictions of this type surface are compared in section 5.

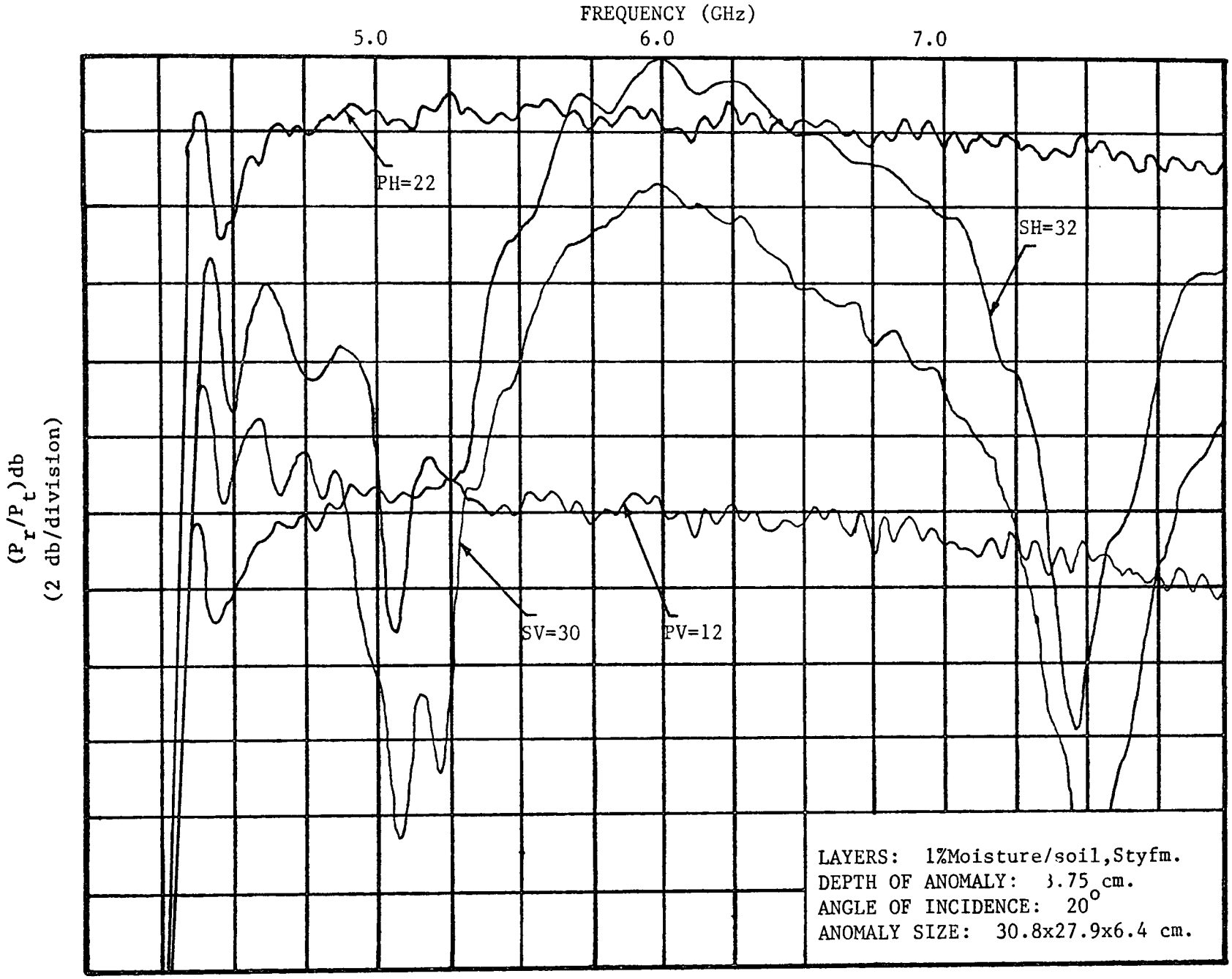

Figure 4.2.4-1 Example of Raw Data
for the Layered Earth Problem

4.3 Field Measurememts

4.3.1 Non-Vegetated Surfaces

Measurements were conducted in the field on a plot of ground that had been stripped of vegetation several weeks prior to data acquisition. This stripping action destroyed the natural texture of the surface, hence, several weeks weathering and herbicide treatments were used to obtain a realistic vegetation-free surface.

The data from the natural terrain exhibited similar characteristics to that of section 4.2.3, i.e. roughness beyond that suggested by visual inspection of the target area. Field data gathering was severely hampered as this situation caused most return signatures to fall below the sensitivity of the equipment used. Furthermore, the measurements that were obtained were altered by a crusting effect, i.e. an approximate 1/2 inch layer which was significantly drier than the subsruface soil.

The field measurement data collected is presented in section 5 where it is likewise analyzed and corrected.

4.3.2 Vegetated Surfaces

Another plot of ground was used to examine the effects of a low level vegetation cover (primarily bermuda grass). The introduction of the cover had marked detrimental effect upon the return signature. Figure 4.3.1-1 illustrates the type of data acquired. The figure represents three clip heights and the stripped soil. Obviously, interpretation of this type data requires a more sophisticated model incorporating the efforts of both roughness and layering. No moisture estimates were made as no suitable models exist for extraction of this information.

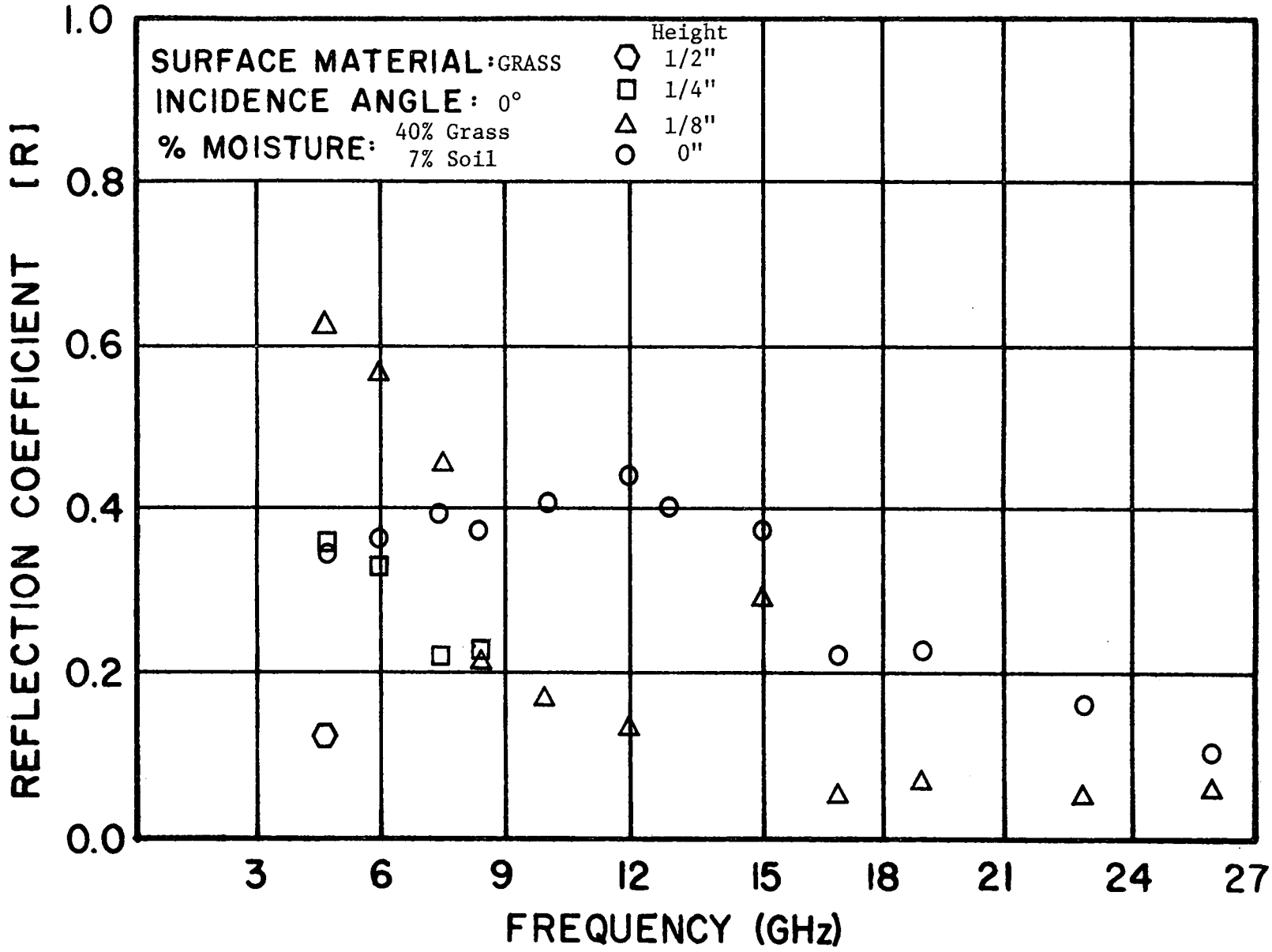

Figure 4.3.1-1 Reflectivity of grass covered soil

5. COMPARISON OF THEORY AND MEASUREMENT DATA

Analysis and use of scattering theories for the elimination of the effects of roughness requires investigation of the parameters affecting rough surface reflection coefficient and scattering cross section. In this section, a comparison is made with previous work, then, a method of correction for roughness is developed using frequency diversity. To verify this method, rough surfaces were measured both in the laboratory and in the field. Predictions of moisture content were made with and without the correction for the effects of roughness. Results of the predictions and limitations of the method are discussed.

5.1 Parameterization

The effective rough surface reflection coefficient

$$\Gamma_h^R = \Gamma_h \, e^{-2\beta^2 \bar{z}^2 \cos^2\theta_o}$$

is derived in Section 2.3. If the height standard deviation (h) is

$$h^2 = \bar{z}^2 \tag{5.1-1}$$

then

$$\Gamma_h^R = \Gamma_h \, e^{-4\pi^2 \left(\frac{h}{\lambda}\right)^2 \cos^2\theta_o} \tag{5.1-2}$$

The roughness factor ($e^{-4\pi^2\left(\frac{h}{\lambda}\right)^2\cos^2\theta_o}$) therefore results in lower reflection coefficients for increasing height deviation, increasing frequency, and decreasing angle of incidence. The effect of angle of incidence is shown as a Fresnel plot in Figure 5.1-1. The ratio (h/λ) determines the effective roughness of the surface. The effect of increasing surface roughness (h) is illustrated in Figure 5.1-2.

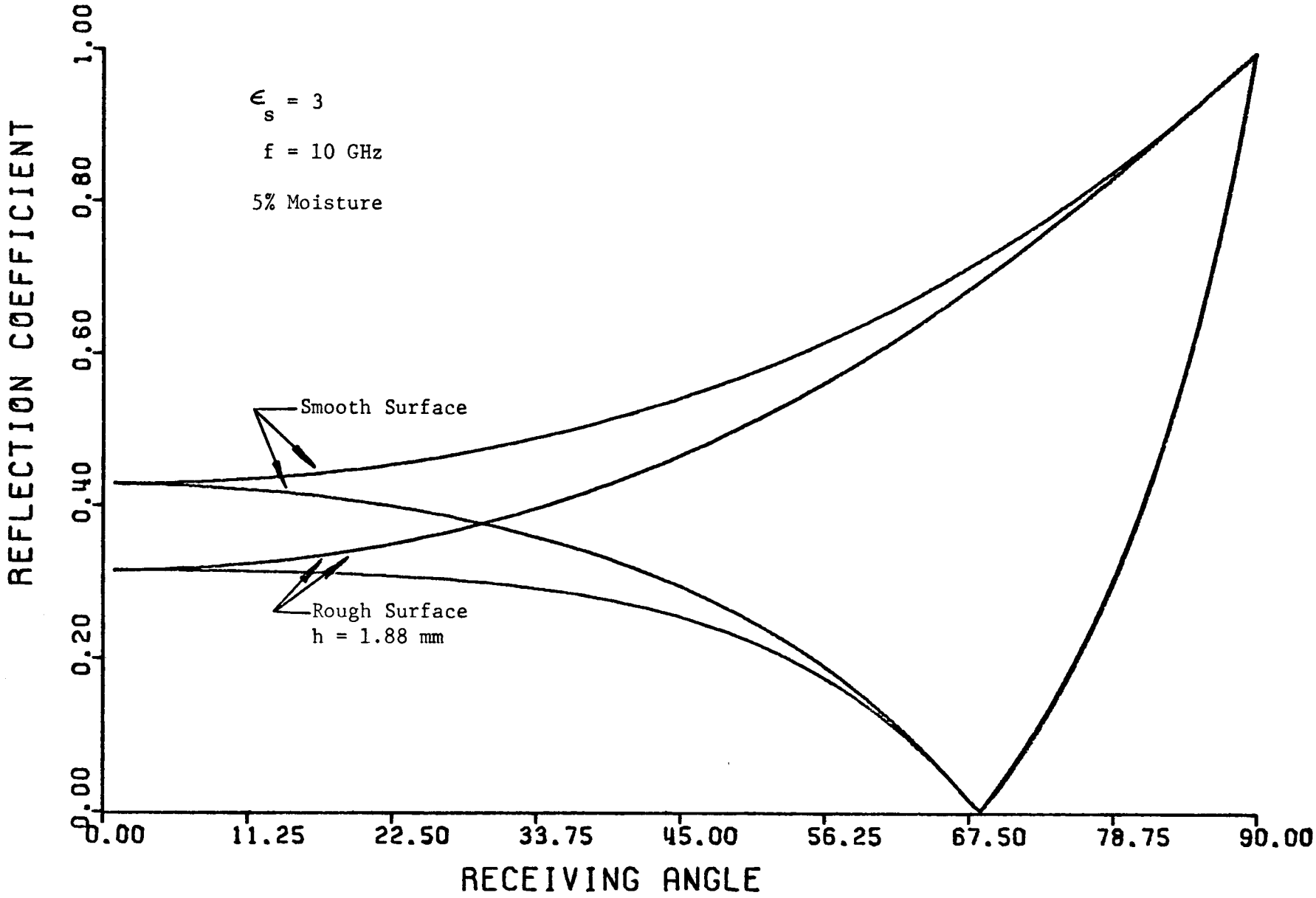

Figure 5.1-1 Comparison of effective rough surface reflection coefficient and the Fresnel reflection coefficient

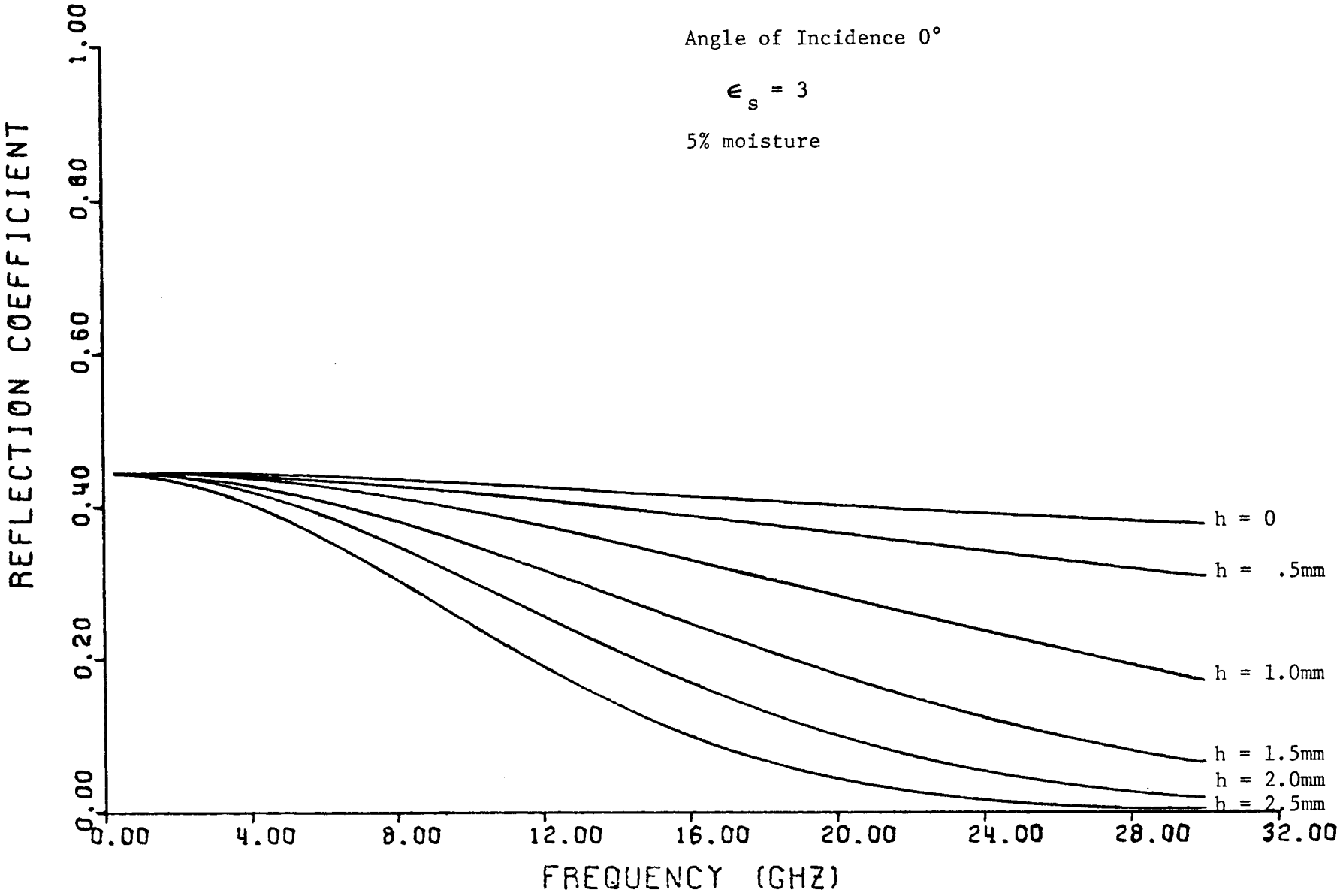

Figure 5.1-2 Effect of increasing surface roughness on reflectivity

The expression for incoherent scattering cross section

$$\sigma_o = 4\beta^4 h^2 V^2 \cos^2\theta_o \cos^2\theta_s T_{h,v} e^{-\frac{V^2\beta^2}{4}(\sin\theta_s\cos\phi_s - \sin\theta_s)^2} \quad (5.1\text{-}3)$$

is derived in Section 2.3. The factor $T_{h,v}$ contains the effects of target composition (relative dielectric constant). The variation of $T_{h,v}$ with angle and dielectric constant, shown in Figure 5.1-3, is similar to variation with reflection coefficient. Increasing roughness (h) increases the incoherent scattering cross section. This effect is illustrated in Figure 5.1-4 for specular scatter and in Figure 5.1-5 for backscatter.

Variation with correlation distance is more complex. A peak in incoherent cross section for backscatter occurs for

$$\frac{V}{\lambda} \approx 0.4 \quad (5.1\text{-}4)$$

for v/λ ratios much greater than this value, or increasing correlation distance (surface effectively smoother), the incoherent cross section decreases. This effect can also be predicted from the definition of incoherence and is illustrated for backscatter in Figure 5.1-6. As the angle of incidence increases from the normal, the incoherent scattering cross section has a general decreasing trend due to the $\cos^2\theta$ term in equation 5.1-3.

Variation of the incoherent scattering cross section with frequency is illustrated in Figures 5.1-4, 5.1-5, 5.1-6. A pattern of incoherent scattering cross section is shown in Figure 5.1-7 for incident radiation at 30^o.

The expression for coherent scattering cross section from section 2.4 is

$$\sigma_o = \frac{\beta^2}{\pi} A \left(\frac{\sin\frac{\beta\xi_x L_x}{2}}{\frac{\beta\xi_x L_x}{2}} \right)^2 |\alpha_{h,v}|^2 e^{-\beta^2 h^2 (\cos\theta_o - \cos\theta_s)^2} \quad (5.1\text{-}5)$$

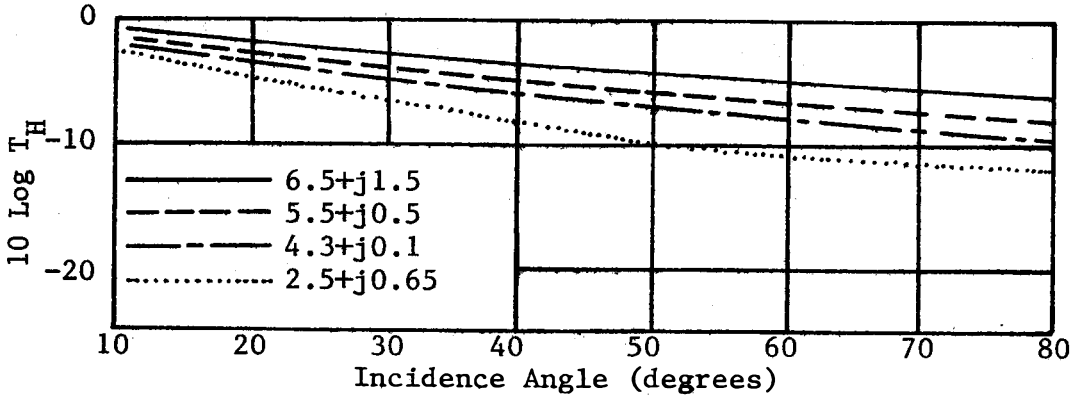

Effect of dielectric constant on return from a slightly rough surface (horizontal polarization)

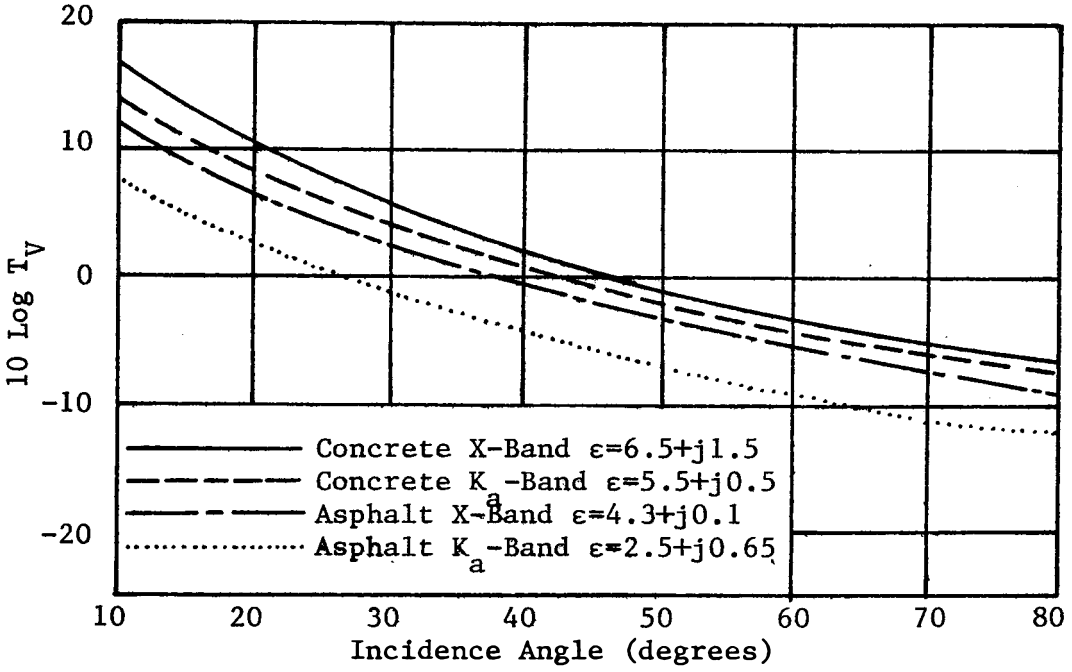

Effect of dielectric constant on return from a slightly rough surface (vertical polarization)

Figure 5.1-3 Effect of relative dielectric constant on $T_{h,v}$ (from Peake, 1959)

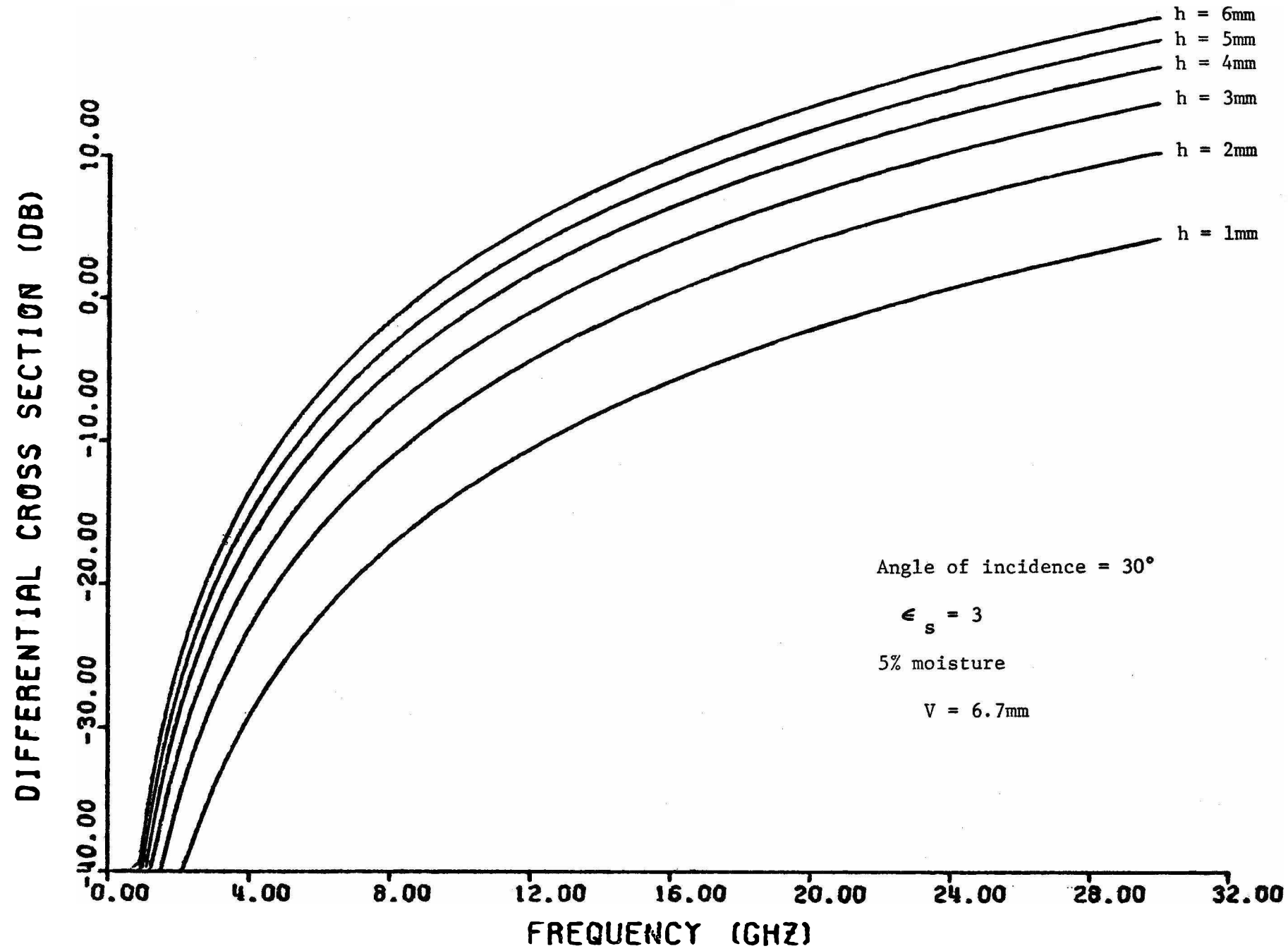

Figure 5.1-4 Effect of roughness on incoherent specular scattering cross section (horizontal polarization)

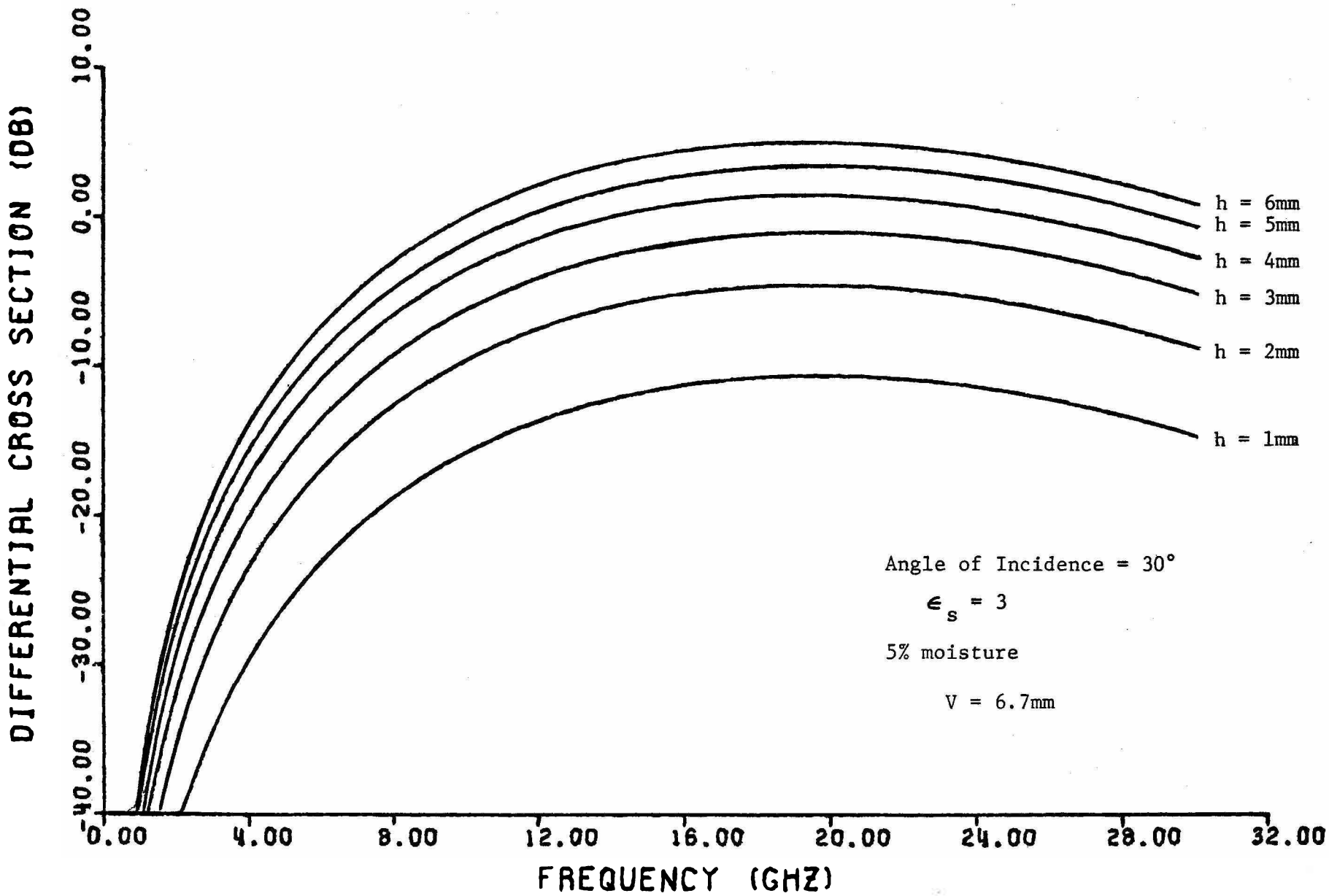

Figure 5.1-5 Effect of roughness on incoherent backscattering cross section (horizontal polarization)

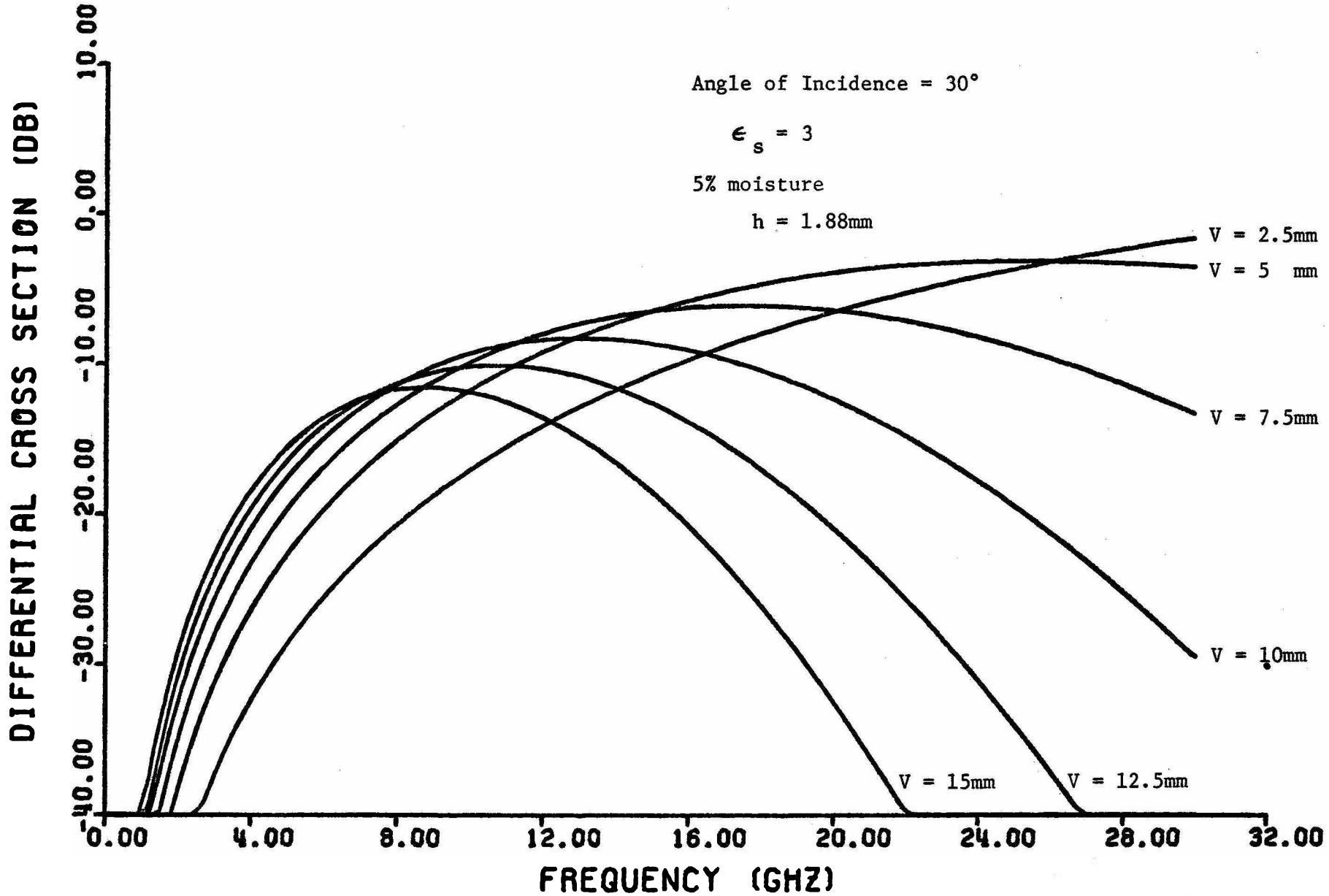

Figure 5.1-6 Effect of correlation distance on incoherent backscattering cross section (horizontal polarization)

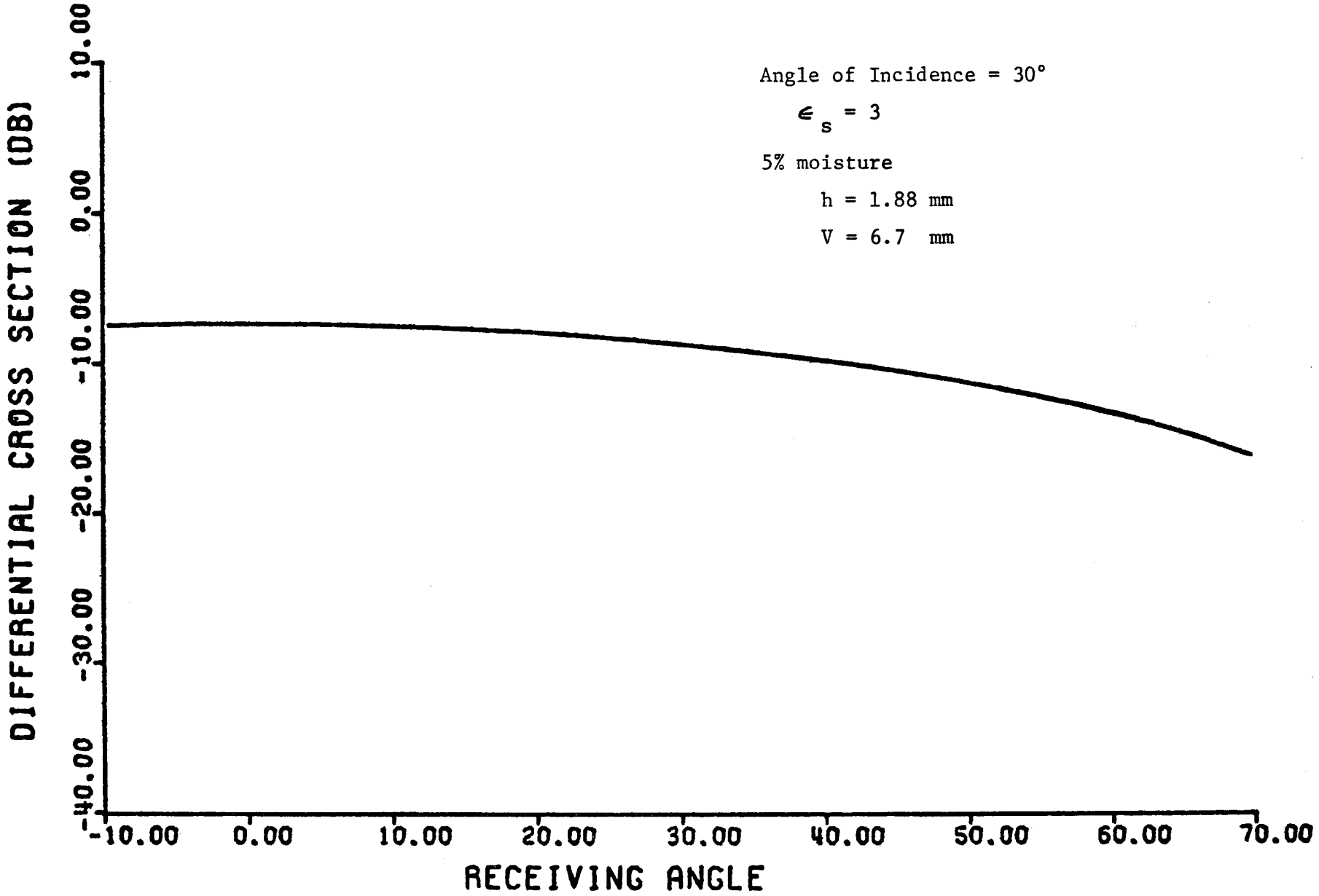

Figure 5.1-7 Pattern of incoherent scattering cross section (horizontal polarization)

An increase in the surface roughness (h) causes a decrease in coherent scattering. This effect is predicted from the definition of coherence and is illustrated in Figure 5.1-8 for specular scattering cross section. The variation with angle for specular scattering cross section is similar to the variation of the coherent reflection coefficient. A change in dielectric constant affects only the Fresnel reflection coefficient term in α. Increasing frequency decreases the coherent cross section and also narrows the lobe structure of the diffraction pattern. For radiation incident at 30^{o}, a pattern of coherent scattering cross section is shown in Figure 5.1-9.

5.2 Comparison with Previous Work

The expression for coherent rough surface reflection coefficient from Section 2.3.3

$$\Gamma_h^R = \Gamma_h \, e^{-2\beta^2 h^2 \cos^2\theta_o} \qquad (5.2\text{-}1)$$

is identical to the factor derived by Ament (1953). This formula for specular reflection is widely accepted and may also be obtained from the Kirchhoff method.

The expression for incoherent backscatter scattering coefficient (γ) was derived by Peake (1959). The relationship between differential scattering cross section and scattering coefficient is

$$\gamma = \frac{\sigma_o}{\cos\theta_o} \qquad (5.2\text{-}3)$$

The expression for incoherent differential backscatter cross section in equation 2.3-31 derived from Peake's expression exhibits a cos θ_o term

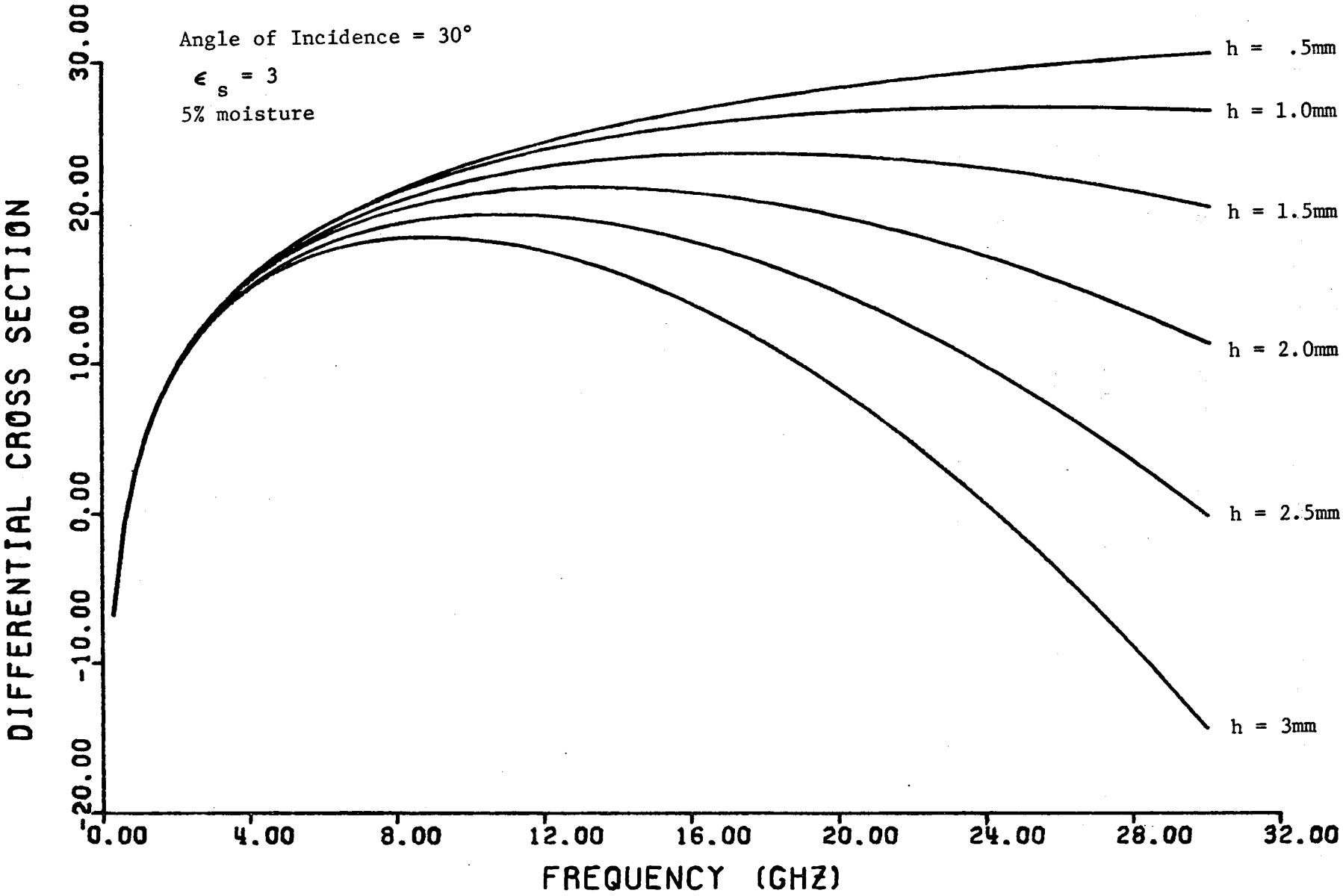

Figure 5.1-8 Effect of roughness on coherent specular scattering cross section (horizontal polarization)

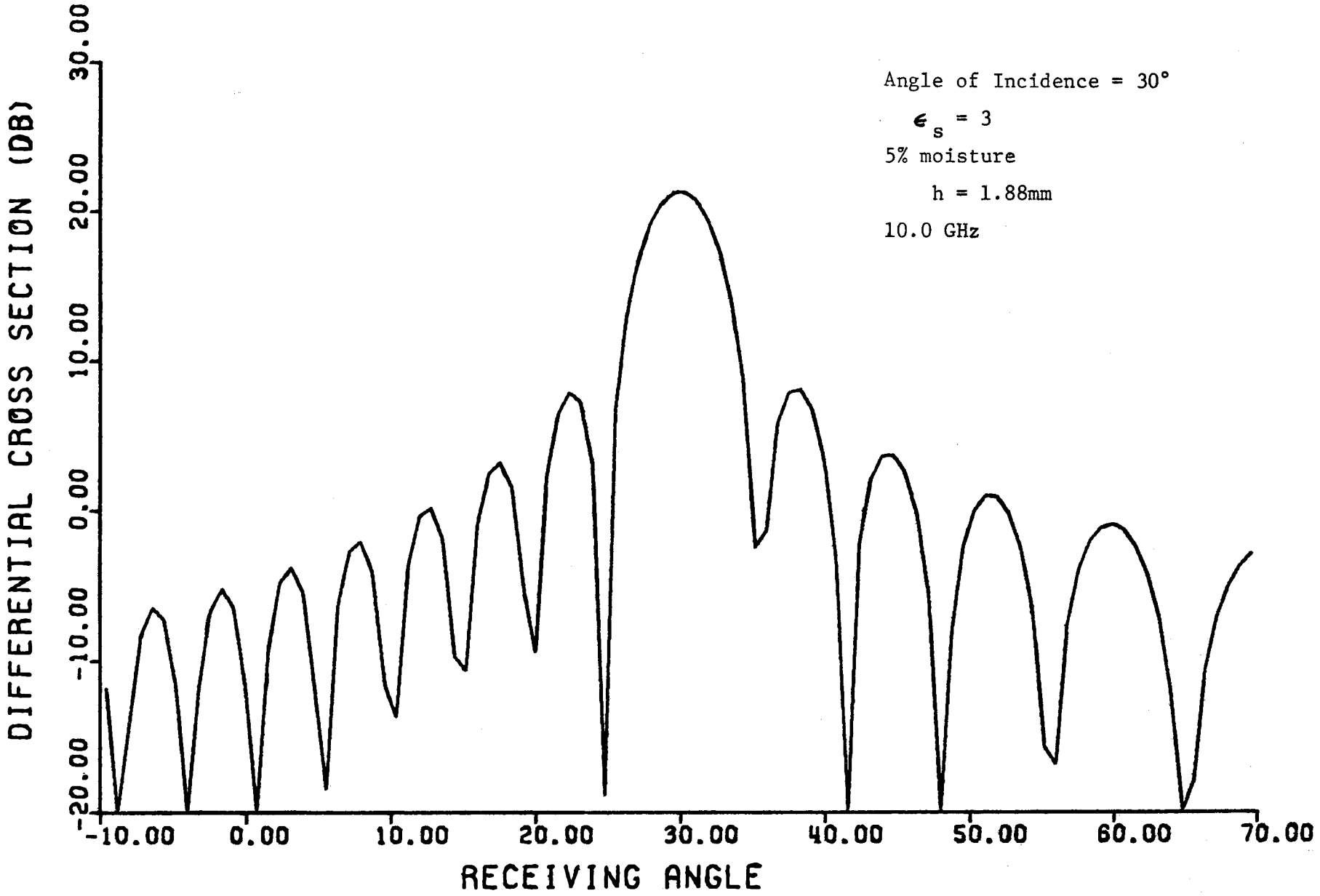

Figure 5.1-9 Pattern of coherent scattering cross section (horizontal polarization)

difference. No data could be taken for the backscatter configuration due to insufficient sensitivity, however, an investigation was made of the prediction of backscatter. The match of theory and data is shown in Figure 5.2-1 (Peake, 1959). The slight discrepancies in theory and data were felt by Peake to be due to errors in estimation of the statistics of the surface and errors in estimation of the dielectric constant. Near grazing incidence, the geometry breaks down due to shadowing. The theory is a better fit for higher frequencies since the coherent component at higher frequencies is negligible. Investigation of the coherent backscatter indicates possible improvement over Peake's theory. Since Peake's system parameters were not known, the coherent component could not be predicted. Therefore, this investigation was applied to the molded surface described in section 4.2.2. The magnitudes are different, however, the trends should be the same. Incoherent backscatter scattering coefficient (γ) is shown in Figure 5.2-2 for the molded surface and the sum of the incoherent and coherent backscatter scattering coefficients is shown in Figure 5.2-3. The wide antenna beamwidths used result in averaging of the nulls in the sum of the incoherent component alone is shown in Figure 5.2-4. Reference to Peake's data (Figure 5.2-1) indicates improvement in the match for horizontal polarization. The improvement in slope is most apparent near normal incidence where the coherent component is most significant. It is felt that the sum of the coherent and incoherent components of backscatter scattering coefficient would produce a significantly better approximation to the actual return.

The sum of the coherent and incoherent components is useful for calculation of the scattering pattern from a rough surface. At different angles across the pattern, either component may be dominant. The sum of the incoherent components for the pattern of scattering cross section are shown

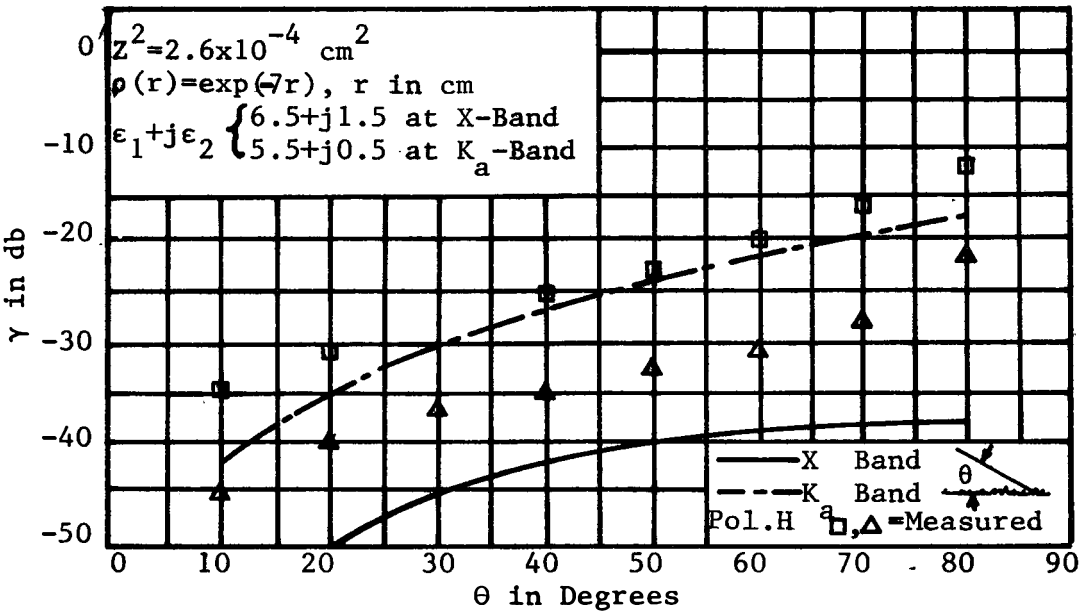

Calculated and measured return from a slightly rough concrete surface (horizontal polarization)

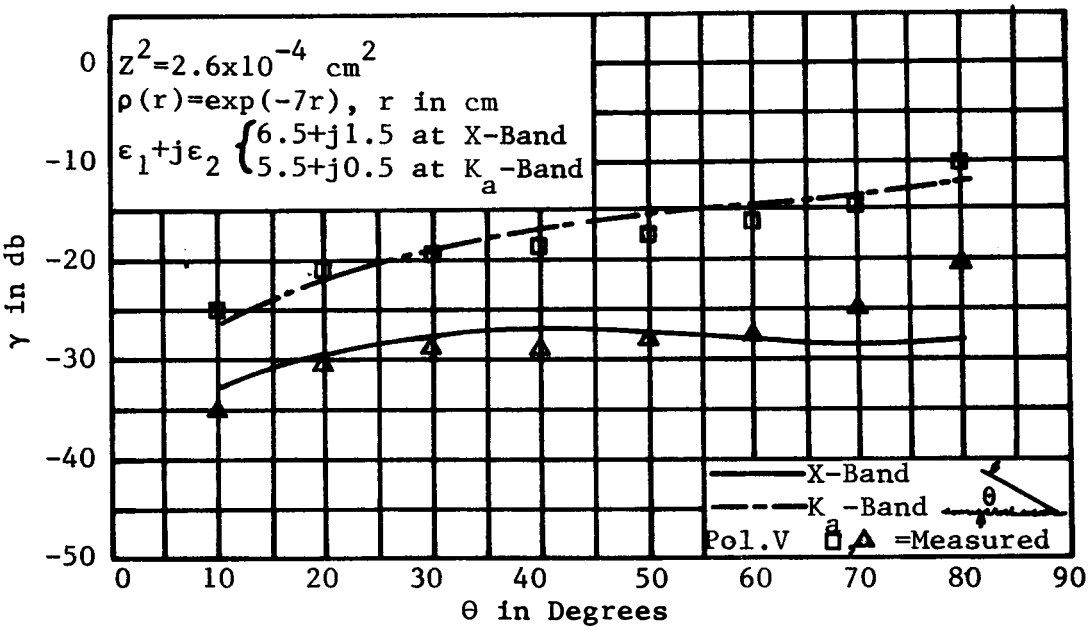

Calculated and measured return from a slightly rough concrete surface (vertical polarization)

Figure 5.2-1 Comparison of incoherent backscatter scattering coefficient and data (from Peake, 1959)

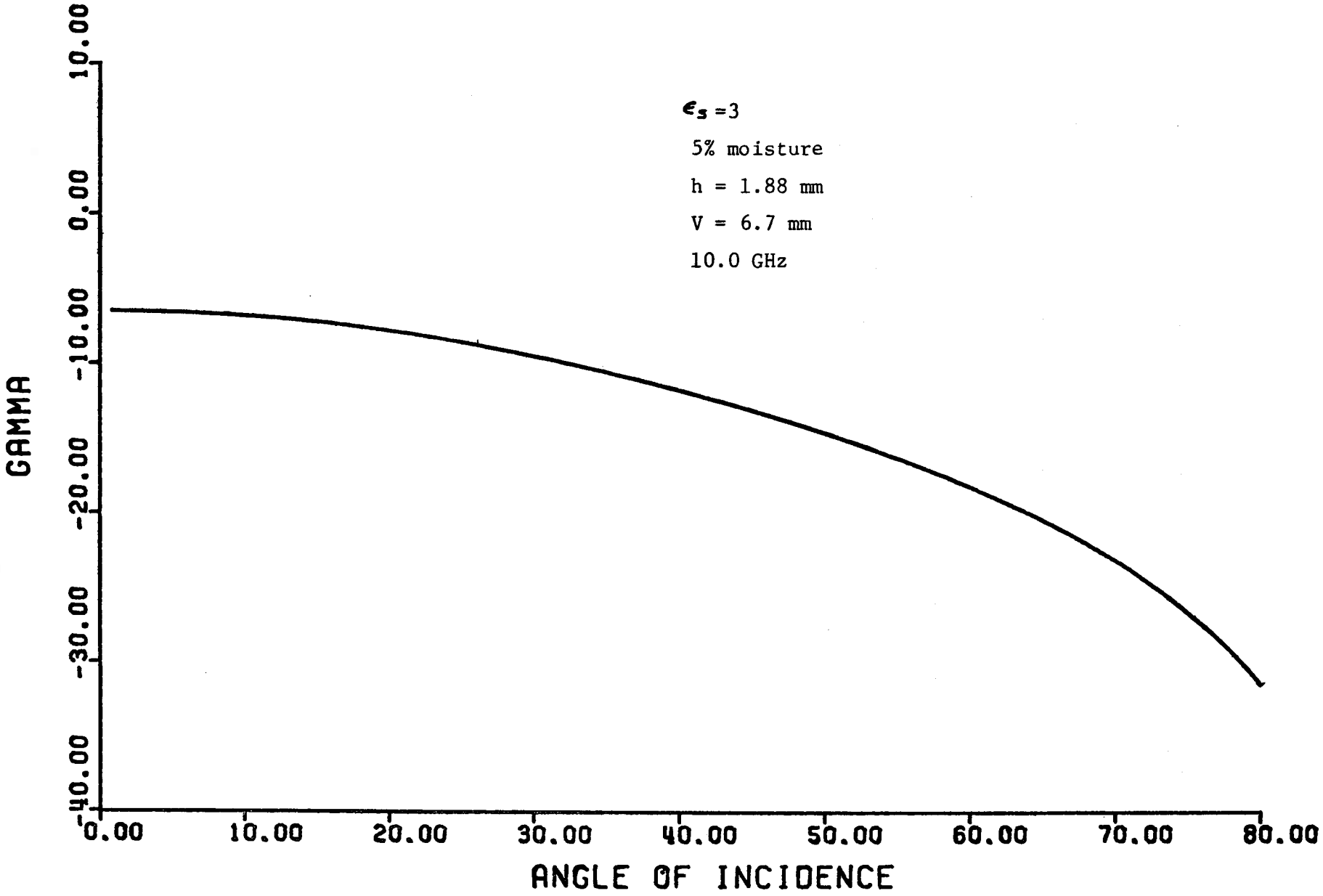

Figure 5.2-2 Incoherent backscattering scattering coefficient for the molded surface (horizontal polarization)

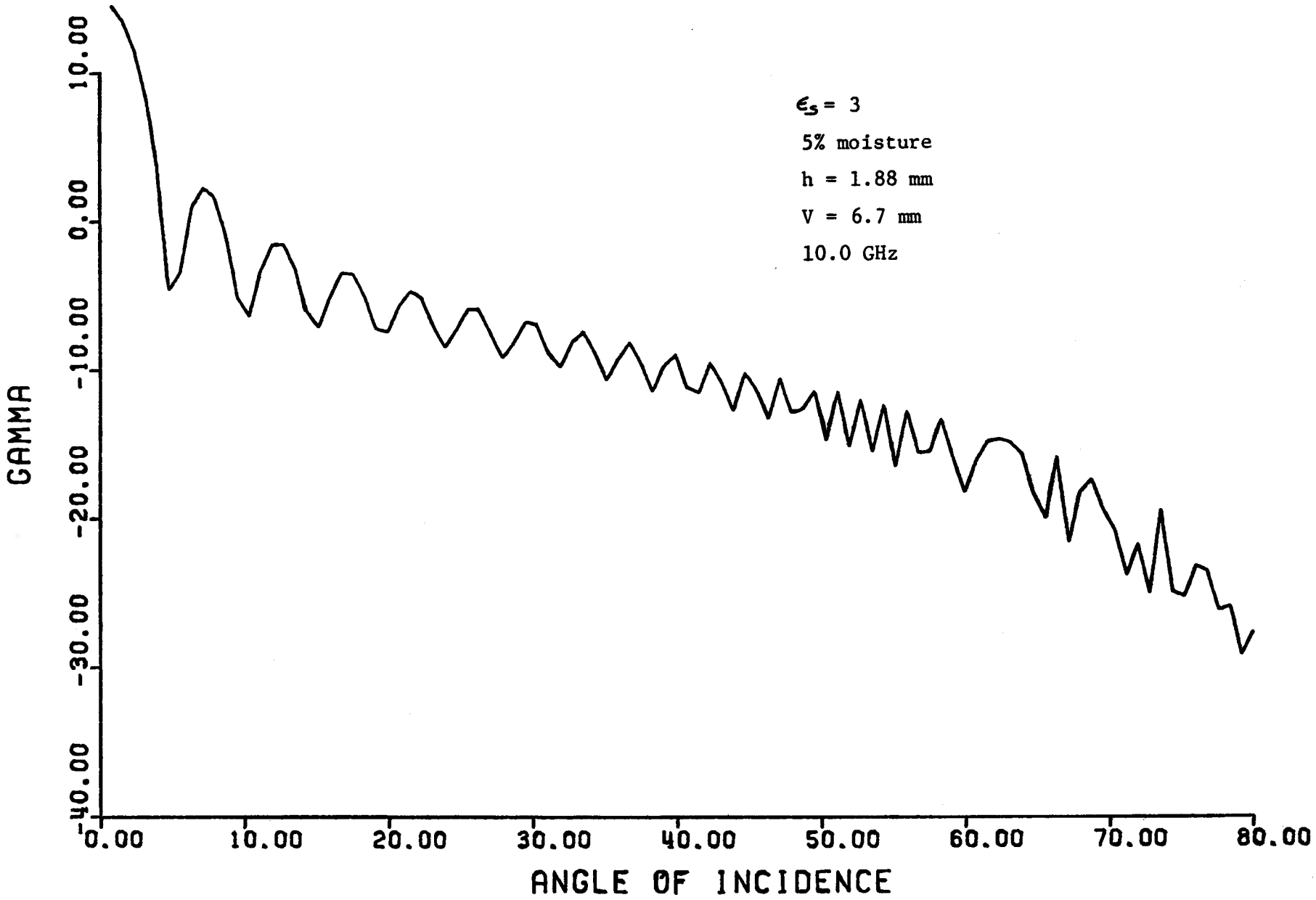

Figure 5.2-3 Sum of incoherent and coherent backscatter scattering coefficient for the molded surface (horizontal polarization)

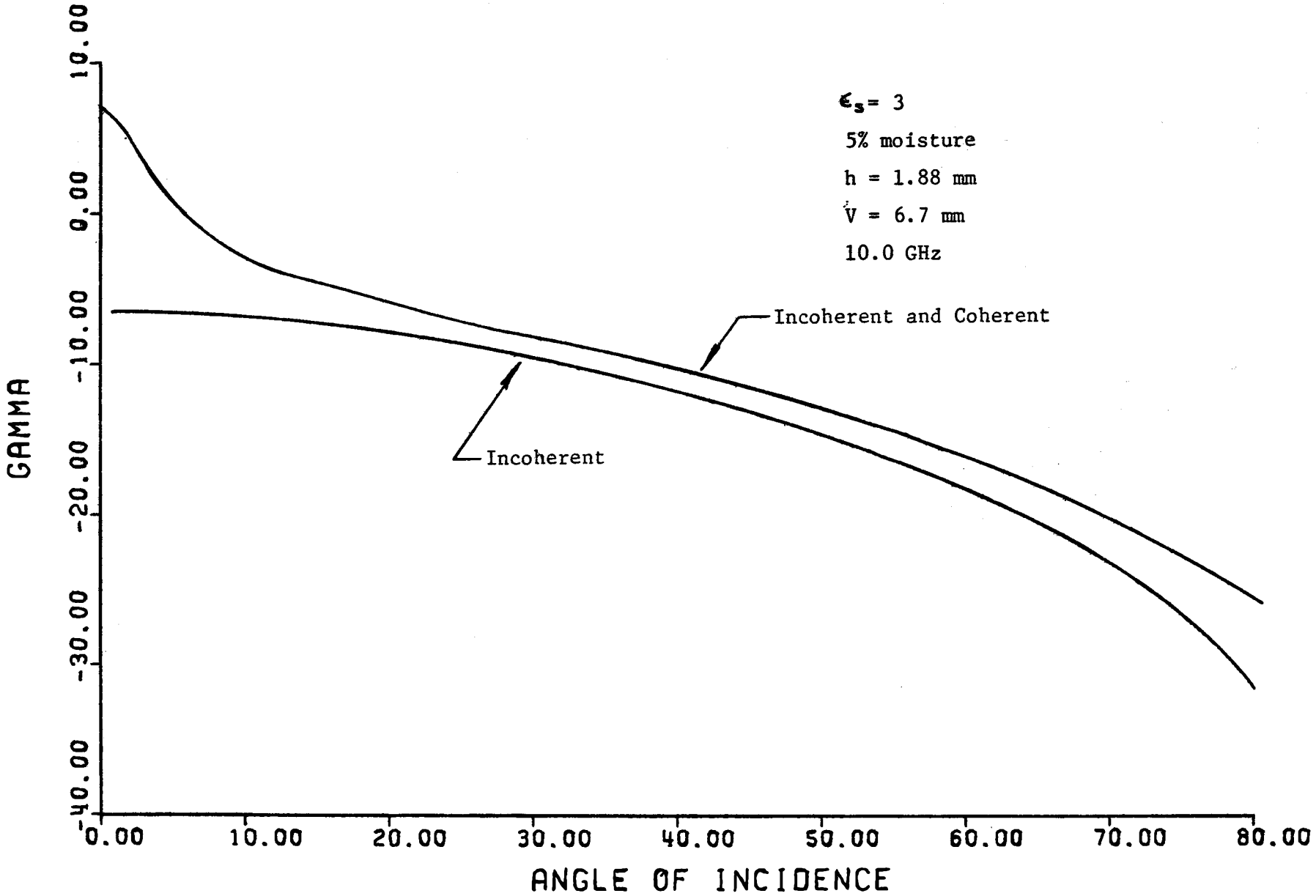

Figure 5.2-4 Comparison of incoherent and the averaged sum of incoherent and coherent backscatter scattering coefficient (horizontal polarization)

in Figure 5.2-5. The antennas used in the measurement system had wide beamwidths, therefore, angular averaging reduced the nulls in the predicted pattern. In Figure 5.2-6, the measured values of the scattering cross section are compared to the theoretical values averaged over the antenna beamwidth (20^{o}). The data agree in shape, however, the predicted magnitudes are slightly high. This was probably due to an inaccurate estimate of the illuminated area or dielectric constant since both affect the magnitude of the coherent component.

5.3 Prediction of Moisture Content

The power returned from a surface could only be measured near the specular angles since the reflectometer-scatterometer lacked sufficient sensitivity. This fact made angular diversity ineffective as a method of separating the effects of surface roughness and dielectric constant. Also angular diversity would be impractical to implement for an airborne system. Since the greatest measurement sensitivity is at the specular angle, this angle is fixed then frequency and polarization diversity are used for the separation. At the specular angle, the coherent component is dominant therefore, the expression for coherent rough surface reflection coefficient is used to express the effects of roughness. This expression was chosen over the coherent cross section expression because of simplicity and ease of measurement.

Separation of the effects of roughness first requires prediction of the roughness, then solution of the inverse scattering problem. The solution to the inverse scattering problem yields the target characteristics in the absence of roughness. The expression used is

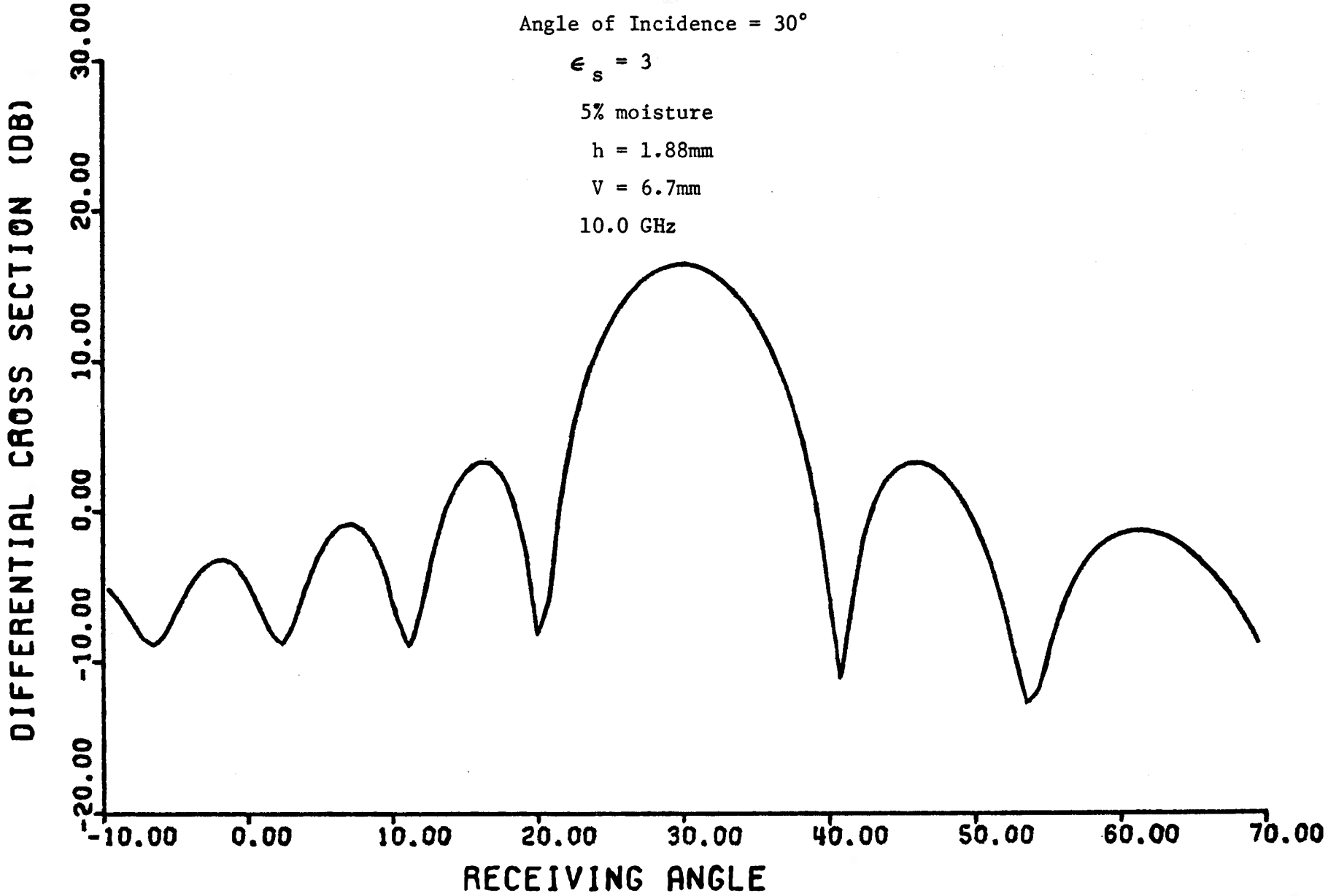

Figure 5.2-5 Pattern of sum of incoherent and coherent scattering cross section (horizontal polarization)

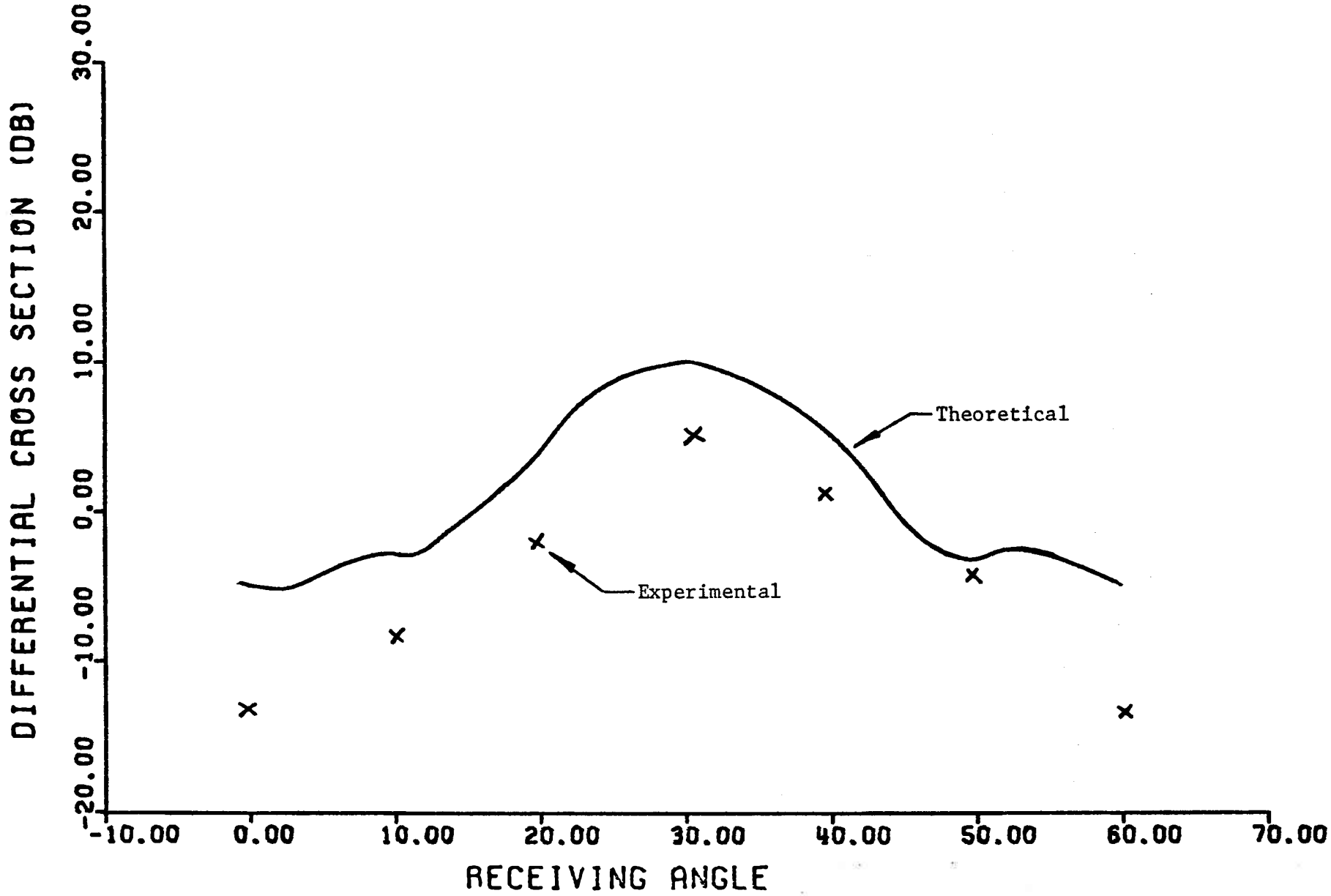

Figure 5.2-6 Average pattern of sum of incoherent and coherent scattering cross section and comparison to data (horizontal polarization)

$$\Gamma_h = \Gamma_h^R e^{2\beta^2 h^2 \cos^2 \theta} \qquad (5.3\text{-}1)$$

If the statistics of the surface are known, then the problem is simple. Figure 5.3-1 demonstrates the use of equation 5.3-1 to correct for the effects of roughness. The corrected curve is a close approximation to the measurements of a smoothed surface. If the statistics of the surface are not known, then diversity in frequency is used to determine the roughness. The experimental measurements were taken from both horizontal and vertical polarizations at 10^o and averaged to give the reflection coefficient at 0^o. The frequency dependence of the power reflection coefficient was then plotted in decibels. This frequency dependence is a result of both surface roughness and the dispersion of water. From Figure 2.1-4 it is apparent that for soils with percent moistures greater than 5 percent, the frequency dependence resulting from the water content is nearly constant. As a result, frequency dependence of the return with respect to moisture content is assumed to be negligible. The frequency dependence of the theoretical power reflection coefficient for different roughness (h) is shown in Figure 5.3-2. The slope of these curves is matched to the frequency dependence of the data and the best fit for roughness (h) is chosen. Then multiplication by the roughness factor

$$e^{2\beta^2 h^2} \qquad (5.3\text{-}2)$$

gives the estimate of the smooth surface reflection coefficient. The use of the roughness correction factor is shown in the correction of the moisture calibration curves for sand (Figure 5.3-3) and soil (Figure 5.3-4). The improvement from the original curves (Figures 4.2-4 and 4.2-5) is significant. The correction was necessary since in some cases the surface

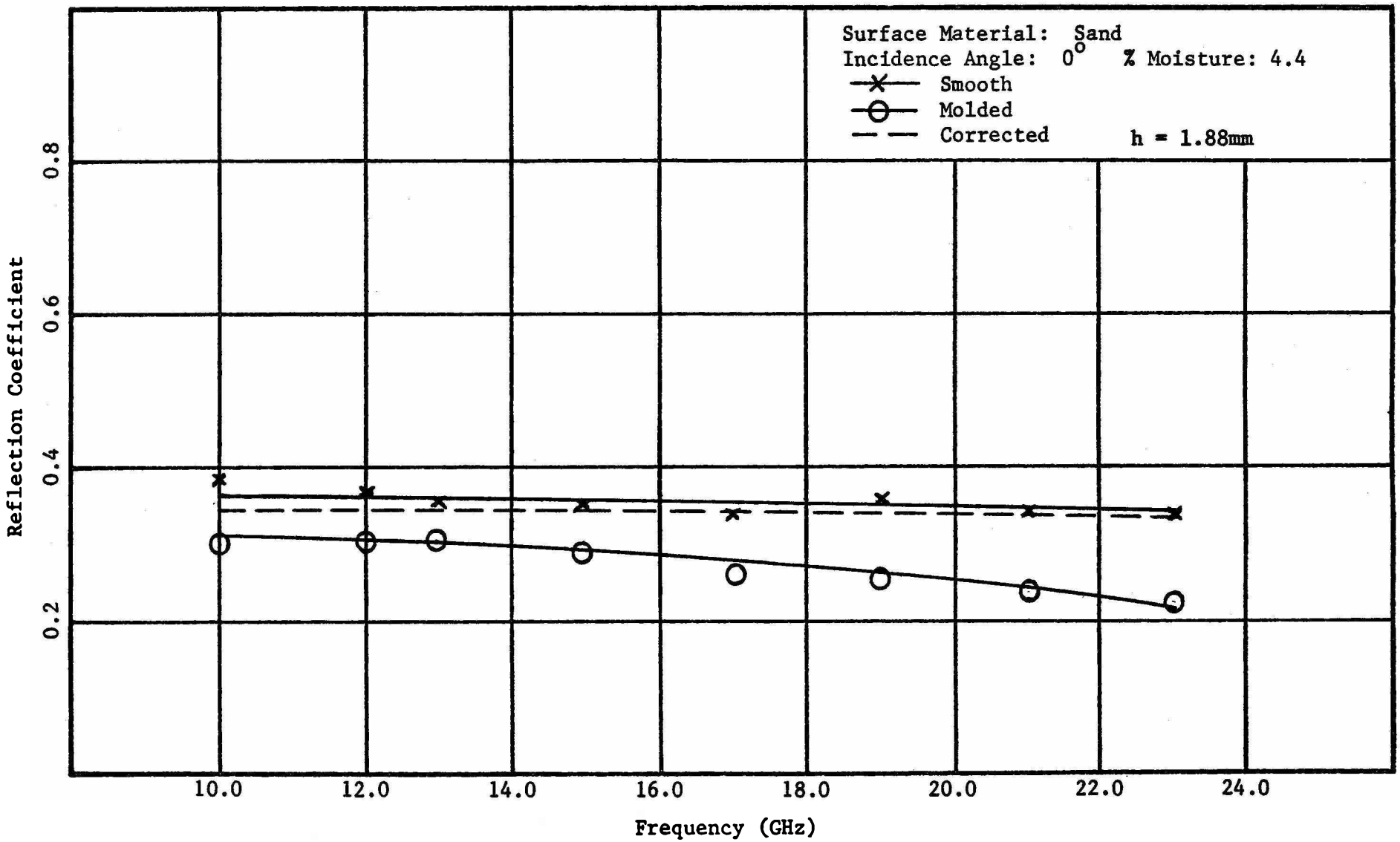

Figure 5.3-1 Correction for roughness of a surface with known statistics

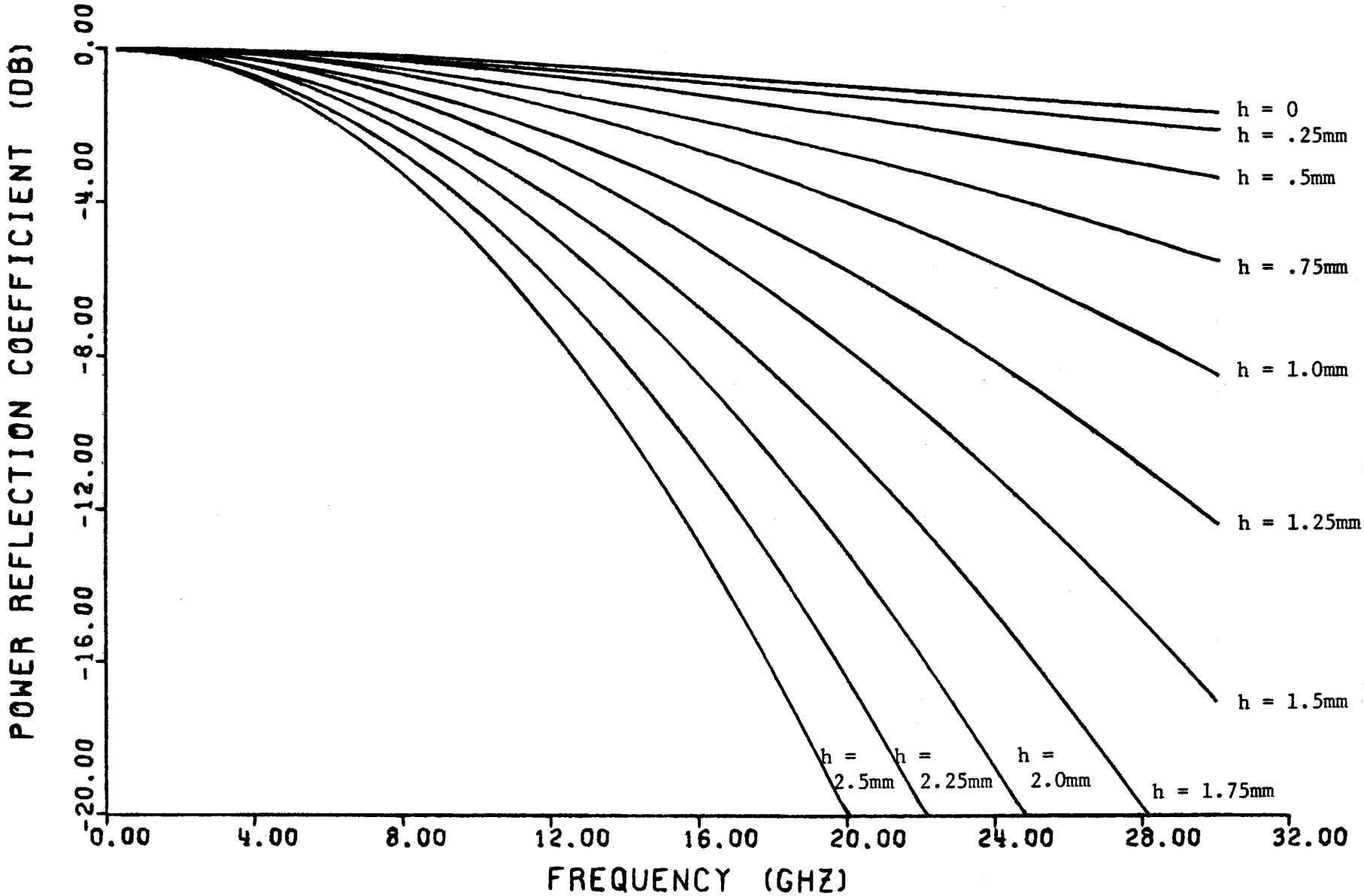

Figure 5.3-2 Effect of roughness on the power reflection coefficient

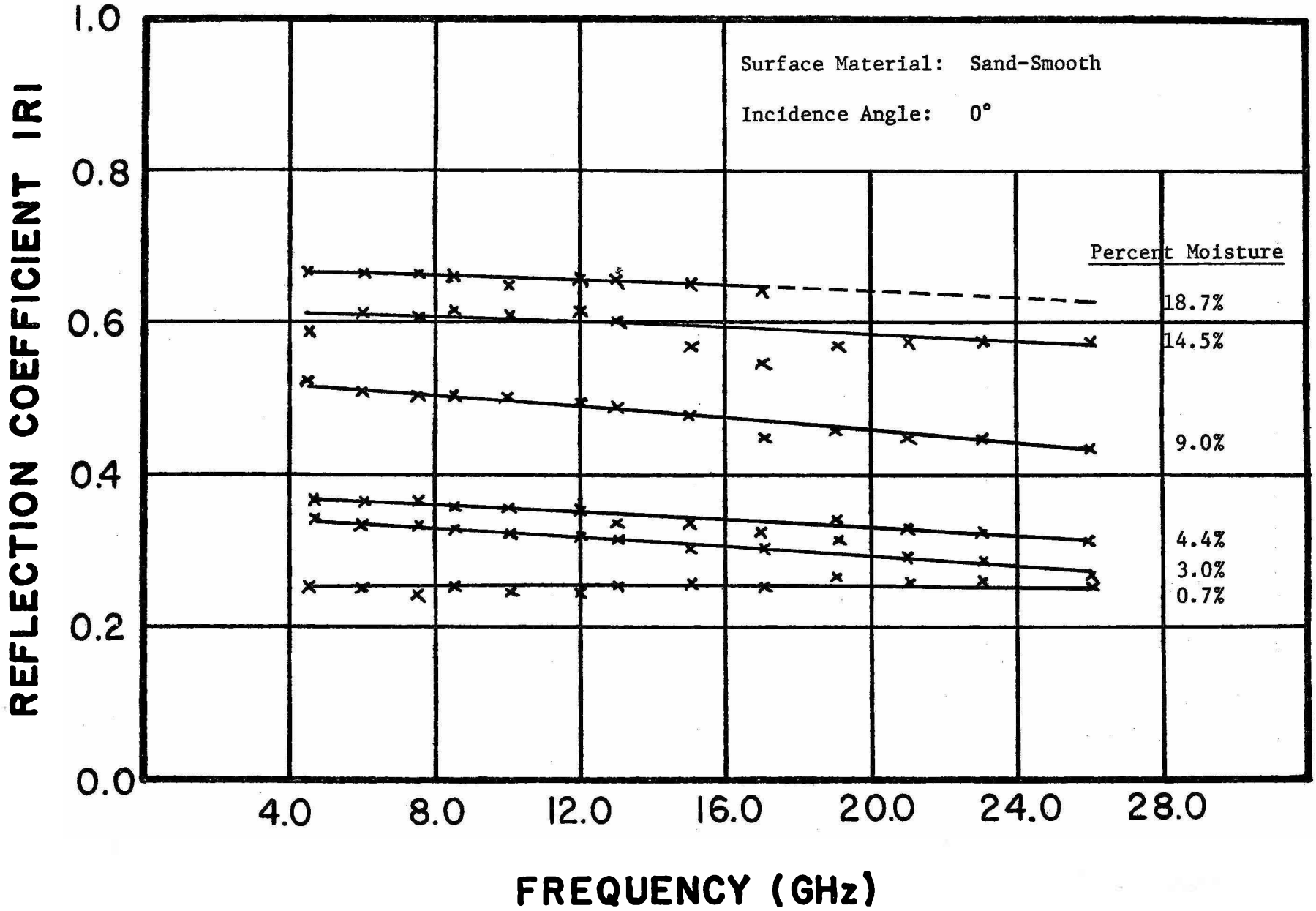

Figure 5.3-3 Sand moisture calibration curve corrected for roughness

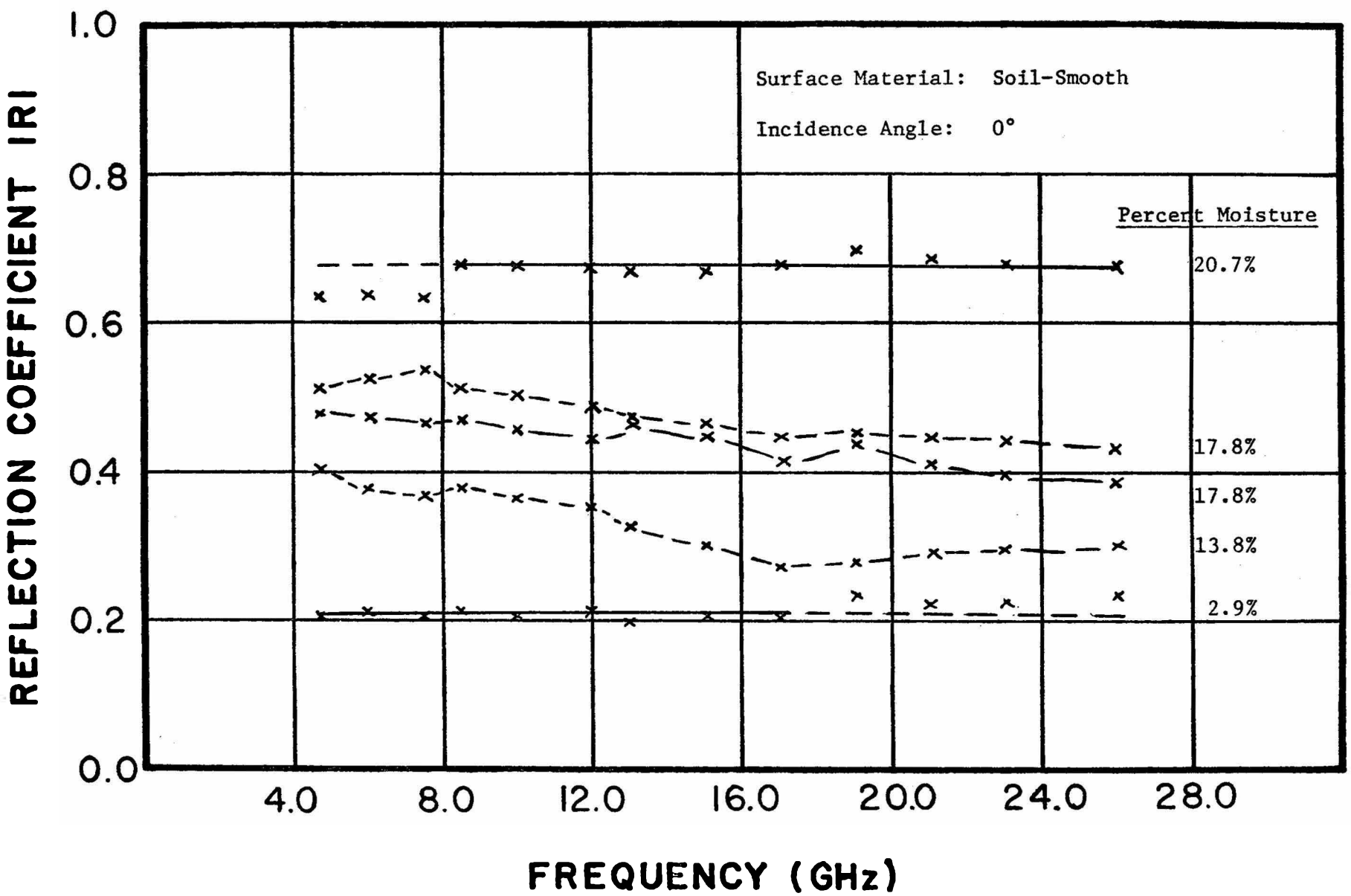

Figure 5.3-4 Soil moisture calibration curve corrected for roughness

could not be sufficiently smoothed to eliminate the roughness effects. The similarity to the theoretical curves (Figure 2.1-4) is obvious.

Elimination of the effects of roughness and the prediction of moisture content may be made by one of two methods. The first is to lower frequency sufficiently that the surface appears smooth. The second is to correct for the effects of roughness. Since the frequency range was set and the surfaces measured appeared rough, the second method must be used. To estimate the moisture content predicted in the presence of roughness, the reflection coefficient from the rough surface was plotted on its respective moisture calibration set (Figure 5.3-3 or Figure 5.3-4). Then the predicted moisture contents were calculated (Table 5.3-1) by a linear interpolation between the two adjacent moisture calibration curves. In some cases due to roughness the return was lower than the lowest moisture calibration curve. The predicted moisture content was then just listed as less than that moisture. To correct for the effects of roughness, the method discussed in the preceding paragraph was used. After correction, the reflection coefficient was also plotted on the respective moisture calibration set and moisture content predicted at several frequencies. These estimates were then averaged and listed in Table 5.3-1. Both laboratory and field measurements were taken on sand and soil. The measured values of soil moisture were calculated from

$$\% \text{ Moisture} = \frac{\text{Wet wt.} - \text{Dry wt}}{\text{Wet wt.}} \qquad (5.3\text{-}3)$$

Measurement of moisture content was done in this manner for matching with the mixing formula for dielectric constant (equation 2.1-3). This method differs from the standard moisture measurements calculated by

$$\% \text{ Moisture} = \frac{\text{Wet wt.} - \text{Dry wt.}}{\text{Dry wt.}} \qquad (5.3\text{-}4)$$

Surface Material	Predicted Moisture Content					Measured Moisture Content
	Uncorrected for Roughness				After Correction for Roughness	
	6 GHz	10 GHz	15 GHz	23 GHz		
1 Molded Sand	1.25	1.97	1.49	.7	3.17	4.29
2 Molded Sand	---	2.54	2.75	.7	4.79	5.6
3 Rough Sand	---	.70	.7	.7	4.70	5.6
4 Very Rough Sand	---	.7	.7	.7	4.90	5.6
5 Molded Soil	18.1	17.9	18.2	16.4	18.5	17.8
6 Field Soil	7.0	10.4	5.8	---	10.6	11.2
7 Molded Soil	---	---	14.4	5.0	15.7	14.8

Table 5.3-1

Moisture Content Predictions

Table 5.3-1 indicates a definite improvement in the estimation of moisture content after correction for roughness. The high uncorrected estimates from Set 5 were probably due to a surface film of water. When the surface of a very wet soil is compressed (application of the mold), water rises to the surface. The estimate for the field data (Set 6) at 10 GHz was also high. It is felt that this was due to some large scale structure or a layering effect as reflectivity was lower for both higher and lower frequencies about 10 GHz.

For the frequency range investigated, the maximum effective roughness (h) that could be measured was approximately four millimeters. The molded surface corresponded generally to an h of around one millimeter. This indicated that for a surface with smooth slopes, height variations up to about one inch could be measured and prediction of moisture made for the frequency range 4.0 to 26.5 GHz. For surfaces with slope variations that were not smooth, the effective roughness appeared much greater for smaller height variations. Therefore, if the roughness was discontinuous, correction can still be made but height variations must be limited to much less than one inch.

Apparently from examination of Sets 2, 3, and 4,correction for roughness may be made regardless of actual roughness. These three sets were made at the same soil moisture content with different types of roughness. Correction was made for effective roughness and the predictions were very close to the same.

The roughness scales commonly occurring in the agricultural situation are much greater than those mentioned above. Therefore, a much lower frequency would be needed to compensate for this increased roughness. Frequencies in the range of 500 MHz to 1 GHz would give a wavelength increase of

approximately 10 and possibly allow prediction of moisture content for roughnesses on the order of a plowed field. An even lower frequency would be desirable, however, this is limited by the size and expense of the antennas.

6. CONCLUSIONS AND RECOMMENDATIONS FOR FUTURE STUDIES

Conclusions

The direct relationship of smooth surface microwave reflectivity and dielectric constant indicated the possibility of relating moisture content and reflectivity due to the large disparity in the dielectric constant of dry soils and water. The experimental program conducted demonstrated the validity of this measurement approach for smooth surfaces and the curves of reflectivity or dielectric constant versus percent moisture content (Figures 4.2.1-8 through 4.2.1-12) permit an exceedingly accurate estimate of moisture content by remote means. This, by itself, provides an improved measurement capability, for the measure is an average over the illuminated area and variation of range or beamwidth permits easy variation of the sample size.

Unfortunately most natural surfaces are neither smooth nor vertically homogeneous and consequently the reflectivity is also a function of the surface structure. The effect of vertical inhomogeneities were investigated through the use of a layered model and it was found that discontinuities in moisture could be detected and estimated for relatively shallow depths. However, this required a continuous broad spectrum measurement system such as developed here with an effective bandwidth compatible with the electrical thickness of the layer.

The effects of surface roughness were first investigated by theoretical analysis of analytically tractable models. This analysis showed the roughness to be wavelength dependent with the effect decreasing as the ratio of mean height deviation to wavelength decreased (frequency decreased). Thus, the effects of roughness could be accounted for by either decreasing frequency until the surface appeared effectively smooth or to solve the inverse scattering

problem of estimating roughness from the broad spectrum measurement and then correcting the measurement for roughness.

The experimental program revealed that the discontinuous nature of naturally occurring rough surfaces made them appear effectively rougher and thus require a substantially lower measurement frequency for the surface to appear essentially smooth. Since the frequency range of the system was limited to 4-26.5 GHz, it was necessary to estimate the surface roughness and correct to an effective smooth surface reflectivity for even the prepared laboratory surfaces.

Using the results derived from the analytical models to correct the measured data, the prediction of moisture content was significantly improved for both laboratory and field measurements and for both continuous and discontinuous surfaces (Table 5.3-1). It is important to note that for discontinuous surfaces, the roughness determined is an "effective" value and not the mean square height deviation used in the analytical expressions. However, the experimental program indicated that use of such an "effective" parameter still provided an excellent estimate of the effective smooth surface reflectivity and, consequently, the percent moisture content.

For the frequency range investigated (4-26.5 GHz), the maximum allowable roughness was approximately one inch. This was limited principally by the effects of discontinuous surface roughness. Extrapolating from these results, it appears that a frequency range of 500 MHz to 1 GHz will be necessary to permit moisture content prediction for most agricultural surfaces. This is near the lower limit of operation for aircraft or spacecraft borne systems, and it is particularly important to note that even in this range roughness effects will <u>not</u> be negligible and a broad spectrum measurement and correction will be required.

Recommendations for Future Studies

The single most important task that should be considered is the extension of this study to include frequencies down to, or below, 1 GHz. In addition, the correction algorithm devised here used the effective smooth surface power reflectivity which involves strictly the coherent reflection component. This is basically what is measured by a passive radiometric system and the algorithm mades use of only frequency diversity. The investigation should be extended to apply the same techniques for investigation of the incoherent component as a function of both frequency and incidence angle.

The effects of vegetation cover should be investigated in the same manner and over approximately the same frequency range. In this investigation, it is essential that the linear depolarized component be recorded in addition to the like polarized component to determine if these data may be used to separate the contributions of surface and volume scattering effects.

The objectives of a future study to extend this program would be as follows:

1) To determine what wavelength must be used for both passive and active sensors so that surface roughness effects are negligible for the purposes of measuring soil moisture and for surfaces representative of bare agricultural fields in various stages of tillage.
2) To determine what range of frequencies, either continuous or discrete, are necessary for both passive and active sensors to estimate the surface roughness of bare agricultural fields and permit correction for the effects of roughness in the measurement of soil moisture.
3) To determine the relative magnitude of vegetation and soil signal components for vegetated surfaces consisting of grass with various

volume densities of both vegetative matter and water.

4) To perform the above measurements with an active system at both backscattering and specular angles to permit correlation of radar cross section and specular reflectivity (emissivity) of the same surface.

5) To correlate the direct measurement of specular reflectivity with passive measurements of emissivity at the same frequency.

6) To measure the linear depolarized return for both vegetated and non-vegetated surfaces to determine if it may be used to help separate the return into surface and volume contributions.

7) To compare high frequency measurements of vegetation with available models to determine if structural effects may be determined by frequency and polarization diversity permitting an estimate of the dielectric characteristics of the vegetation volume.

Such an advanced study could be accomplished with relatively minor modifications to the system developed in this program. Basically, the requirements would be to:

1) Increase frequency coverage with the addition of plug-ins, antennas, and associated hardware.

2) Increase system sensitivity by modifying to permit operation as a frequency modulation-continuous wave reflectometer utilizing intermediate frequency amplification.

3) Improve mobility of system by mobile mounting on a small trailer.

BIBLIOGRAPHY

Abramowitz, M. and Stegun, I. A., (Editors), Handbook of Mathematical Functions, U. S. Department of Commerce, National Bureau of Standards, Applied Mathematics Series 55, 1964.

Ament, W. S., "Toward a Theory of Reflection by a Rough Surface," Proc. IRE, Vol. 41, pp. 142-146, 1953.

Beckman, P. and Spizzichino, A., The Scattering of Electromagnetic Waves from Rough Surfaces, The MacMillan Co., New York, 1963.

Davis, B. R., Lundien, J. R., and Williamson, A. N. Jr., "Feasibility of the Use of Radar to Detect Surface and Ground Water," Technical Report No. 3-727, U.S. Army Engineering Waterways Experiment Station, Vicksburg, Mississippi, April, 1966.

Edgerton, A. T., Ruskey, F., Williams, D., Stogryn, A., Poe, G., Meeks, D., and Russell, O., "Microwave Emission Characteristics of Natural Materials," Microwave Division Aerojet-General Corporation, Report No. 9016R-8, El Monte, California, 1971.

Grant, E., Buchanan, T., and Cook, H., "Dielectric Behavior of Water at Microwave Frequencies," J. Chem. Phys., Vol. 26, p. 156, 1957.

Hoskyn, J. P. and Bryan, B. B., "Subsurface Irrigation Research in Arkansas," Water Resources Research Center, No. 3, Series 176, Univ. of Arkansas, June, 1969.

Lundien, J. R., "Terrain Analysis by Electromagnetic Means, Report 2," Technical Report No. 3-693, U.S. Army Engineer Waterways Experiment Station, Vicksburg, Mississippi, September, 1966.

Malmberg, C. and Margott, A., "Dielectric Constant of Water from 0° to 100°C," J. Res. Nat. Bur. Standards, Vol. 56, No. 1, 1956.

Peake, W. H., "The Interaction of Electromagnetic Waves with Some Natural Surfaces," Ph.D. Dissertation, Ohio State University, Columbus, Ohio, 1959.

Peake, W. H., "Terrain Radar Scatter-Experimental and Theoretical," Presented at the Western Electronic Show and Convention, August, 1968.

Poe, G., Stogryn, A., and Edgerton, A. T., "Determination of Soil Moisture Content Using Microwave Radiometry," Final Report No. 1684 FR-1 for DOC Contract No. 0-35239, Aerojet-General Corp., Microwave Div., El Monte, California, 1971.

Ramo, S., Whinnery, J. R., and Van Duzer, T., Fields and Waves in Communications Electronics, John Wiley & Sons, Inc., New York, 1967.

Rayleigh, L. D., The Theory of Sound, 3rd. ed., MacMillian, London, 1896.

Rice, S. O., "Reflection of Electromagnetic Waves from Slightly Rough Surfaces," Communications in Pure and Applied Mathematics, Vol. 4, pp. 351-378, 1951.

Rouse, J. W., Jr., "The Frequency Dependence of Backscatter from Rough Surfaces," CRES Technical Report 133-4, University of Kansas, September, 1968.

Ruck, G. T., Barrick, D. E., Stuart, W. D., and Kirchbaum, C. K., Radar Cross Section Handbook, Plenum Press, New York, 1970.

Skolnik, M. I., Introduction to Radar Systems, McGraw-Hill Book Co., New York, 1962.

Stratton, J. A., Electromagnetic Theory, McGraw-Hill Book Co., New York, 1941.

Valenzuela, C. R., "Depolarization of EM Waves by Slightly Rough Surfaces," IEEE Trans. on Antennas and Propagation, Vol. AP-15, No. 4, July 1967.

Von Hipple, A. R., (Ed.), Dielectric Materials and Applications, The MIT Press, Cambridge, Mass., 1954.

APPENDIX A

CONVERSION OF DIFFERENTIAL RADAR SCATTERING CROSS SECTION TO EFFECTIVE REFLECTION COEFFICIENT

For a radar operating in a bistatic configuration, two different terms can be used to express the target parameters. Differential radar scattering cross section is the term normally used to express target characteristics. However, for the bistatic case and particularly for reception at the specular angle, it is often convenient to express the target characteristics by an effective reflection coefficient. This reflection coefficient could then be compared to the Fresnel reflection coefficient for a smooth semi-infinite medium. A relationship is therefore needed between radar scattering cross section and the effective reflection coefficient to facilitate conversion between the two methods of expressing target characteristics.

The normal form for the radar equation is

$$P_r = \frac{P_t G_t G_r \lambda^2}{(4\pi)^3 R^4} \sigma \qquad \text{(A1)}$$

where G_t is the gain of the transmitting antenna, G_r is the gain of the receiving antenna, P_r is the recieved power, P_t is the transmitted power, R is the range, is the wavelength and is the radar scattering cross section of the target. Cross section has units of area. This unit is normalized to a differential scattering cross section (σ_o)

$$\sigma_o = \frac{\sigma}{A} \qquad \text{(A2)}$$

where A is the illuminated area. The derivation of the radar equation

assumes equal ranges to transmitter and receiver, constant range across the illuminated area, a uniform wquare beam across the illuminated area, constant scattering cross section across the illuminated area, and uniform illumination of the receiving aperture.

Using image theory and an effective reflection coefficient for the surface, a similar form of the radar equation may be developed (Peake 1968). From image theory, the range is doubled. An effective electric field reflaction coefficient Γ^R_{eff} is used as the surface parameter. The resulting formula for received power is

$$P_r = \frac{P_t G_t G_r}{4\pi (2R)^2} \left|\Gamma^R_{eff}\right|^2 \qquad \text{(A3)}$$

The resulting relationship between differential radar cross section and effective reflection coefficient is thus

$$\left|\Gamma^R_{eff}\right|^2 = \frac{\sigma_o A}{\pi R^2} \qquad \text{(A4)}$$

DERIVATION OF SMALL PERTURBATION
SCATTERING COEFFICIENTS

APPENDIX B

In this appendix, the scattering coefficients from S. O. Rice (1951) are formulated.

REPRESENTATION OF THE ROUGH SURFACE

First of all, the surface is represented as the product of two one-dimensional Fourier series. The surface is assumed to be periodic with period L. This will be no restriction on the generality of the representation of the surface, however, since L will be made very large. The coefficients of this series are taken to be random. The surface is therefore,

$$z = f(x,y) = \sum_m \sum_n [A_m \cos(a_m x) + B_m \sin(a_m x)][C_n \cos(a_n y) + D_n \sin(a_n y)] \tag{B1}$$

$$a = \frac{2\pi}{L} \qquad m > 0,\ n > 0$$

where A, B, C and D are independent random coefficients and m and n are integers greater than zero.

$$z = \sum_m \sum_n [A_m C_n \cos(a_m x) + B_m C_n \sin(a_m x)] \cos(a_n y) + [A_m D_n \cos(a_m x) + B_m D_n \sin(a_m x)] \sin(a_n y) \tag{B2}$$

Since the surface is a Fourier series representation, A must be even and B must be odd with respect to the sign of m. This is likewise true for C and D with respect to the sign of n. Let,

$$\begin{aligned} a_{mn} &= A_m C_n \\ b_{mn} &= B_m C_n \\ c_{mn} &= A_m D_n \\ d_{mn} &= B_m D_n \end{aligned} \tag{B3}$$

now the surface becomes

$$z = \sum_m \sum_n \left[a_{mn} \cos(a_m x) + b_{mn} \sin(a_m x) \right] \cos(a_n y)$$

$$+ \left[c_{mn} \cos(a_m x) + d_{mn} \sin(a_m x) \right] \sin(a_n y) \qquad \text{(B4)}$$

$$m > 0, \; n > 0$$

Expressing the series as an exponential series by Euler's formulas,

$$z = \sum_m \sum_n \left[a_{mn} \tfrac{1}{2} \left(e^{j a_m x} + e^{-j a_m x} \right) + b_{mn} \tfrac{1}{j2} \left(e^{j a_m x} - e^{-j a_m x} \right) \right]$$

$$\cdot \tfrac{1}{2} \left(e^{j a_n y} + e^{-j a_n y} \right) + \left[c_{mn} \tfrac{1}{2} \left(e^{j a_m x} + e^{-j a_m x} \right) \right.$$

$$\left. + d_{mn} \tfrac{1}{j2} \left(e^{j a_m x} - e^{-j a_m x} \right) \right] \cdot \tfrac{1}{2} \left(e^{j a_n y} - e^{-j a_n y} \right)$$

$$= \tfrac{1}{4} \sum_m \sum_n \left[(a_{mn} - j b_{mn} - j c_{mn} - d_{mn}) \, e^{j(a_m x + a_n y)} \right.$$

$$+ (a_{mn} - j b_{mn} + j c_{mn} + d_{mn}) \, e^{j(a_m x - a_n y)} \qquad \text{(B5)}$$

$$+ (a_{mn} + j b_{mn} - j c_{mn} + d_{mn}) \, e^{j(-a_m x + a_n y)}$$

$$\left. + (a_{mn} + j b_{mn} + j c_{mn} - d_{mn}) \, e^{j(-a_m x - a_n y)} \right)$$

The only assumptions made are that a_{mn}, b_{mn}, c_{mn}, and d_{mn} are independent random variables that are gaussian distributed with zero mean and the same variance of $4\pi^2 \, W(p,q)/L^2$. Also it is assumed that for given values of m and n, the real and imaginary parts of the random coefficients have the same variance irregardless of the sign on m and n $W(p,q)$ is the roughness distribution function of the surface. $W(p,q)\,dpdq$ is a measure of the contribution of the Fourier components with radian frequencies between p and p + dp in the x direction and q and q + dq in the y direction. Also the surface can be represented by its height correlation function $\bar{z}^2 \, \rho \, (\xi,\eta)$. Here $\bar{z}^2$ is the mean square height of the surface $\bar{z}^2 = \langle f^2(x,y) \rangle$ and $\rho(\xi,\eta)$ is the auto correlation of the surface.

The height correlation function and the roughness distribution functions form a Fourier transform pair.

$$W(p,q) = \frac{1}{\pi^2} \iint_{-\infty}^{\infty} \bar{z}^2 \rho(\xi,\eta)\, e^{j(p\xi+q\eta)}\, d\xi\, d\eta \tag{B6}$$

The surface can also be expressed as

$$z = \sum_m \sum_n \left(\frac{a_{mn} + j\, b_{mn} + j\, c_{mn} - d_{mn}}{4} \right) e^{j(-a_m x - a_n y)} \tag{B7}$$

$$-\infty < m < \infty \quad , \quad -\infty < n < \infty$$

since the sign on the coefficients is affected by their evenness or oddness. For example, $a_{mn} = A_m C_n$ where A_m and C_n are even. Therefore, for $m>0$, $n>0$ there will be no sign change. Now for $m<0$, $n<0$ or $-m>0$, $-n>0$

$$\begin{aligned} a_{-m-n} &\rightarrow a_{mn} \\ b_{-m-n} &\rightarrow -b_{mn} \\ c_{-m-n} &\rightarrow -c_{mn} \\ d_{-m-n} &\rightarrow d_{mn} \end{aligned} \tag{B8}$$

therefore, for -m and -n the summed term is

$$\frac{a_{mn} - j\, b_{mn} - j\, c_{mn} - d_{mn}}{4} \qquad \exp\,(iamx + iany)$$

which is identical to the first term of equation 5. A similar procedure for $m<0$, $n>0$ and $m>0$, $n<0$ gives the other two terms of equation 5, therefore, equation 7 is a complete representation of the surface. Now let $P(m,n) = (a_{mn} + j\, b_{mn} + j\, c_{mn} - d_{mn}/4)$ which is a new random variable with the restriction that $P(-m,-n) = \underline{P}^*(m,n)$. This condition is necessary to make f(x,y) real. The properties of P(m,n) result from being the summation of the a,b,c, and d terms. $\langle\,\rangle$ denotes average. The mean value is

$$\langle P(m,n) \rangle = 0 \tag{B9}$$

since the P(m,n) are independent

$$\langle P(m,n)\ P(u,v)\rangle = 0 \quad (-m,-n) \neq (u,v) \tag{B10}$$

The variance of P(m,n) results from P(m,n) being the sum of four random variables. Since the mean is zero, the mean square value equals the variance.

$$\langle P(m,n)\, P^*(m,n)\rangle = \frac{1}{16}\left[4\left(4\pi^2 W(p,q)/L^2\right)\right] = \pi^2 W(p,q)/L^2$$

$$p = 2\pi m/L \tag{B11}$$
$$q = 2\pi n/L$$
$$W(p,q) = W(|p|,|q|)$$

The equation for the surface is therefore,

$$z = f(x,y) = \sum_{m\,n} P(m,n)\, e^{-j a(mx+ny)} \tag{B12}$$
$$a = 2\pi/L$$

The above equation states that the surface is periodic in both x and y with period L where L is assumed to be large. Therefore, the surface is effectively random.

The two vectors which define the surface at a point are the tangent vectors to the surface at the point. The equation for the surface is

$$f = x\hat{a}_x + y\hat{a}_y + z\hat{a}_z \tag{B13}$$

The resulting tangent vectors are

$$T_x = 1\,\hat{a}_x + f_x\,\hat{a}_z \tag{B14}$$
$$T_y = 1\,\hat{a}_y + f_y\,\hat{a}_z$$

The normal to the surface is then

$$N = \frac{T_x \times T_y}{|T_x \times T_y|} \tag{B15}$$

$$N = \frac{-f_x\hat{a}_x - f_y\hat{a}_y + \hat{a}_z}{\sqrt{1+f_x^2+f_y^2}}$$

Separating N into its components gives

$$N_x = -f_x/\sqrt{1+f_x^2+f_y^2}$$
$$N_y = -f_y/\sqrt{1+f_x^2+f_y^2} \tag{B16}$$
$$N_z = 1/\sqrt{1+f_x^2+f_y^2}$$

SCATTERING FROM A DIELECTRIC BOUNDARY - HORIZONTAL POLARIZATION

For the case of a horizontally polarized wave incident at a dielectric boundary, the geometry is shown in Figure B.1.

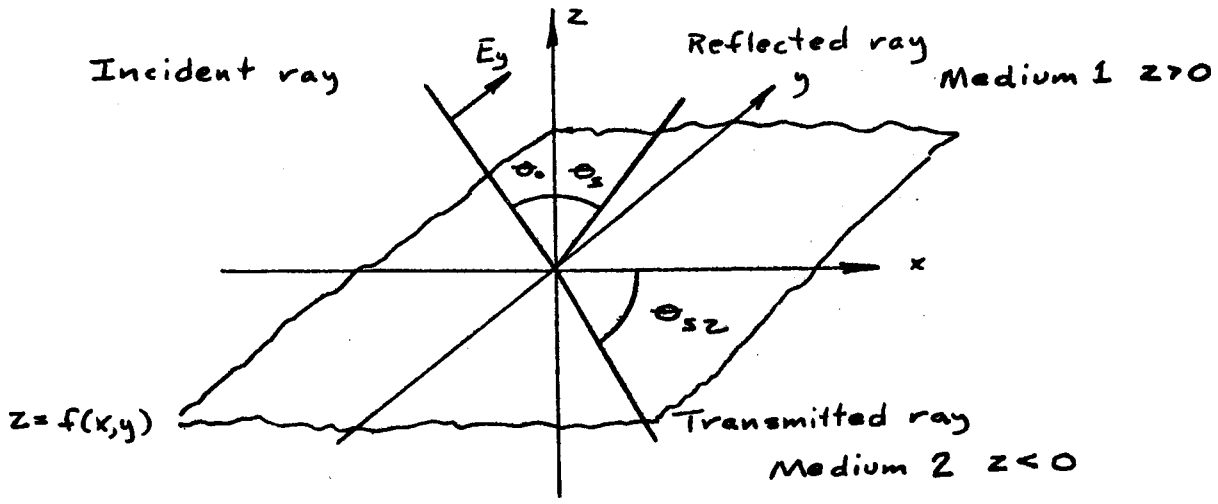

Figure B.1

The incident field is assumed to be of unit intensity. Then the electric fields can be expressed as equation 17.

$$E_x = \begin{cases} \sum_{mn} A_{mn} E(m,n,z) & z > f \\ \sum_{mn} G_{mn} F(m,n,z) & z < f \end{cases}$$

$$E_y = \begin{cases} E^+ + \sum_{mn} B_{mn} E(m,n,z) & z > f \\ E^- + \sum_{mn} H_{mn} F(m,n,z) & z < f \end{cases} \qquad \text{(B17)}$$

$$E_z = \begin{cases} \sum_{mn} C_{mn} E(m,n,z) & z > f \\ \sum_{mn} I_{mn} F(m,n,z) & z < f \end{cases}$$

$$E(m,n,z) = e^{-ja(mx+ny)-jb(m,n)z} e^{j\omega t}$$

$$F(m,n,z) = e^{-ja(mx+ny)+jc(m,n)z} e^{j\omega t}$$

The summations on m and n extend from $-\infty$ to $+\infty$. The exponential forms for (m,n,z) and F(m,n,z) ensure that the fields satisfy the wave equation.

For medium 1, the scattered field must have the same propagation constant as the incident field. If β is the propagation constant for medium 1 (here assumed to be free space, then

$$\beta^2 = a^2m^2 + a^2n^2 + b^2(m,n)$$

$$b(m,n) = (\beta^2 - a^2m^2 - a^2n^2)^{1/2} \tag{B18}$$

Now medium 2 is assumed to have relative permeability of one and relative dielectric constant of ϵ_r. Also medium 2 has conductivity g, therefore, the propagation constant is

$$\gamma = \beta\sqrt{\epsilon_r + g/j\omega\epsilon_0}$$

$$\gamma^2 = a^2m^2 + a^2n^2 + c^2(m,n) \tag{B19}$$

$$c(m,n) = (\gamma^2 - a^2m^2 - a^2n^2)^{1/2}$$

The time variation term $e^{j\omega t}$ will be understood in the following. Also the conductivity is assumed to be zero.

The E^+ term in equation 17 is the sum of the incident and reflected rays. If we define

$$\alpha = \sin\theta_0$$

$$\gamma = \cos\theta_0$$

$$\alpha' = \sin\theta_{s2}$$

$$\gamma' = \cos\theta_{s2}$$

for horizontal polarization, the incident field is in the y-direction. The direction of propagation for the incident field is

$$e^{-j\beta(\alpha x - \gamma z)}$$

and for the reflected field

$$e^{-j\beta(\alpha x + \gamma z)}$$

therefore, for unit incident intensity, in medium 1

$$E^{+} = e^{j\beta\alpha x}\left[e^{+j\beta\gamma z} + \Gamma_h e^{-j\beta\gamma z}\right] \tag{B20}$$

likewise, in medium 2

$$E^{-} = -T_h e^{-j\gamma(\alpha' x + \gamma' z)} \tag{B21}$$

Here Γ and T are the Fresnel reflection and transmission coefficients given in equation 22.

$$\Gamma_h = \frac{\beta\gamma - \gamma\gamma'}{\beta\gamma + \gamma\gamma'}$$
$$T_h = \frac{2\beta\gamma}{\beta\gamma + \gamma\gamma'} \tag{B22}$$

Snell's law requires that

$$\beta\alpha = \gamma\alpha' \tag{B23}$$

The component of the propagation constant in the x-direction is βx. For the field to be periodic in x and y of a period L, βx must be an integer multiple of $a = 2\pi/L$

$$a\nu = \beta\alpha \qquad \nu \text{ an integer} \tag{B24}$$

From this it follows that the angle of incidence θ_o is restricted to certain values, however, L is assumed very large, therefore, a ν exists for approximately any angle of incidence.

Now the coefficients A_{mn}, B_{mn}, C_{mn}, G_{mn}, H_{mn}, and I_{mn} will be determined using the divergency relation, boundary conductions, and the assumption that the surface has small height variations with respect to wavelength. We assume that βf, f_x, and f_y are on the same order of smallness which will be denoted as $O(f)$. The second order terms will be designated $O(f^2)$. All terms smaller than $O(f^2)$ will be neglected. The above conditions on the surface require small height variations and smooth

slopes on the surface.

EVALUATION OF COEFFICIENTS

The boundary conditions at the sruface require continuity of the electric and magnetic fields. If N, as in equation 15, is the normal to the surface and E is the electric field vector, then the tangential component of the electric field is

$$E - N(E \cdot N) \tag{B25}$$

The tangential components of Ex, Ey, and Ex, must all be continuous, therefore,

$$E_x - N_x (E_x N_x + E_y N_y + E_z N_z)$$
$$E_y - N_y (E_x N_x + E_y N_y + E_z N_z)$$
$$E_z - N_z (E_x N_x + E_y N_y + E_z N_z)$$

must be continuous at the boundary. However, if two of the components are continuous the other is also continuous. This can be shown by multiplying the x-component by N_x and the y-component by N_y and adding. Therefore, unless N_z is zero, the component will also be continuous at the boundary. The boundary conditions necessary to evaluate the coefficients of the fields are the continuity of the following terms at the boundary.

$$E_x - N_x (E_x N_x + E_y N_y + E_z N_z)$$
$$E_y - N_y (E_x N_x + E_y N_y + E_z N_z) \tag{B26}$$
$$H_x - N_x (H_x N_x + H_y N_y + H_z N_z)$$
$$H_y - N_y (H_x N_x + H_y N_y + H_z N_z)$$

With the assumption that f, f_x, and f_y are $O(f)$, the expansion of N_z is

$$N_z = (1 + f_x^2 + f_y^2)^{-1/2}$$
$$\approx 1 - \tfrac{1}{2}(f_x^2 + f_y^2) \qquad \text{(B27)}$$
$$= 1 + O(f^2)$$

Therefore, N_x and N_y become

$$N_x = -f_x\,[1 + O(f^2)] = -f_x + O(f^3) \qquad \text{(B28)}$$
$$N_y = -f_y\,[1 + O(f^2)] = -f_y + O(f^3)$$

At the surface z = f the E^+ ray is $O(1)$ since when expanded in a series

$$E^+ = e^{j\beta\alpha x}\left(e^{j\beta\gamma f} + \Gamma e^{-j\beta\gamma f}\right)$$
$$= \left[(1+\Gamma)\cos\beta\gamma f + j(1-\Gamma)\sin\beta\gamma f\right] e^{j\beta\alpha x}$$
$$= (1+\Gamma)\left(1 - \frac{\beta^2\gamma^2 f^2}{2} - \cdots\right) e^{j\beta\alpha x}$$
$$= O(1)$$

then E_y is $O(1)$. Assume E_x and E_y, being scattered waves, are $O(f)$. Then the first two terms in Equation 23, ignoring $O(f^3)$ terms become

$$E_x - N_x N_y E_y - N_x N_z E_z$$
$$E_y - N_y^2 E_y - N_y N_z E_z$$

For the last two terms of equation 23 following field relationship is required

$$\nabla \times E = -\mu \frac{\partial H}{\partial t}$$

Since the time factor is e^{-iwt}, in phasor notation

$$\nabla \times E = -j\omega\mu H$$

The -iwt coefficient will be common to all terms and may be dropped.

$$H \Rightarrow \left(\frac{\partial E_z}{\partial y} - \frac{\partial E_y}{\partial z}\right)\bar{a}_x + \left(\frac{\partial E_x}{\partial z} - \frac{\partial E_z}{\partial x}\right)\bar{a}_y + \left(\frac{\partial E_y}{\partial x} - \frac{\partial E_x}{\partial y}\right)\bar{a}_z$$

Therefore the last two terms of equation 23 become

$$\left(\frac{\partial E_z}{\partial y} - \frac{\partial E_y}{\partial z}\right) - N_x^2\left(\frac{\partial E_z}{\partial y} - \frac{\partial E_y}{\partial z}\right) - N_x N_y\left(\frac{\partial E_x}{\partial z} - \frac{\partial E_z}{\partial x}\right) - N_x N_z\left(\frac{\partial E_y}{\partial x} - \frac{\partial E_x}{\partial y}\right)$$

$$\left(\frac{\partial E_x}{\partial z} - \frac{\partial E_z}{\partial x}\right) - N_x N_y\left(\frac{\partial E_z}{\partial y} - \frac{\partial E_y}{\partial z}\right) - N_y^2\left(\frac{\partial E_x}{\partial z} - \frac{\partial E_z}{\partial x}\right) - N_y N_z\left(\frac{\partial E_y}{\partial x} - \frac{\partial E_x}{\partial y}\right)$$

Now assuming N_x, N_y, E_x, E_z, and their partials are $O(f)$ and $N_z = 1$. The continuity terms become

$$E_x - N_x N_y E_y - N_x E_z$$

$$E_y - N_y^2 E_y - N_y E_z \tag{B29}$$

$$\frac{\partial E_z}{\partial y} - (1 - N_x^2)\frac{\partial E_y}{\partial z} - N_x \frac{\partial E_y}{\partial x} + N_x \frac{\partial E_x}{\partial y}$$

$$\frac{\partial E_x}{\partial z} - \frac{\partial E_z}{\partial x} + N_x N_y \frac{\partial E_y}{\partial z} - N_y \frac{\partial E_y}{\partial x} - N_y \frac{\partial E_x}{\partial y}$$

From the Fresnel reflection coefficients, $1 + \Gamma = T$. The $N_x N_y E_y$ and $N_y^2 E_y$ terms drop out thwn the boundary conditions are applied since the specular rays of E_y are $O(f^2)$

$$E^+ + E^- = e^{-j\beta\alpha x}\left(e^{j\beta\gamma f} + \Gamma e^{-j\beta\gamma f} - T e^{j T\gamma f}\right)$$

$$= e^{-j\beta\alpha x} f^2 \frac{T}{2}\left(T^2\gamma'^2 - \beta^2\gamma^2\right)$$

Let

$$U = \frac{T}{2}\left(T^2\gamma'^2 - \beta^2\gamma^2\right) \tag{B30}$$

Therefore, the $N_x N_y E_y$ and $N_y^2 E_y$ terms drop out since they are $O(f^4)$.

Also the $N_x^2 \frac{\partial Ey}{\partial z}$ and $N_x N_y \frac{\partial Ey}{\partial x}$ terms will drop out, however, here $O(f^3)$ terms are needed since the derivative is taken.

$$\frac{\partial E_y}{\partial z} = \frac{\partial}{\partial z}\left(E^+ + E^-\right)$$

$$= \frac{\partial}{\partial z}\left[e^{-j\beta\alpha x}\left(1 + j\beta\gamma f - \frac{\beta^2\gamma^2 f^2}{2} - j\frac{\beta^3\gamma^3 f^3}{6} + \Gamma - j\beta\gamma f\Gamma\right.\right. \tag{B31}$$

$$\left.\left. - \Gamma\frac{\beta^2\gamma^2 f^2}{2} + j\frac{f^3\Gamma\beta^3\gamma^3}{6} - T - j T\gamma\gamma' f T + T\frac{T^2\gamma'^2 f^2}{2} + j\frac{f^3 T^3\gamma'^3}{6}\right)\right]$$

$$= e^{-j\beta\alpha x}\left[2fU + jU T\gamma\gamma' f^2\right]$$

Therefore, $N_x^2 \frac{\partial Ey}{\partial x}$ and $N_x N_y \frac{\partial Ey}{\partial x}$ are $O(f^3)$ and are dropped.

Therefore, at z = f the boundary conditions are

$$\sum_{mn} A_{mn} E(m,n,f) - N_x \sum_{mn} C_{mn} E(m,n,f) = \sum_{mn} G_{mn} F(m,n,f) - N_x \sum_{mn} I_{mn} F(m,n,f)$$

$$E^+ + \sum_{mn} B_{mn} E(m,n,f) - N_y \sum_{mn} C_{mn} E(m,n,f) = E^- + \sum_{mn} H_{mn} F(m,n,f) - N_y \sum_{mn} I_{mn} F(m,n,f)$$

$$\frac{\partial}{\partial y}\left(\sum_{mn} C_{mn} E(m,n,f)\right) - \frac{\partial}{\partial z}\left(E^+ + \sum_{mn} B_{mn} E(m,n,f)\right) - N_x \frac{\partial}{\partial x}\left(E^+ + \sum_{mn} B_{mn} E(m,n,f)\right)$$

$$+ N_x \frac{\partial}{\partial y}\left(\sum_{mn} A_{mn} E(m,n,f)\right) = \frac{\partial}{\partial y}\left(\sum_{mn} I_{mn} F(m,n,f)\right) - \frac{\partial}{\partial z}\left(E^- + \sum_{mn} H_{mn} F(m,n,f)\right) \qquad \text{(B32)}$$

$$- N_x \frac{\partial}{\partial x}\left(E^- + \sum_{mn} H_{mn} F(m,n,f)\right) + N_x \frac{\partial}{\partial y}\left(\sum_{mn} G_{mn} F(m,n,f)\right)$$

$$\frac{\partial}{\partial z}\left(\sum_{mn} A_{mn} E(m,n,f)\right) - \frac{\partial}{\partial x}\left(\sum_{mn} C_{mn} E(m,n,f)\right) - N_y \left(E^+ + \sum_{mn} B_{mn} E(m,n,f)\right)$$

$$+ N_y \frac{\partial}{\partial y}\left(\sum_{mn} A_{mn} E(m,n,f)\right) = \frac{\partial}{\partial z}\left(\sum_{mn} G_{mn} F(m,n,f)\right) - \frac{\partial}{\partial x}\left(\sum_{mn} I_{mn} F(m,n,f)\right)$$

$$- N_y \frac{\partial}{\partial x}\left(E^- + \sum_{mn} H_{mn} F(m,n,f) + N_y \left(\sum_{mn} G_{mn} F(m,n,f)\right)\right)$$

Dropping $O(f^3)$ terms.

$$\sum_{mn} \left[(A_{mn} - f_x C_{mn}) E(m,n,f) - (G_{mn} + f_x I_{mn}) F(m,n,f)\right] = 0$$

$$e^{-j\beta x} f^2 U + \sum_{mn} \left[(B_{mn} + f_y C_{mn}) E(m,n,f) - (H_{mn} + f_y I_{mn}) F(m,n,f)\right] = 0$$

$$\sum_{mn} \left[-j a_n C_{mn} + j b(m,n) B_{mn} - j a_m f_x B_{mn} + f_x j a_n A_{mn}\right] E(m,n,f)$$

$$-2f U e^{-j\beta x} - j f^2 U \tau' e^{j\beta x} = \sum_{mn} \left[-j a_n I_{mn} - j c(m,n) H_{mn}\right. \qquad \text{(B33)}$$

$$\left. - j a_m f_x H_{mn} + f_x j a_n G_{mn}\right] F(m,n,f)$$

$$\sum_{mn} \left[-j b(m,n) A_{mn} + j a_m C_{mn} - f_y j a_n B_{mn} + f_y j a_n A_{mn}\right] E(m,n,f)$$

$$= \sum_{mn} \left[j c(m,n) G_{mn} + j a_n I_{mn} - f_y j a_m H_{m,n} + f_y j a_n G_{mn}\right] F(m,n,f)$$

Now the series representations E(m,n,f) and F(m,n,f) out to $O(f)$ are

$$E(m,n,f) = E(m,n,0)\left[1 - j b(m,n) f - b^2(m,n) f^2 - \cdots\right]$$

$$= E(m,n,0)\left[1 - j b(m,n) f\right] \qquad \text{(B34)}$$

$$F(m,n,f) = F(m,n,0)\left[1 + j c(m,n) f\right]$$

E(m,n,f) and F(m,n,0) are equal. Now the coefficients A_{mn}, B_{mn}, C_{mn},

G_{mn}, H_{mn}, and I_{mn} are separated into terms of different orders. $A_{mn}^{(1)}$ implied the first order term of A_{mn}.

$$A_{mn} = A_{mn}^{(1)} + A_{mn}^{(2)} + \cdots \tag{B35}$$

The other terms are treated likewise. Then dropped terms higher than $O(f^3)$ the boundary conditions become

$$\sum_{mn} \left[\left(A_{mn}^{(1)} + A_{mn}^{(2)} + f_x C_{mn}^{(1)} \right) (1 - j\, b(m,n) f \right.$$
$$\left. - \left(G_{mn}^{(1)} + G_{mn}^{(2)} + f_x I_{mn}^{(1)} \right) (1 + j\, c(m,n) f) \right] = 0$$

$$e^{-j\beta\alpha x} f^2 U + \sum_{mn} \left[\left(B_{mn}^{(1)} + B_{mn}^{(2)} + f_y C_{mn}^{(1)} \right) (1 - j\, b(m,n) f) \right.$$
$$\left. - \left(H_{mn}^{(1)} + H_{mn}^{(2)} + f_y I_{mn}^{(1)} \right) (1 + j\, c(m,n) f) \right] E(m,n,0) = 0$$

$$\sum_{mn} \left[\left(-j\alpha_n C_{mn}^{(1)} - j\alpha_n C_{mn}^{(2)} + j\, b(m,n)\, B_{mn}^{(1)} + j\, b(m,n) B_{mn}^{(2)} - j\alpha_m f_x B_{mn}^{(1)} + j\alpha_n f_x A_{mn}^{(1)} \right.\right.$$
$$(1 - j\, b(m,n) f) - \left(-j\alpha_n I_{mn}^{(1)} - j\alpha_n I_{mn}^{(2)} - j\, c(m,n)\, H_{mn}^{(1)} - j\, c(m,n)\, H_{mn}^{(2)} \right.$$
$$\left.\left. - j\alpha_m f_x H_{mn}^{(1)} + j\alpha_n f_x G_{mn}^{(1)} \right) (1 + j\, c(m,n) f) \right] E(m,n,0) \tag{B36}$$
$$- e^{-j\beta\alpha x} U (2f + j f^2 \gamma\gamma') = 0$$

$$\sum_{mn} \left[\left(-j\, b(m,n) A_{mn}^{(1)} - j\, b(m,n) A_{mn}^{(2)} + j\alpha_m C_{mn}^{(1)} + j\alpha_m C_{mn}^{(2)} - f_y j\alpha_m B_{mn}^{(1)} + j\alpha_n f_y A_{mn}^{(1)} \right) \right.$$
$$(1 - j\, b(m,n) f) - \left(j\, c(m,n)\, G_{mn}^{(1)} + j\, c(m,n)\, G_{mn}^{(2)} + j\alpha_m I_{mn}^{(1)} + j\alpha_m I_{mn}^{(2)} \right.$$
$$\left. \left. - j\alpha_m f_y H_{mn}^{(1)} + j\alpha_n f_y G_{mn}^{(1)} \right) (1 + j\, c(m,n) f) \right] E(m,n,0) = 0$$

Since

$$f = \sum_{mn} P(m,n)\, e^{-j\alpha(mx + ny)}$$

$$E(m,n,0) = e^{-j\alpha(mx+ny)}$$

therefore, (B37)

$$f = \sum_{mn} P(m,n)\, E(m,n,0)$$

$$\begin{bmatrix} f \\ f_x \\ f_y \end{bmatrix} = \sum_{\mu\nu} \begin{bmatrix} 1 \\ -j\alpha\mu \\ -j\alpha\nu \end{bmatrix} P(\mu,\nu)\, E(\mu,\nu,0)$$

Therefore, as an example of the use of equation 37 for the term $fe^{-i\beta\alpha x}$, the third equation of equation 36 is

$$f e^{-j\beta\alpha x} = f e^{-j a v x} = \sum_{uv} P(u,v)\, E(m,n,0)$$

$$= \sum_{mn} P(m-v,n)\, E(m,n,0)$$

where u = m − v and v = n

Equating the first order terms in Equation 35,

$$A_{mn}^{(1)} = G_{mn}^{(1)}$$

$$B_{mn}^{(1)} = H_{mn}^{(1)}$$

$$-j a_n (C_{mn}^{(1)} - I_{mn}^{(1)}) + j\, b(m,n)\, B_{mn}^{(1)} + j\, c(m,n)\, H_{mn}^{(1)} - 2U P(m-v,n) = 0 \qquad \text{(B38)}$$

$$-j\, b(m,n)\, A_{mn}^{(1)} + j a_m (C_{mn}^{(1)} - I_{mn}^{(1)} - j\, c(m,n)\, G_{mn}^{(1)} = 0$$

Let

$$d(m,n) = b(m,n) + c(m,n)$$

$$A_{mn}^{(1)} = G_{mn}^{(1)}$$

$$B_{mn}^{(1)} = H_{mn}^{(1)} \qquad \text{(B39)}$$

$$-j a_n (C_{mn}^{(1)} - I_{mn}^{(1)}) + j\, d(m,n)\, B_{mn}^{(1)} = 2U P(m-v,n)$$

$$a_m (C_{mn}^{(1)} - I_{mn}^{(1)}) - d(m,n)\, A_{mn}^{(1)} = 0$$

Since it is assumed that the regions are charge free, the divergence condition $\nabla \cdot \mathcal{E} = 0$ must be satisfied for both medium 1 and medium 2.

$$a_m A_{mn}^{(1)} + a_n B_{mn}^{(1)} + b(m,n)\, C_{mn}^{(1)} = 0$$

$$a_m G_{mn}^{(1)} + a_n H_{mn}^{(1)} - c(m,n)\, I_{mn}^{(1)} = 0 \qquad \text{(B40)}$$

Equations 39 and 40 give six equations to solve for the six unknowns. Solving these equations simultaneously gives euqation 41, if

$$D_{mn} = a^2 m^2 + a^2 n^2 + b(m,n)\, c(m,n)$$

$$A_{mn}^{(1)} = G_{mn}^{(1)} = \frac{j 2U a^2 m n\, P(m-v,n)}{d(m,n)\, D_{mn}}$$

$$B_{mn}^{(1)} = H_{mn}^{(1)} = \frac{j 2U P(m-v,n)}{d(m,n)} \left[\frac{a^2 n^2}{D_{mn}} - 1\right] \qquad \text{(B41)}$$

$$C_{mn}^{(1)} = \frac{j 2U a_n c(m,n)\, P(m-v,n)}{d(m,n)\, D_{mn}}$$

$$I_{mn}^{(1)} = \frac{-j 2U a_n b(m,n)\, P(m-v,n)}{d(m,n)\, D_{mn}}$$

The determination fo the second order coefficients requires some additional equations which are derived below. The substitution of

$$\sum_{mn} \begin{bmatrix} f \\ f_x \\ f_y \end{bmatrix} J_{mn} E(m,n,o) \tag{B42}$$

for f in Equation 37 where J_{mn} is an arbitrary function of m and n yields

$$\sum_{mn} \begin{bmatrix} f \\ f_x \\ f_y \end{bmatrix} J_{mn} E(m,n,o) = \sum_{mn} \sum_{kl} \begin{bmatrix} 1 \\ -j a(m-k) \\ -j a(n-l) \end{bmatrix} J_{kl} P(m-k,n-l) E(m,n,o) \tag{B43}$$

From the definitions of b(m,n) and c(m,n)

$$c^2(m,n) - b^2(m,n) = \beta^2 (\epsilon_r - 1) \tag{B44}$$

Taking the difference of the two first order divergence conditions given in Equation 40 yields

$$b(m,n) C_{mn}^{(1)} + c(m,n) I_{mn}^{(1)} = 0 \tag{B45}$$

Also,

$$e^{-j a \nu x} f^2 = \sum_{mn} P(m,n) E(m,n,o) \cdot \sum_{kl} P(k,l) E(k,l,o) e^{-j a \nu x}$$

$$= \sum_{mnkl} P(m,n) P(k,l) E(m+k+\nu, n+l, o)$$

substituting k = k−ν and $l = l$ yields

$$= \sum_{mnkl} P(m,n) P(k-\nu, l) E(m+k, n+l, o)$$

then substituting m = m + k and N = n + l yields

$$f^2 e^{-j a \nu x} = \sum_{mnkl} P(m-k,n-l) P(k-\nu, l) E(m,n,o) \tag{B46}$$

Then equating the second order terms in Equation 36 gives

$$[A_{mn}^{(2)} + f_x C_{mn}^{(1)}](1-jb(m,n)f) - [G_{mn}^{(1)} + f_x I_{mn}^{(1)}](1+jc(m,n)f) = 0$$

$$f^2 e^{-j\alpha_0 x} + \sum_{mn} [(B_{mn}^{(2)} + f_y C_{mn}^{(1)})(1-jb(m,n)f) - (H_{mn}^{(2)} + f_y I_{mn}^{(1)})(1+jc(m,n)f)] E(m,n,0) = 0$$

$$\sum_{mn} [(-j\alpha_n C_{mn}^{(2)} + jb(m,n) B_{mn}^{(2)} - j\alpha_m f_x B_{mn}^{(1)} + j\alpha_n f_x A_{mn}^{(1)})(1-jb(m,n)f) - (-j\alpha_n I_{mn}^{(2)} - jc(m,n) H_{mn}^{(2)} - j\alpha_m f_x H_{mn}^{(1)} + j\alpha_n f_x G_{mn}^{(1)})(1+jc(m,n)f) \cdot E(m,n,0) - j e^{-j\beta_0 x} U f^2 \gamma\gamma' = 0 \quad \text{(B47)}$$

$$[-jb(m,n) A_{mn}^{(2)} + j\alpha_m C_{mn}^{(2)} - j\alpha_m f_y B_{mn}^{(1)} + j\alpha_n f_y A_{mn}^{(1)}](1-jb(m,n)f) - [jc(m,n) G_{mn}^{(2)} + j\alpha_m I_{mn}^{(2)} - j\alpha_m f_y H_{mn}^{(1)} + j\alpha_n f_y G_{mn}^{(1)}](1+jc(m,n)f) = 0$$

substitution of Equation 46 in Equation 47 yields

$$[A_{mn}^{(2)} + f_x C_{mn}^{(1)}](1-jb(m,n)f) - [G_{mn}^{(1)} + f_x I_{mn}^{(1)}](1+jc(m,n)f) = 0$$

$$\sum_{kl} [P(m-k,n-l) P(k-\nu,l)] + (B_{mn}^{(2)} + f_y C_{mn}^{(1)})(1-jb(m,n)f) - (H_{mn}^{(2)} + f_y I_{mn}^{(1)})(1+jc(m,n)f) = 0$$

$$-j\gamma\gamma' U \sum_{kl} [P(m-k,n-l) P(k-\nu,l)] + (-j\alpha_n C_{mn}^{(2)} + jb(m,n) B_{mn}^{(2)} - j\alpha_m f_x B_{mn}^{(1)} + j\alpha_n f_x A_{mn}^{(1)})(1-jb(m,n)f) - (-j\alpha_n I_{mn}^{(2)} - jc(m,n) H_{mn}^{(2)} - j\alpha_m f_x H_{mn}^{(1)} + j\alpha_n f_x G_{mn}^{(1)})(1+jc(m,n)f) = 0 \quad \text{(B48)}$$

$$[-jb(m,n) A_{mn}^{(2)} + j\alpha_m C_{mn}^{(2)} - j\alpha_m f_y B_{mn}^{(1)} + j\alpha_n f_y A_{mn}^{(1)}](1-jb(m,n)f) - [jc(m,n) G_{mn}^{(2)} + j\alpha_m I_{mn}^{(2)} - j\alpha_m f_y H_{mn}^{(1)} + j\alpha_n f_y G_{mn}^{(1)}](1+jc(m,n)f) = 0$$

Using Equation 48 and the divergence condition for the second order terms

$$\alpha_m A_{mn}^{(2)} + \alpha_n B_{mn}^{(2)} + b(m,n) C_{mn}^{(2)} = 0$$

$$\alpha_m G_{mn}^{(2)} + \alpha_n H_{mn}^{(2)} - c(m,n) I_{mn}^{(2)} = 0 \quad \text{(B49)}$$

Equations 48 and 49 give six equations to solve for the six second order coefficients. The solution to these equations for $z > 0$ is

$$d(m,n)\,D_{mn}\,A_{mn}^{(2)} = a^2m^2\,b(m,n)\,h_1 + (D_{mn} - a^2m^2)(c(m,n)\,h_1 - h_4) + a^2mn\,(b(m,n)\,h_2 - c(m,n)\,h_2 + h_3)$$

$$d(m,n)\,D_{mn}\,B_{mn}^{(2)} = a^2n^2\,b(m,n)\,h_2 + (D_{mn} - a^2n^2)(c(m,n)\,h_3 - h_3) + a^2mn\,(b(m,n)\,h_1 - c(m,n)\,h_1 + h_4)$$

$$d(m,n)\,D_{mn}\,C_{mn}^{(2)} = \gamma^2 a\,(mh_1 + nh_2) + c(m,n)\,a\,(mh_4 + nh_3) \qquad \text{(B50)}$$

where

$$h_1 = j\,am \sum_{kl} (C_{kl}^{(1)} - I_{kl}^{(1)})\,P(m-k, n-l)$$

$$h_2 = \sum_{kl} [U P(k-\nu, l) + j\,an\,(C_{kl}^{(1)} - I_{kl}^{(1)}]\,P(m-k, n-l)$$

$$h_3 = j \sum_{kl} [U\gamma\gamma' P(k-\nu, l) + \beta^2(\epsilon-1)\,B_{kl}^{(1)}]\,P(m-k, n-l] \qquad \text{(B51)}$$

$$h_4 = j\,\beta^2(\epsilon_t - 1) \sum_{kl} A_{kl}^{(1)}\,P(m-k, n-l)$$

The evaluation of the second order coefficients requires calculations of the average of Q(m,n,k,1), where

$$Q(m,n,k,l) = P(k-\nu, l)\,P(m-k, n-l) \qquad \text{(B52)}$$

From Equations 10 and 11,

$$\langle Q(m,n,k,l)\rangle = \langle P(k-\nu, l)\,P(m-k, n-l)\rangle \qquad (m,n) \neq (\nu,0)$$

$$= \begin{cases} 0 & \\ \dfrac{\pi^2}{L^2}\,W(ak - a\nu, al) & (m,n) = (\nu,0) \end{cases} \qquad \text{(B53)}$$

SCATTERING FROM A DIELECTRIC BOUNDARY - VERTICAL POLARIZATION

For the case of a vertically polarized wave incident on a dielectric boundary, the geometry is shown in Figure B.2.

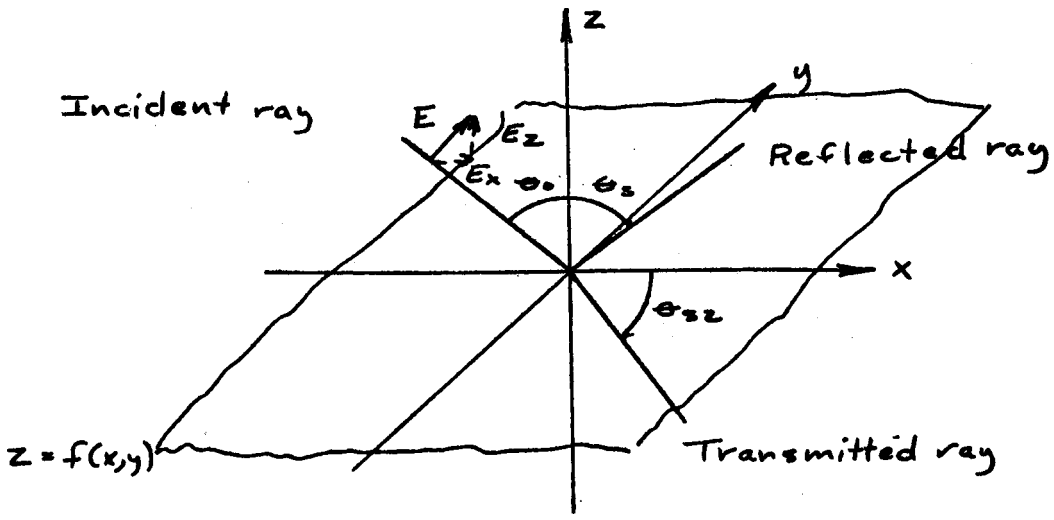

Figure B.2

The incident field is of unit intensity. Then the electric fields can be expressed as equation 54.

$$E_x = \begin{cases} E_x^+ + \sum_{mn} A_{mn} E(m,n,z) \\ E_x^- + \sum_{mn} G_{mn} F(m,n,z) \end{cases}$$

$$E_y = \begin{cases} \sum_{mn} B_{mn} E(m,n,z) \\ \sum_{mn} H_{mn} F(m,n,z) \end{cases}$$

$$E_z = \begin{matrix} E_z^+ + \sum_{mn} C_{mn} E(m,n,z) \\ E_z^- + \sum_{mn} I_{mn} F(m,n,z) \end{matrix} \qquad \text{(B54)}$$

$$E(m,n,z) = e^{-j\,a(mx+ny)\,-j\,b(m,n)\,z}\, e^{j\omega t}$$

$$F(m,n,z) = e^{-j\,a(mx+ny)\,+j\,c(m,n)\,z}\, e^{j\omega t}$$

The Fresnel reflection and transmission coefficients for a verticlly polarized wave as rations of the magnetic field intensity are given

below.

$$\Gamma_v = \frac{\gamma\gamma - \beta\gamma'}{\gamma\gamma + \beta\gamma'}$$

$$T_v = \frac{2\gamma\gamma'}{\gamma\gamma + \beta\gamma} \tag{B55}$$

The incident ray is $e^{-j\beta(\alpha x - \gamma z)}$. The specular ray is $e^{-j\beta(\alpha x + \gamma z)}$

Therefore

$$\begin{aligned} E_x^+ &= \gamma e^{-j\beta\alpha x}\left[e^{j\beta\gamma z} - \Gamma_v e^{-j\beta\gamma z}\right] \\ E_x^- &= \frac{\beta}{\gamma}\gamma' T_v e^{-\gamma(\alpha' x - \gamma' z)} \\ E_z^+ &= \alpha e^{-j\beta\alpha x}\left[e^{j\beta\gamma z} + \Gamma_v e^{-j\beta\gamma z}\right] \\ E_z^- &= \frac{\beta}{\gamma}\alpha' T_v e^{-j\gamma(\alpha' x - \gamma' z)} \end{aligned} \tag{B56}$$

The method of solution is similar to the horizontally polarized case.

The resulting coefficients are given below (Rice 1951).

$$A_{mn}^{(1)} = \left[j\alpha a_m \gamma b(m,n) - j\beta\gamma'(D_{mn} - a^2 h^2)\right] \frac{2UP(m-v,h)}{\gamma d(m,n) D_{mn}}$$

$$B_{mn}^{(1)} = \left[j\alpha\gamma b(m,n) + j a_m \beta\gamma'\right] \frac{2 a_n UP(m-v,h)}{\gamma d(m,n) D_{mn}} \tag{B57}$$

$$C_{mn}^{(1)} = \left[j a_m \gamma' c(m,n) - j\gamma a^2(m^2+h^2)\right] \frac{2UP(m-v,h)}{\gamma d(m,n) D_{mn}}$$

APPENDIX C
INTEGRALS

Evaluation of the roughness distribution function requires taking the Fourier transform of the mean square height of the surface ($\overline{z^2}$) times the auto correlation function ($\rho(r)$). The transformation is defined in Equation 6 of Appendix B. The transform of W(am-av,o) after conversion to cylindrical coordinates is

$$W(am-av,o) = \frac{\bar{z}^2}{\pi^2}\int_0^{\infty}\int_0^{2\pi}\rho(r)\,e^{i(am-av)r\cos\psi}\,r\,dr\,d\psi$$
$$= \frac{\bar{z}^2}{\pi^2}\int_0^{\infty}\left[\int_0^{2\pi}e^{ihr\cos\psi}\,d\psi\right]r\,dr \qquad (C1)$$

where $h = am-av = \beta(\sin\theta_s\cos\theta_s - \sin\theta_o)$

To perform the angular integration, equation 9.6.16 from the Handbook of Mathematical Functions (Abramowitz, M., and Stegun, I. A. (Eds.), U.S. Department of Commerce, March 1965) is used.

$$I_o(z) = \frac{1}{\pi}\int_0^{\pi}e^{z\cos\theta}\,d\theta \qquad (C2)$$

Since cos θ is an even function

$$2\pi I_o(z) = \int_0^{2\pi}e^{z\cos\theta}\,d\theta \qquad (C3)$$

also

$$I_o(z) = J_o(iz) \qquad (C4)$$

therefore, substitution of z = ihr yields

$$2\pi J_o(-hr) = \int_0^{2\pi}e^{ihr\cos\psi}\,d\psi \qquad (C5)$$

And,

$$W(am-av,o) = \frac{2\bar{z}^2}{\pi}\int_0^{\infty}r\rho(r)J_o(-hr)\,dr \qquad (C6)$$

If a Gaussian correlation function is chosen

$$\rho(r) = e^{-\frac{r^2}{V^2}} \tag{C7}$$

where V is the correlation distance.

From the same reference, Equation 11.4.29 is

$$\int_0^\infty e^{-a^2 t^2} t^{\nu+1} J_\nu(bt)\, dt = \frac{b^\nu}{(2a^2)^{\nu+1}}\, e^{-\frac{b^2}{4a^2}} \tag{C8}$$

$$\text{where } \Re(\nu) > -1$$

$$\Re(a^2) > 0$$

where $\Re$ designates the real part of the argument.

If

$$\nu = 0$$

$$a^2 = \frac{1}{V^2}$$

$$b = ih$$

$$t = r \tag{C9}$$

$$W(am - a\nu, o) = \frac{\bar{z}^2 V^2}{4\pi}\, e^{-\frac{V^2\beta^2}{4}(\sin\theta_s \cos\phi_s - \sin\theta_o)^2}$$

The integral in Equation 2.3-26, therefore, reduces to

$$\int_0^\infty \int_0^{2\pi} \rho(r)\, e^{i\beta r(\cos\phi_s \sin\theta_s - \sin\theta_o)\cos\psi}\, r\, dr\, d\psi$$

$$= 4\pi V^2 e^{-V^2\beta^2(\sin\theta_s \cos\phi_s - \sin\theta_o)^2} \tag{C10}$$

APPENDIX D

TABULATED DATA

REFLECTIVITY DATA FOR SAND - SMOOTH

FREQUENCY (GHz)	% MOISTURE (By Weight)	POLARIZATION	INCIDENCE ANGLE 10°	20°	30°	40°	50°	60°	70°
4.75	0.26	H	0.243	0.248	0.257	0.302	0.363		
6.0	0.26	H	0.269	0.282	0.302	0.355	0.398		
7.5	0.26	H	0.229	0.243	0.282	0.331	0.367		
4.75	0.26	V	0.257	0.232	0.202	0.200	0.110		
6.0	0.26	V	0.251	0.240	0.224	0.214	0.096		
7.5	0.26	V	0.232	o.204	0.216	0.200	0.100		
4.75	3.03	H	0.309	0.320	0.343	0.380	0.447		
6.0	3.03	H	0.299	0.302	0.331	0.372	0.437		
7.5	3.03	H	0.305	0.320	0.343	0.389	0.437		
4.75	3.03	V	0.305	0.295	0.263	0.224	0.158		
6.0	3.03	V	0.285	0.285	0.266	0.216	0.158		
7.5	3.03	V	0.309	0.302	0.272	0.226	0.158		
4.75	5.45	H	0.394	0.389	0.420	0.457	0.479		
6.0	5.45	H	0.380	0.398	0.427	0.457	0.468		
7.5	5.45	H	0.367	0.385	0.412	0.467	0.479		
4.75	5.45	V	0.380	0.363	0.343	0.302	0.232		
6.0	5.45	V	0.376	0.363	0.437	0.299	0.251		
7.5	5.45	V	0.372	0.359	0.339	0.313	0.248		
4.75	10.0	H	0.432	0.432	0.447	0.501	0.537		
6.0	10.0	H	0.417	0.412	0.447	0.495	0.543		
7.5	10.0	H	0.412	0.417	0.442	0.484	0.525		
4.75	10.0	V	0.412	0.394	0.367	0.331	0.263		

REFLECTIVITY DATA FOR SAND - SMOOTH

FREQUENCY	% MOISTURE	POLARIZATION	INCIDENCE ANGLE						
(GHz)	(By Weight)		10°	20°	30°	40°	50°	60°	70°
6.0	10.0	V	0.407	0.385	0.363	0.331	0.275		
7.5	10.0	V	0.380	0.372	0.355	0.316	0.266		
4.75	14.0	H	0.624	0.624	0.631	0.668	0.700		
6.0	14.0	H	0.610	0.638	0.638	0.668	0.700		
7.5	14.0	H	0.596	0.610	0.617	0.661	0.700		
4.75	14.0	V	0.610	0.603	0.562	0.525	0.452		
6.0	14.0	V	0.596	0.596	0.596	0.519	0.452		
7.5	14.0	V	0.563	0.575	0.550	0.507	0.452		
4.75	18.4	H	0.716	0.716	0.741	0.759	0.750		
6.0	18.4	H	0.700	0.708	0.708	0.759	0.759		
7.5	18.4	H	0.700	0.708	0.716	0.741	0.741		
4.75	18.4	V	0.684	0.684	0.661	0.610	0.531		
6.0	18.4	V	0.668	0.668	0.646	0.596	0.525		
7.5	18.4	V	0.661	0.668	0.646	0.603	0.513		
8.5	1.22	H	0.243	0.245	0.275	0.324	0.385	0.462	0.596
9.0	1.22	H	0.245	0.245	0.275	0.320	0.389	0.479	0.589
10.0	1.22	H	0.260	0.261	0.282	0.331	0.385	0.468	0.569
11.0	1.22	H	0.269	0.272	0.302	0.339	0.417	0.484	0.596
12.0	1.22	H	0.285	0.299	0.309	0.359	0.417	0.507	0.603
12.4	1.22	H	0.282	0.288	0.320	0.347	0.422	0.501	0.589
8.5	1.22	V	0.234	0.224	0.193	0.170	0.075	0.000	0.355
9.0	1.22	V	0.240	0.219	0.191	0.141	0.080	0.000	0.285

REFLECTIVITY DATA FOR SAND - SMOOTH

FREQUENCY (GHz)	% MOISTURE (By Weight)	POLARIZATION	INCIDENCE ANGLE 10°	20°	30°	40°	50°	60°	70°
10.0	1.22	V	0.251	0.234	0.191	0.157	0.072	0.000	0.162
11.0	1.22	V	0.254	0.243	0.221	0.160	0.090	0.000	0.263
12.0	1.22	V	0.272	0.248	0.224	0.176	0.105	0.000	0.130
12.4	1.22	V	0.266	0.248	0.214	0.168	0.112	0.000	0.124
8.5	4.30	H	0.327	0.343	0.385	0.422	0.479	0.569	0.707
9.0	4.30	H	0.320	0.339	0.376	0.412	0.468	0.569	0.692
10.0	4.30	H	0.316	0.327	0.363	0.407	0.462	0.556	0.653
11.0	4.30	H	0.316	0.320	0.351	0.398	0.462	0.543	0.684
12.0	4.30	H	0.299	0.309	0.339	0.385	0.452	0.550	0.661
12.4	4.30	H	0.295	0.422	0.324	0.372	0.447	0.531	0.646
8.5	4.30	V	0.320	0.305	0.275	0.248	0.164	0.064	0.335
9.0	4.30	V	0.326	0.305	0.285	0.232	0.172	0.151	0.335
10.0	4.30	V	0.305	0.299	0.272	0.232	0.145	0.079	0.176
11.0	4.30	V	0.292	0.288	0.263	0.240	0.150	0.112	0.269
12.0	4.30	V	0.285	0.279	0.272	0.229	0.164	0.129	0.245
12.4	4.30	V	0.288	0.279	0.266	0.207	0.162	0.126	0.200
8.5	4.75	H	0.347	0.351	0.380	0.380	0.479	0.468	0.569
9.0	4.75	H	0.339	0.347	0.376	0.476	0.473	0.462	0.562
10.0	4.75	H	0.331	0.343	0.372	0.385	0.462	0.457	0.525
11.0	4.75	H	0.347	0.339	0.372	0.385	0.468	0.452	0.550
12.0	4.75	H	0.335	0.339	0.367	0.385	0.462	0.447	0.543
12.4	4.75	H	0.331	0.331	0.363	0.389	0.457	0.452	0.531
8.5	4.75	V	0.339	0.309	0.302	0.257	0.157	0.010	0.251
9.0	4.75	V	0.327	0.309	0.309	0.232	0.170	0.100	0.299
10.0	4.75	V	0.320	0.309	0.299	0.232	0.145	0.050	0.162

REFLECTIVITY DATA FOR SAND - SMOOTH

FREQUENCY (GHz)	% MOISTURE (By Weight)	POLARIZATION	INCIDENCE ANGLE 10°	20°	30°	40°	50°	60°	70°
11.0	4.75	V	0.316	0.309	0.309	0.340	0.150	0.072	0.184
12.0	4.75	V	0.331	0.299	0.316	0.234	0.162	0.089	0.214
12.4	4.75	V	0.320	0.305	0.302	0.324	0.158	0.088	0.202
8.5	6.15	H	0.398	0.394	0.442	0.452	0.513	0.603	0.733
9.0	6.15	H	0.380	0.389	0.417	0.452	0.507	0.603	0.813
10.0	6.15	H	0.380	0.380	0.412	0.452	0.507	0.603	0.692
11.0	6.15	H	0.398	0.398	0.417	0.452	0.513	0.596	0.716
12.0	6.15	H	0.376	0.385	0.403	0.447	0.507	0.589	0.716
12.4	6.15	H	0.380	0.385	0.407	0.447	0.519	0.582	0.708
8.5	6.15	V	0.389	0.363	0.309	0.295	0.195	0.070	0.299
9.0	6.15	V	0.363	0.363	0.327	0.272	0.207	0.146	0.339
10.0	6.15	V	0.367	0.355	0.327	0.279	0.182	0.101	0.182
11.0	6.15	V	0.363	0.359	0.335	0.292	0.197	0.127	0.191
12.0	6.15	V	0.376	0.385	0.403	0.447	0.507	0.589	0.269
12.4	6.15	V	0.363	0.359	0.331	0.272	0.202	0.146	0.257
8.5	11.40	H	0.457	0.473	0.490	0.531	0.569	0.653	0.759
9.0	11.40	H	0.457	0.468	0.484	0.513	0.575	0.653	0.733
10.0	11.40	H	0.457	0.457	0.479	0.519	0.569	0.638	0.716
11.0	11.40	H	0.462	0.457	0.479	0.507	0.556	0.631	0.733
12.0	11.40	H	0.442	0.432	0.468	0.501	0.543	0.617	0.700
12.4	11.40	H	0.427	0.437	0.462	0.495	0.543	0.617	0.692
8.5	11.40	V	0.457	0.422	0.403	0.372	0.299	0.178	0.221
9.0	11.40	V	0.452	0.432	0.407	0.351	0.295	0.220	0.292
10.0	11.40	V	0.442	0.442	0.403	0.351	0.275	0.191	0.180
11.0	11.40	V	0.442	0.432	0.398	0.343	0.272	0.207	0.178

REFLECTIVITY DATA FOR SAND - SMOOTH

FREQUENCY (GHz)	% MOISTURE (By Weight)	POLARIZATION	INCIDENCE ANGLE 10°	20°	30°	40°	50°	60°	70°
12.0	11.40	V	0.422	0.417	0.398	0.335	0.272	0.207	0.254
12.4	11.40	V	0.432	0.417	0.380	0.331	0.263	0.207	0.232
8.5	12.15	H	0.473	0.473	0.495	0.543	0.610	0.676	0.804
9.0	12.15	H	0.462	0.479	0.501	0.543	0.596	0.668	0.891
10.0	12.15	H	0.452	0.460	0.495	0.531	0.582	0.676	0.785
11.0	12.15	H	0.473	0.484	0.490	0.531	0.582	0.653	0.776
12.0	12.15	H	0.457	0.462	0.479	0.513	0.569	0.661	0.794
12.4	12.15	H	0.462	0.473	0.479	0.519	0.562	0.653	0.794
8.5	12.15	V	0.473	0.447	0.407	0.385	0.305	0.166	0.214
9.0	12.15	V	0.457	0.447	0.417	0.376	0.309	0.240	0.299
10.0	12.15	V	0.422	0.422	0.412	0.372	0.282	0.186	0.200
11.0	12.15	V	0.422	0.432	0.403	0.380	0.282	0.211	0.207
12.0	12.15	V	0.452	0.442	0.403	0.347	0.295	0.237	0.295
12.4	12.15	V	0.452	0.427	0.394	0.359	0.285	0.224	0.282
8.5	16.57	H	0.676	0.668	0.684	0.716	0.716	0.785	0.841
9.0	16.57	H	0.661	0.676	0.684	0.708	0.750	0.794	0.851
10.0	16.75	H	0.661	0.676	0.684	0.716	0.759	0.794	0.841
11.0	16.75	H	0.767	0.661	0.684	0.716	0.750	0.776	0.841
12.0	16.75	H	0.668	0.661	0.661	0.707	0.750	0.776	0.841
12.4	16.75	H	0.653	0.646	0.676	0.708	0.759	0.767	0.316
8.5	16.75	V	0.661	0.614	0.603	0.589	0.501	0.389	0.048
9.0	16.75	V	0.646	0.638	0.603	0.631	0.495	0.398	0.219
10.0	16.75	V	0.646	0.638	0.610	0.575	0.507	0.412	0.285
11.0	16.75	V	0.661	0.631	0.617	0.575	0.507	0.407	0.229
12.0	16.75	V	0.643	0.631	0.617	0.569	0.513	0.398	0.269

REFLECTIVITY DATA FOR SAND - SMOOTH

FREQUENCY (GHz)	% MOISTURE (By Weight)	POLARIZATION	INCIDENCE ANGLE 10°	20°	30°	40°	50°	60°	70°
12.4	16.57	V	0.646	0.638	0.582	0.569	0.495	0.398	0.315
8.5	17.54	H	0.692	0.692	0.692	0.724	0.776	0.813	0.871
9.0	17.54	H	0.676	0.692	0.700	0.724	0.776	0.813	0.861
10.0	17.54	H	0.684	0.676	0.692	0.724	0.776	0.813	0.861
11.0	17.54	H	0.692	0.676	0.692	0.724	0.759	0.822	0.881
12.0	17.54	H	0.684	0.892	0.700	0.724	0.776	0.822	0.861
12.4	17.54	H	0.692	0.699	0.692	0.733	0.785	0.832	0.832
8.5	17.54	V	0.676	0.638	0.610	0.575	0.525	0.417	0.126
9.0	17.54	V	0.646	0.646	0.617	0.562	0.519	0.427	0.257
10.0	17.54	V	0.661	0.631	0.617	0.575	0.519	0.427	0.295
11.0	17.54	V	0.676	0.638	0.617	0.589	0.525	0.447	0.240
12.0	17.54	V	0.661	0.646	0.617	0.575	0.537	0.447	0.335
12.4	17.54	V	0.668	0.646	0.617	0.598	0.543	0.468	0.355
13.0	0.31	H	0.288	0.305	0.339	0.367	0.427	0.495	
15.0	0.31	H	0.279	0.299	0.324	0.359	0.442	0.501	
17.0	0.31	H	0.285	0.299	0.320	0.355	0.422	0.495	
13.0	0.31	V	0.279	0.275	0.237	0.372	0.140		
15.0	0.31	V	0.269	0.251	0.245	0.363	0.141		
17.0	0.31	V	0.272	0.257	0.237	0.363	0.129		
13.0	4.27	H	0.269	0.279	0.305	0.339	0.403	0.519	
15.0	4.27	H	0.251	0.248	0.282	0.320	0.385	0.501	
17.0	4.27	H	0.221	0.229	0.254	0.299	0.363	0.457	
13.0	4.27	V	0.263	0.240	0.211	0.170	0.105	0.065	

REFLECTIVITY DATA FOR SAND - SMOOTH

FREQUENCY (GHz)	% MOISTURE (By Weight)	POLARIZATION	INCIDENCE ANGLE 10°	20°	30°	40°	50°	60°	70°
15.0	4.27	V	0.234	0.214	0.200	0.164	0.090	0.079	
17.0	4.27	V	0.204	0.191	0.172	0.136	0.086	0.045	
13.0	6.30	H	0.316	0.339	0.372	0.427	0.495	0.569	
15.0	6.30	H	0.295	0.313	0.339	0.394	0.479	0.543	
17.0	6.30	H	0.254	0.282	0.309	0.363	0.452	0.513	
13.0	6.30	V	0.302	0.302	0.288	0.254	0.188	0.143	
15.0	6.30	V	0.275	0.263	0.251	0.232	0.158	0.127	
17.0	6.30	V	0.257	0.240	0.232	0.197	0.141	0.080	
13.0	7.10	H	0.427	0.442	0.457	0.501	0.562	0.646	
15.0	7.10	H	0.417	0.422	0.452	0.490	0.550	0.638	
17.0	7.10	H	0.398	0.412	0.437	0.452	0.513	0.613	
13.0	7.10	V	0.427	0.412	0.376	0.335	0.272	0.170	
15.0	7.10	V	0.412	0.385	0.363	0.316	0.251	0.166	
17.0	7.10	V	0.372	0.359	0.347	0.288	0.229	0.136	
13.0	15.80	H	0.610	0.624	0.653	0.668	0.707	0.767	
15.0	15.80	H	0.603	0.603	0.631	0.653	0.692	0.733	
17.0	15.80	H	0.569	0.582	0.610	0.617	0.661	0.707	
13.0	15.80	V	0.575	0.562	0.543	0.501	0.447	0.372	
15.0	15.80	V	0.562	0.537	0.513	0.479	0.417	0.363	
17.0	15.80	V	0.556	0.513	0.531	0.462	0.398	0.339	
13.0	16.80	H	0.692	0.700	0.708	0.759	0.794	0.832	
15.0	16.80	H	0.700	0.692	0.716	0.750	0.776	0.822	

REFLECTIVITY DATA FOR SAND - SMOOTH

FREQUENCY (GHz)	% MOISTURE (By Weight)	POLARIZATION	INCIDENCE ANGLE 10°	20°	30°	40°	50°	60°	70°
17.0	16.80	H	0.676	0.684	0.700	0.741	0.767	0.822	
13.0	16.80	V	0.700	0.676	0.653	0.603	0.556	0.462	
15.0	16.80	V	0.708	0.676	0.661	0.610	0.525	0.452	
17.0	16.80	V	0.700	0.692	0.653	0.582	0.513	0.412	
19.0	0.31	H	0.260	0.275	0.309	0.343	0.417	0.519	
23.0	0.31	H	0.254	0.269	0.295	0.324	0.398	0.513	
26.0	0.31		0.243	0.257	0.288	0.309	0.380	0.490	
19.0	0.31	V	0.254	0.243	0.224	0.180	0.108		
23.0	0.31	V	0.269	0.248	0.226	0.184	0.123		
26.0	0.31	V	0.260	0.245	0.219	0.178	0.129		
19.0	3.80	H	0.269	0.272	0.295	0.343	0.403	0.484	
23.0	3.80	H	0.243	0.251	0.275	0.320	0.380	0.462	
26.0	3.80	H	0.221	0.234	0.260	0.302	0.359	0.442	
19.0	3.80	V	0.221	0.209	0.193	0.164	0.116	0.081	
23.0	3.80	V	0.211	0.202	0.178	0.133	0.099	0.054	
26.0	3.80	V	0.200	0.191	0.178	0.132	0.080	0.066	
19.0	6.30	H	0.351	0.355	0.394	0.427	0.501	0.589	
23.0	6.30	H	0.320	0.320	0.351	0.385	0.457	0.550	
26.0	6.30	H	0.299	0.309	0.343	0.359	0.432	0.479	
19.0	6.30	V	0.331	0.320	0.282	0.243	0.180	0.115	
23.0	6.30	V	0.292	0.272	0.257	0.211	0.153	0.122	
26.0	6.30	V	0.285	0.254	0.229	0.186	0.141	0.095	

REFLECTIVITY DATA FOR SAND - SMOOTH

FREQUENCY (GHz)	% MOISTURE (By Weight)	POLARIZATION	INCIDENCE ANGLE 10°	20°	30°	40°	50°	60°	70°
19.0	7.10	H	0.385	0.394	0.442	0.442	0.525	0.676	
23.0	7.10	H	0.363	0.376	0.398	0.422	0.484	0.646	
26.0	7.10	H	0.351	0.367	0.398	0.407	0.462	0.610	
19.0	7.10	V	0.385	0.369	0.335	0.288	0.224	0.141	
23.0	7.10	V	0.363	0.347	0.316	0.266	0.195	0.143	
26.0	7.10	V	0.335	0.331	0.299	0.254	0.178	0.119	
19.0	15.80	H	0.537	0.531	0.562	0.610	0.653	0.700	
23.0	15.80	H	0.484	0.507	0.531	0.582	0.638	0.676	
26.0	15.80	H	0.447	0.462	0.501	0.562	0.617	0.653	
19.0	15.80	V	0.525	0.484	0.490	0.447	0.398	0.331	
23.0	15.80	V	0.495	0.462	0.457	0.417	0.363	0.316	
26.0	15.80	V	0.452	0.417	0.447	0.407	0.339	0.272	
19.0	16.80	H	0.631	0.631	0.661	0.700	0.759	0.794	
23.0	16.80	H	0.603	0.610	0.638	0.692	0.759	0.804	
26.0	16.80	H	0.603	0.603	0.617	0.653	0.733	0.785	
19.0	16.80	V	0.661	0.653	0.624	0.589	0.507	0.427	
23.0	16.80	V	0.676	0.661	0.603	0.575	0.501	0.417	
26.0	16.80	V	0,661	0.646	0.610	0.562	0.490	0.389	

REFLECTIVITY DATA FOR SAND - ROUGH

FREQUENCY (GHz)	% MOISTURE (By Weight)	POLARIZATION	INCIDENCE ANGLE 10°	20°	30°	40°	50°	60°	70°
4.75	0.26	H	0.197	0.202	0.237	0.254	0.299		
6.0	0.26	H	0.234	0.237	0.272	0.302	0.331		
7.5	0.26	H	0.209	0.219	0.263	0.313	0.324		
4.75	0.26	V	0.219	0.202	0.174	0.123	0.106		
6.0	0.26	V	0.229	0.211	0.195	0.138	0.090		
7.5	0.26	V	0.234	0.200	0.200	0.148	0.100		
4.75	3.03	H	0.234	0.248	0.272	0.299	0.372		
6.0	3.03	H	0.243	0.245	0.269	0.302	0.367		
7.5	3.03	H	0.229	0.240	0.305	0.336	0.363		
4.75	3.03	V	0.237	0.224	0.200	0.170	0.129		
6.0	3.03	V	0.240	0.226	0.211	0.174	0.135		
7.5	3.03	V	0.243	0.260	0.248	0.195	0.155		
4.75	5.45	H	0.295	0.288	0.339	0.359	0.437		
6.0	5.45	H	0.266	0.263	0.331	0.347	0.432		
7.5	5.45	H	0.257	0.269	0.347	0.347	0.432		
4.75	5.45	V	0.292	0.263	0.266	0.232	0.186		
6.0	5.45	V	0.269	0.243	0.248	0.202	0.164		
7.5	5.45	V	0.288	0.266	0.272	0.202	0.157		
4.75	10.00	H	0.355	0.355	0.398	0.437	0.501		
6.0	10.00	H	0.376	0.380	0.407	0.442	0.501		
7.5	10.00	H	0.394	0.412	0.447	0.462	0.513		
4.74	10.00	V	0.347	0.327	0.324	0.292	0.243		

REFLECTIVITY DATA FOR SAND - ROUGH

FREQUENCY (GHz)	% MOISTURE (By Weight)	POLARIZATION	INCIDENCE ANGLE 10°	20°	30°	40°	50°	60°	70°
6.0	10.00	V	0.372	0.359	0.343	0.302	0.248		
7.5	10.00	V	0.412	0.398	0.380	0.324	0.263		
4.75	14.0	H	0.537	0.550	0.589	0.617	0.638		
6.0	14.0	H	0.575	0.562	0.603	0.610	0.646		
7.5	14.0	H	0.610	0.610	0.631	0.631	0.638		
4.75	14.0	V	0.543	0.519	0.519	0.457	0.403		
6.0	14.0	V	0.575	0.562	0.562	0.468	0.403		
7.5	14.0	V	0.610	0.575	0.569	0.495	0.417		
4.75	18.4	H	0.562	0.569	0.617	0.668	0.759		
6.0	18.4	H	0.582	0.569	0.617	0.676	0.794		
7.5	18.4	H	0.631	0.624	0.692	0.700	0.804		
4.75	18.4	V	0.537	0.543	0.525	0.525	0.484		
6.0	18.4	V	0.556	0.537	0.537	0.543	0.473		
7.5	18.4	V	0.661	0.624	0.631	0.582	0.589		

REFLECTIVITY DATA FOR SAND - ROUGH

FREQUENCY (GHz)	% MOISTURE (By Weight)	POLARIZATION	INCIDENCE ANGLE 10°	20°	30°	40°	50°	60°	70°
8.5	1.22	H	0.182	0.182	0.260	0.327	0.343	0.422	0.562
10.0	1.22	H	0.186	0.182	0.234	0.295	0.343	0.412	0.490
12.0	1.22	H	0.184	0.188	0.237	0.294	0.339	0.403	0.513
8.5	1.22	V	0.193	0.193	0.136	0.088	0.037	0.025	0.376
10.0	1.22	V	0.182	0.191	0.146	0.071	0.040	0.023	0.174
12.0	1.22	V	0.184	0.178	0.145	0.068	0.052	0.020	0.257
8.5	4.30	H	0.316	0.331	0.355	0.385	0.427	0.501	0.646
10.0	4.30	H	0.288	0.260	0.331	0.355	0.427	0.490	0.569
12.0	4.30	H	0.288	0.288	0.305	0.316	0.398	0.457	0.550
8.5	4.30	V	0.302	0.288	0.263	0.200	0.148	0.081	0.432
10.0	4.30	V	0.266	0.260	0.240	0.197	0.141	0.054	0.120
12.0	4.30	V	0.254	0.240	0.204	0.162	0.117	0.063	0.088
8.5	4.75	H	0.316	0.320	0.355	0.389	0.432	0.490	0.653
10.0	4.75	H	0.302	0.309	0.331	0.363	0.422	0.490	0.610
12.0	4.75	H	0.295	0.292	0.313	0.339	0.417	0.479	0.562
8.5	4.75	V	0.305	0.299	0.263	0.207	0.155	0.055	0.367
10.0	4.75	V	0.282	0.269	0.254	0.191	0.151	0.035	0.138
12.0	4.75	V	0.269	0.245	0.226	0.188	0.136	0.048	0.178
8.5	6.15	H	0.305	0.327	0.339	0.389	0.447	0.507	0.653
10.0	6.15	H	0.295	0.309	0.339	0.363	0.427	0.501	0.575
12.0	6.15	H	0.299	0.295	0.309	0.351	0.427	0.490	0.537

RELFECTIVITY DATA FOR SAND - ROUGH

FREQUENCY (GHz)	% MOISTURE (By Weight)	POLARIZATION	INCIDENCE ANGLE 10°	20°	30°	40°	50°	60°	70°
8.5	6.15	V	0.305	0.299	0.269	0.219	0.164	0.088	0.363
10.0	6.15	V	0.282	0.269	0.251	0.211	0.148	0.060	0.132
12.0	6.15	V	0.269	0.254	0.229	0.195	0.146	0.089	0.174
8.5	11.4	H	0.442	0.452	0.479	0.519	0.569	0.631	0.741
10.0	11.4	H	0.432	0.437	0.452	0.490	0.543	0.603	0.638
12.0	11.4	H	0.398	0.394	0.417	0.437	0.507	0.562	0.603
8.5	11.4	V	0.447	0.427	0.398	0.355	0.288	0.166	0.295
10.0	11.4	V	0.398	0.398	0.372	0.335	0.260	0.155	0.186
12.0	11.4	V	0.389	0.351	0.324	0.272	0.237	0.197	0.247
8.5	12.15	H	0.427	0.447	0.468	0.525	0.550	0.596	0.708
10.0	12.15	H	0.407	0.412	0.447	0.479	0.537	0.569	0.668
12.0	12.15	H	0.398	0.403	0.417	0.457	0.525	0.575	0.537
8.5	12.15	V	0.447	0.437	0.394	0.347	0.292	0.178	0.343
10.0	12.15	V	0.432	0.389	0.385	0.335	0.275	0.150	0.130
12.0	12.15	V	0.432	0.363	0.335	0.305	0.248	0.193	0.132
8.5	16.57	H	0.638	0.575	0.603	0.603	0.676	0.684	0.684
10.0	16.57	H	0.575	0.525	0.589	0.582	0.668	0.653	0.676
12.0	16.57	H	0.484	0.484	0.543	0.582	0.653	0.653	0.578
8.5	16.57	V	0.562	0.484	0.501	0.457	0.394	0.204	0.316
10.0	16.57	V	0.525	0.442	0.468	0.437	0.355	0.221	0.195
12.0	16.57	V	0.525	0.442	0.457	0.452	0.407	0.275	0.359

REFLECTIVITY DATA FOR SAND - ROUGH

FREQUENCY (GHz)	% MOISTURE (By Weight)	POLARIZATION	INCIDENCE ANGLE 10°	20°	30°	40°	50°	60°	70°
8.5	17.54	H	0.692	0.692	0.700	0.759	0.794	0.861	0.923
10.0	17.54	H	0.708	0.692	0.724	0.767	0.794	0.871	0.881
12.0	17.54	H	0.716	0.700	0.716	0.767	0.724	0.851	0.881
8.5	17.54	V	0.676	0.668	0.603	0.610	0.519	0.389	0.188
10.0	17.54	V	0.700	0.653	0.646	0.617	0.519	0.417	0.305
12.0	17.54	V	0.676	0.708	0.661	0.624	0.562	0.467	0.403
13.0	0.31	H	0.209	0.224	0.245	0.282	0.320	0.409	
15.0	0.31	H	0.200	0.200	0.224	0.226	0.309	0.385	
17.0	0.31	H	0.158	0.176	0.204	0.257	0.295	0.359	
13.0	0.31	V	0.193	0.191	0.174	0.141	0.077		
15.0	0.31	V	0.162	0.162	0.145	0.120	0.069		
17.0	0.31	V	0.148	0.141	0.132	0.112	0.055		
13.0	4.27	H	0.257	0.266	0.288	0.327	0.394	0.490	
15.0	4.27	H	0.234	0.240	0.275	0.313	0.385	0.484	
17.0	4.27	H	0.200	0.207	0.243	0.292	0.363	0.457	
13.0	4.27	V	0.254	0.234	0.219	0.182	0.116	0.158	
15.0	4.27	V	0.229	0.214	0.200	0.170	0.112	0.066	
17.0	4.27	V	0.197	0.191	0.174	0.157	0.110	0.056	
13.0	6.30	H	0.292	0.309	0.339	0.398	0.468	0.543	
15.0	6.30	H	0.269	0.275	0.309	0.363	0.442	0.513	
17.0	6.30	H	0.229	0.243	0.275	0.327	0.412	0.495	

REFLECTIVITY DATA FOR SAND - ROUGH

FREQUENCY (GHz)	% MOISTURE (By Weight)	POLARIZATION	INCIDENCE ANGLE 10°	20°	30°	40°	50°	60°	70°
13.0	6.30	V	0.282	0.279	0.251	0.229	0.164	0.127	
15.0	6.30	V	0.251	0.240	0.226	0.200	0.146	0.115	
17.0	6.30	V	0.226	0.221	0.197	0.172	0.136	0.072	
13.0	7.10	H	0.376	0.385	0.393	0.437	0.513	0.596	
15.0	7.10	H	0.351	0.359	0.385	0.412	0.490	0.589	
17.0	7.10	H	0.305	0.324	0.347	0.376	0.452	0.569	
13.0	7.10	V	0.355	0.343	0.313	0.275	0.224	0.105	
15.0	7.10	V	0.331	0.313	0.288	0.254	0.224	0.133	
17.0	7.10	V	0.282	0.272	0.257	0.209	0.186	0.108	
13.0	15.80	H	0.556	0.575	0.610	0.617	0.661	0.733	
15.0	15.80	H	0.562	0.562	0.575	0.596	0.631	0.708	
17.0	15.80	H	0.479	0.490	0.562	0.550	0.589	0.684	
13.0	15.80	V	0.519	0.507	0.501	0.462	0.403	0.343	
15.0	15.80	V	0.495	0.470	0.462	0.432	0.376	0.343	
17.0	15.80	V	0.468	0.447	0.437	0.412	0.355	0.305	
19.0	0.31	H	0.162	0.158	0.202	0.272	0.295		
23.0	0.31	H	0.040	0.065	0.119	0.211	0.279		
26.0	0.31	H	0.035	0.042	0.063	0.180	0.240		
19.0	0.31	V	0.133	0.151	0.136	0.112	0.069		
23.0	0.31	V	0.052	0.077	0.086	0.087	0.050		
26.0	0.31	V	0.042	0.036	0.046	0.076	0.044		
19.0	3.80	H	0.207	0.219	0.248	0.285	0.351	0.473	

REFLECTIVITY DATA FOR SAND - ROUGH

FREQUENCY (GHz)	% MOISTURE (By Weight)	POLARIZATION	INCIDENCE ANGLE 10°	20°	30°	40°	50°	60°	70°
23.0	6.30	H	0.101	0.133	0.197	0.295	0.385	0.479	
26.0	6.30	H	0.025	0.050	0.120	0.234	0.324	0.447	
19.0	6.30	V	0.191	0.186	0.178	0.155	0.114	0.090	
23.0	6.30	V	0.146	0.148	0.153	0.129	0.094	0.065	
26.0	6.30	V	0.119	0.114	0.105	0.091	0.074	0.079	
19.0	7.10	H	0.266	0.285	0.327	0.380	0.457	0.603	
23.0	7.10	H	0.178	0.209	0.257	0.305	0.407	0.562	
26.0	7.10	H	0.119	0.148	0.209	0.251	0.372	0.531	
19.0	7.10	V	0.254	0.245	0.237	0.234	0.153	0.115	
23.0	7.10	V	0.146	0.155	0.146	0.140	0.119	0.107	
26.0	7.10	V	0.080	0.091	0.099	0.076	0.077	0.097	
19.0	15.80	H	0.351	0.372	0.417	0.452	0.525	0.610	
23.0	15.80	H	0.285	0.313	0.363	0.394	0.457	0.543	
26.0	15.80	H	0.209	0.216	0.299	0.339	0.417	0.501	
19.0	15.80	V	0.417	0.398	0.407	0.376	0.389	0.305	
23.0	15.80	V	0.339	0.339	0.343	0.335	0.320	0.275	
26.0	15.80	V	0.272	0.272	0.305	0.376	0.363	0.309	

REFLECTIVITY DATA FOR SOIL - SMOOTH

FREQUENCY (GHz)	% MOISTURE (By Weight)	POLARIZATION	INCIDENCE ANGLE 10°	20°	30°	40°	50°	60°	70°
4.75	1.0	H	0.224	0.248	0.263	0.305	0.343		
6.0	1.0	H	0.224	0.234	0.251	0.305	0.339		
7.5	1.0	H	0.229	0.240	0.260	0.299	0.351		
8.5	1.0	H	0.229	0.240	0.269	0.316	0.355		
10.0	1.0	H	0.234	0.234	0.275	0.316	0.339		
12.0	1.0	H	0.234	0.234	0.269	0.316	0.363		
4.75	1.0	V	0.232	0.209	0.184	0.130	0.072		
6.0	1.0	V	0.219	0.209	0.172	0.130	0.072		
7.5	1.0	V	0.219	0.209	0.184	0.127	0.074		
8.5	1.0	V	0.219	0.214	0.195	0.162	0.083		
10.0	1.0	V	0.219	0.209	0.188	0.155	0.081		
12.0	1.0	V	0.224	0.214	0.186	0.148	0.085		
4.75	5.12	H	0.339	0.359	0.385	0.417	0.473		
6.0	5.12	H	0.355	0.367	0.376	0.422	0.447		
7.5	5.12	H	0.363	0.380	0.376	0.442	0.479		
8.5	5.12	H	0.316	0.316	0.339	0.380	0.469		
10.0	5.12	H	0.313	0.324	0.351	0.385	0.437		
12.0	5.12	H	0.309	0.324	0.347	0.389	0.437		
4.75	5.12	V	0.339	0.320	0.295	0.251	0.166		
6.0	5.12	V	0.351	0.324	0.295	0.245	0.162		
7.5	5.12	V	0.339	0.339	0.302	0.251	0.191		
8.5	5.12	V	0.301	0.295	0.275	0.237	0.182		
10.0	5.12	V	0.305	0.295	0.275	0.240	0.178		
12.0	5.12	V	0.302	0.295	0.263	0.276	0.164		

REFLECTIVITY DATA FOR SOIL - SMOOTH

FREQUENCY (GHz)	% MOISTURE (By Weight)	POLARIZATION	INCIDENCE ANGLES 10°	20°	30°	40°	50°	60°	70°
4.75	9.1	H	0.320	0.335	0.355	0.398	0.473		
6.0	9.1	H	0.376	0.376	0.412	0.422	0.459		
7.5	9.1	H	0.355	0.363	0.389	0.432	0.457		
8.5	9.1	H	0.422	0.447	0.501	0.531	0.662		
10.0	9.1	H	0.437	0.447	0.437	0.479	0.556		
12.0	9.1	H	0.417	0.432	0.468	0.507	0.562		
4.75	9.1	V	0.295	0.327	0.309	0.232	0.186		
6.0	9.1	V	0.339	0.398	0.376	0.248	0.186		
7.5	9.1	V	0.316	0.403	0.376	0.251	0.178		
8.5	9.1	V	0.427	0.422	0.398	0.367	0.282		
10.0	9.1	V	0.427	0.427	0.398	0.355	0.282		
12.0	9.1	V	0.412	0.407	0.385	0.339	0.282		
4.74	13.6	H	0.562	0.569	0.575	0.603	0.589		
6.0	13.6	H	0.531	0.569	0.556	0.603	0.646		
7.5	13.6	H	0.513	0.531	0.550	0.596	0.724		
8.5	13.6	H	0.507	0.495	0.562	0.562	0.603		
10.0	13.6	H	0.501	0.519	0.525	0.569	0.589		
12.0	13.6	H	0.457	0.473	0.519	0.550	0.562		
4.75	13.6	V	0.582	0.562	0.501	0.468	0.372		
6.0	13.6	V	0.525	0.543	0.479	0.473	0.389		
7.5	13.6	V	0.479	0.468	0.427	0.427	0.442		
8.5	13.6	V	0.525	0.495	0.484	0.432	0.380		
10.0	13.6	V	0.513	0.473	0.447	0.427	0.347		
12.0	13.6	V	0.437	0.457	0.432	0.412	0.363		

REFLECTIVITY DATA FOR SOIL - SMOOTH

FREQUENCY (GHz)	% MOISTURE (By Weight)	POLARIZATION	INCIDENCE ANGLE 10°	20°	30°	40°	50°	60°	70°
4.75	17.0	H	0.631	0.631	0.538	0.661	0.692		
6.0	17.0	H	0.624	0.638	0.676	0.708	0.716		
7.5	17.0	H	0.631	0.638	0.657	0.708	0.724		
8.5	17.0	H	0.603	0.610	0.638	0.692	0.716		
10.0	17.0	H	0.596	0.610	0.631	0.684	0.750		
12.0	17.0	H	0.589	0.603	0.610	0.678	0.708		
4.75	17.0	V	0.624	0.610	0.569	0.531	0.479		
6.0	17.0	V	0.631	0.638	0.610	0.519	0.473		
7.5	17.0	V	0.646	0.617	0.610	0.582	0.501		
8.5	17.0	V	0.596	0.575	0.556	0.531	0.468		
10.0	17.0	V	0.575	0.575	0.550	0.543	0.490		
12.0	17.0	V	0.582	0.562	0.562	0.513	0.462		
4.75	23.0	H	0.776	0.741	0.767	0.776	0.813		
6.0	23.0	H	0.741	0.692	0.724	0.776	0.794		
7.5	23.0	H	0.804	0.741	0.794	0.804	0.841		
8.5	23.0	H	0.724	0.750	0.770	0.832	0.841		
10.0	23.0	H	0.733	0.750	0.804	0.813	0.871		
12.0	23.0	H	0.700	0.724	0.794	0.832	0.841		
4.75	23.0	V	0.724	0.716	0.700	0.638	0.575		
6.0	23.0	V	0.708	0.692	0.668	0.646	0.562		
7.5	23.0	V	0.785	0.724	0.759	0.653	0.638		
8.5	23.0	V	0.708	0.716	0.692	0.691	0.631		
10.0	23.0	V	0.724	0.724	0.741	0.708	0.617		
12.0	23.0	V	0.733	0.733	0.750	0.724	0.631		

REFLECTIVITY DATA FOR SOIL - ROUGH

FREQUENCY (GHz)	% MOISTURE (By Weight)	POLARIZATION	INCIDENCE ANGLE 10°	20°	30°	40°	50°	60°	70°
4.75	1.0	H	0.166	0.182	0.251	0.320	0.417		
6.0	1.0	H	0.158	0.162	0.234	0.288	0.398		
7.5	1.0	H	0.146	0.143	0.224	0.251	0.398		
8.5	1.0	H	0.186	0.209	0.245	0.245	0.372		
10.0	1.0	H	0.186	0.214	0.251	0.275	0.389		
12.0	1.0	H	0.170	0.214	0.214	0.275	0.347		
4.75	1.0	V	0.153	0.164	0.172	0.127	0.063		
6.0	1.0	V	0.148	0.155	0.170	0.116	0.060		
7.5	1.0	V	0.135	0.130	0.172	0.120	0.060		
8.5	1.0	V	0.191	0.170	0.182	0.120	0.234		
10.0	1.0	V	0.200	0.191	0.191	0.138	0.224		
12.0	1.0	V	0.186	0.170	0.158	0.132	0.114		
4.75	5.12	H	0.305	0.324	0.339	0.447	0.550		
6.0	5.12	H	0.302	0.324	0.324	0.407	0.562		
7.5	5.12	H	0.288	0.295	0.302	0.417	0.596		
8.5	5.12	H	0.331	0.324	0.412	0.437	0.596		
10.0	5.12	H	0.355	0.367	0.437	0.484	0.589		
12.0	5.12	H	0.385	0.427	0.447	0.513	0.562		
4.75	5.12	V	0.302	0.288	0.275	0.240	0.182		
6.0	5.12	V	0.282	0.292	0.266	0.216	0.193		
7.5	5.12	V	0.316	0.279	0.269	0.243	0.211		
8.5	5.12	V	0.331	0.302	0.316	0.240	0.204		
10.0	5.12	V	0.385	0.355	0.351	0.269	0.186		
12.0	5.12	V	0.427	0.398	0.355	0.251	0.166		

REFLECTIVITY DATA FOR SOIL - ROUGH

FREQUENCY	% MOISTURE	POLARIZATION	INCIDENCE ANGLE						
(GHz)	(By Weight)		10°	20°	30°	40°	50°	60°	70°
4.75	9.1	H	0.257	0.279	0.327	0.398	0.495		
6.0	9.1	H	0.260	0.272	0.320	0.355	0.484		
7.5	9.1	H	0.251	0.263	0.339	0.376	0.479		
8.5	9.1	H	0.335	0.437	0.427	0.398	0.550		
10.0	9.1	H	0.309	0.407	0.380	0.363	0.537		
12.0	9.1	H	0.282	0.351	0.335	0.407	0.543		
4.75	9.1	V	0.263	0.251	0.251	0.234	0.195		
6.0	9.1	V	0.263	0.254	0.248	0.200	0.186		
7.5	9.1	V	0.282	0.269	0.285	0.243	0.197		
8.5	9.1	V	0.363	0.302	0.359	0.347	0.229		
10.0	9.1	V	0.309	0.320	0.359	0.355	0.202		
12.0	9.1	V	0.234	0.269	0.288	0.288	0.172		
4.75	13.6	H	0.537	0.556	0.624	0.661	0.832		
6.0	13.6	H	0.531	0.525	0.610	0.676	0.851		
7.5	13.6	H	0.537	0.543	0.631	0.692	0.832		
8.5	13.6	H	0.335	0.351	0.437	0.537	0.562		
10.0	13.6	H	0.335	0.335	0.407	0.543	0.543		
12.0	13.6	H	0.313	0.324	0.355	0.468	0.519		
4.75	13.6	V	0.525	0.507	0.501	0.468	0.380		
6.0	13.6	V	0.537	0.525	0.519	0.432	0.427		
7.5	13.6	V	0.556	0.543	0.513	0.484	0.479		
8.5	13.6	V	0.351	0.343	0.363	0.335	0.279		
10.0	13.6	V	0.343	0.335	0.339	0.331	0.245		
12.0	13.6	V	0.331	0.302	0.302	0.275	0.232		

REFLECTIVITY DATA FOR SOIL - ROUGH

FREQUENCY (GHz)	% MOISTURE (By Weight)	POLARIZATION	INCIDENCE ANGLE 10°	20°	30°	40°	50°	60°	70°
4.75	17.0	H	0.562	0.575	0.653	0.631	0.708		
6.0	17.0	H	0.582	0.589	0.638	0.646	0.741		
7.5	17.0	H	0.646	0.624	0.653	0.661	0.708		
8.5	17.0	H	0.631	0.631	0.653	0.684	0.638		
10.0	17.0	H	0.569	0.631	0.562	0.708	0.653		
12.0	17.0	H	0.575	0.582	0.537	0.646	0.596		
4.75	17.0	V	0.556	0.543	0.507	0.490	0.479		
6.0	17.0	V	0.550	0.569	0.556	0.473	0.484		
7.5	17.0	V	0.624	0.582	0.582	0.519	0.484		
8.5	17.0	V	0.582	0.575	0.582	0.519	0.417		
10.0	17.0	V	0.543	0.596	0.531	0.562	0.432		
12.0	17.0	V	0.562	0.556	0.495	0.537	0.427		